Cape Peninsula University of Technology

Facile sensor based on thiol capped quantum dots for sensing of Human epidermal growth factor receptor (HER-2)

by

Madillo Jemina Mareka

Thesis submitted in fulfilment of the requirements for the degree.

Master of Technology:

in the Faculty of Applied of science

at the Cape Peninsula University of Technology

Supervisor: DR. N. Ndube-Tsolekile
Co-supervisor: Prof. M.C. Matoetoe

Bellville
September 2023

DECLARATION

I, **Madillo Jemina Mareka**, declare that the contents of this thesis/dissertation represent my own unaided work and that the thesis/dissertation has not previously been submitted for academic examination towards any qualification. Furthermore, it represents my own opinions and not necessarily those of the Cape Peninsula University of Technology.

Signed:  **Date: August 2023**

ABSTRACT

Quantum dots (QDs) are a novel class of materials that have attracted much interest in the fields of biology, material science, and physical optics. Herein, we report the facile synthesis of thiol-protected SnS QDs for HER-2 sensor fabrication. The QDs were synthesized using two synthetic methods with different sulfur sources (sodium sulfide (Na_2S) vs. thiourea). The synthesis was performed by heating in the presence of simple precursors in a diol-stabilized chemical medium. To improve material stabilization and bio-compatibility, three thiols, namely, Glutathione (GSH), L-Cysteine (L-cyst) and Mercapto-propanoic acid (MPA), were investigated as potential capping agents in each method. The effect of synthetic parameters such as reaction time, Sn: S ratio, reaction solvent (H_20 vs. $C_3H_8O_2$), reaction method (heat vs. reflux), ZnS shell and pH were also investigated to obtain optimum reaction conditions. An optical property comparison between the two methods was conducted. SnS QDs synthesized using method 2 exhibited high PL peak intensities at 1:1 Sn:S and pH 6 when L-Cysteine is used as a thiol capping agent. Adding the ZnS shell on the SnS QDs enhanced the PL intensity in both methods. Subsequently, L-Cysteine capped SnS QDs were synthesized using heat-up method at Sn:S ratio (1:1), and pH 6 with 30 min reaction time. These QDs were used as labels to create a sensor for HER2 biomarker detection.The optical properties of the synthesized QDs were characterized using ultraviolet-visible (UV–Vis), photoluminescence (PL) spectroscopy, and energy dispersive spectroscopy (EDS). The size and the shape of the QDs were confirmed using dynamic light scattering (DLS), scanning electron microscope (SEM), and transmission electron microscope (TEM).

The electroactivity of the as-synthesized L-cyst-SnS/ZnS QDs were successfully investigated using non-film (L-cyst-SnS/ZnS (solution) and film (L-cyst-SnS/ZnS/GCE) modes. Electroactivity properties were studied using Cyclic voltammetry (CV) and differential-pulse

voltammetry (DPV). A choice was made between non-film and film methods based on depicted electroactivity and the film preparation problems encountered. The effect of varying supporting electrolytes was made using aqueous hydrochloric acid and Phosphate-buffered saline (PBS). PBS showed better electroactivity; hence, used in chemical reactivity and electron transfer kinetics of L-cyst-SnS/ZnS QDs studies. Both Randles-Sevcik and Lavron's method results for the core-shell L-Cyst-SnS/ZnS (non-film) QDs showed enhanced electrochemical properties, such as heterogeneous electron-rate constants at 6.72x10-5 $cm.s^{-1}$ and diffusion coefficients (D) of 9.43x10-3 cm^2s^{-1}, in comparison to the reported values. These results suggest the formation of smaller L-cyst-SnS/ZnS QDs which might be the cause of aggregation. The L-cyst-SnS/ZnS (non-film) was successfully employed for sensing of HER-2. Different operating conditions were evaluated for the successful detection of the HER-2 biomarker. The electrochemical interaction between the biomarker and the as-synthesized L-Cyst-SnS/ZnS QDs were carried out using CV, DPV and SWV respectively at different time intervals. The findings showed time-depent interactions between the biomarker and the QDs. Amongst all the methods assessed, SWV technique demonstrated superior sensitivity in HER-2 detection, hence it was selected as the best method. The addition of Glutaraldehyde as a cross-linker led to an enhanced peak of the HER-2. The developed L-Cyst-SnS/ZnS (non-film) QDs sensor demonstrated an optimal limit of detection of 0.23 ng/mL. Additionally, the limits of quantification (LOQ) were determined to be 0.77 ng/mL, and the linear dynamic range of the method was obtained between 0.99 ng/mL and 3.3 ng/mL. The proposed sensor showed great potential for detecting HER-2 in real samples.

ACKNOWLEDGEMENTS

First and foremost, I would like to thank my grand creator, Jehovah God, who has given me the wisdom and strength to complete this study. To my supervisor, Dr Ndube-Tsolekile, thank you, for the knowledge, support, and guidance throughout this entire project. I will never forget the massages of encouragement and quotes you sent especially when I felt tired and drained. You have set an example for me and many younger generations of female scientist moving through the ranks. May God bless you. To my co-supervisor professor Mangaka Matoetoe, thank you for the constant support and advice through all the stages of writing my project. To the late Dr Bongiwe Silwana, thank you for the contribution in this research, your keen scientific insights has benefitted me. To Dr Fredrick Oluoch Okumu , thank you for your thoughtful insights, critical reflection and your willgness to help in this research. To all my lab members, thank you very much for always being so supportive and reliable. To Ken Grieves, Christopher Perrang and Dr Ashwell Makan your unwavering presence and support was felt, thank you. To my mom, Mamokoena (Masamoele Mareka) and sisters (Ntsebo Mareka and Reamoehetse Mareka), words cannot express how grateful I am for the constant support over the years, especially emotionally (Kealeboha Batloung babatle). To Mrs Vusiwe Tsetsana thank you for playing the role of being a parent. Your prayers have helped me persevere. Dr. Gillian Arendse, words cannot explain how much your everlasting faith in me has meant to me; you have supported me throughout my academic career. I highly value your presence in my life, and I hope you are aware and proud of the significant influence you have had in defining my career. Lastly, I would like to express my heartfelt appreciation to Cape Peninsula University of Technology for giving me the opportunity to carry out this project.

The financial assistance of Duram smart paint towards this research is acknowledged. Opinions expressed in this thesis and the conclusions arrived at, are those of the author, and are not necessarily to be attributed to Duram smart paint.

DEDICATION

This is for my late father Joseph Mareka (Motloung waka you are dearly missed) and Dr Gillian Arendse (biae dankie vir alles wat jy vir my gedoen het).

"For I well know the thoughts that I am thinking toward you,' declares Jehovah, 'thoughts of peace, and not of calamity, to give you a future and a hope'' (Jeremiah 29:11).

TABLE OF CONTENTS

CHAPTER 4: FABRICATION OF ELECTROCHEMICAL HER-2 SENSOR

CHAPTER 4: CONCLUSIONS AND RECOMMENDATIONS

List of figures

List of Tables

List of diagrams

Glossary

Abbreviation/Acronym	Definition/meaning.
ASV	Anodic stripping voltammetry
CV	Cyclic voltammetry
DLS	Dynamic light scattering
DPASV	Differential pulse anodic stripping voltammetry
DPV	Differential pulse voltammetry
EDS	Energy dispersive spectroscopy
EIS	Electrochemical impedance spectroscopy
FTIR	Fourier-transform infrared spectroscopy
FWHM	Full-width half maximum
GCE	Glassy carbon electrode
GA	Glutaraldehyde
GSH	Glutathione
HCL	Hydrochloric acid
HER-2	Human epidermal growth factor receptor 2
L-Cyst	L-Cysteine
PBS	Phosphate buffer
PL	Photoluminescence
PXRD	Powder-X-ray diffraction
PG	Propylene glycol
QDs	Quantum dots
SEM	Scanning electron microscope
SnS	Tin Sulfide

TEM	Transmission electron microscope
UV	Ultraviolet-visible spectroscopy
ZnS	Zinc sulfide

Research outputs

1. Publications

i. Madillo Mareka, Mangaka Matoetoe, Ncediwe Tsolekile.2024. One-pot synthesis optimization of thiol-capped SnS and SnS/ZnS QDs for photocatalytic degradation of Rhodamine 6G. Heliyon 10:1

2. Conference presentations

i. 10th South African Nanotechnology Initiative-Nanoscience Young Researcher's symposium (SANI-NYRS): National. 7-8 October 2021. (**Ora**l) Madillo Mareka, Ncediwe Tsolekile, Mangaka C. Matoetoe. Title: pH sensitive Thiol Capped SnS QDs: Synthesis and Optical properties. (**Grand prize winner**).

ii. SACI Central Section Annual Young Chemists Symposium: National.19 August 2022. (**Oral**). Madillo Mareka, Ncediwe Tsolekile, Mangaka C. Matoetoe. Title: Synthesis of highly stable SnS QDs: Photocatalytic degradation of Rhodamine R6G.

CHAPTER 1

INTRODUCTION

1.1. Background

Cancer-related incidences and deaths are arising around the world. In 2018, the world health organization (WHO) reported that cancer is one of the leading causes of mortality (World health organization, no date). Screening and early detection of cancer increases the chances of successful treatment of the disease and accessible health facilities (Lu et al., 2016). Oncological imaging and biopsy-cytology specimens are the most widely used techniques for early cancer detection. However, these invasive conventional detection methods are time-consuming, expensive and have low sensitivity. Therefore, developing a rapid, new low-cost, and highly sensitive method is critical to enable early cancer diagnosis.

Nanotechnology (Quantum dots)

Nanotechnology has brought new hope in cancer therapy resulting in development of rapid diagnosis strategies. Due to their size-dependent chemical and physical properties, nanoparticles (NPs) have been used in medical field for cancer research. Quantum dots (QDs) have been promising NPs for biological applications due to their excellent optoelectronic properties and spectral tunability, allowing their use in ultraviolet and near-infrared regions (Yadav et al., 2016). Apart from these advantages, QDs have proven to be the leading tags or labels used in bio-imaging and other biological applications due to their excellent fluorescent properties which can be used in-vivo and in-vitro imaging (Pereira et al., 2019). Traditional QDs are inorganic, therefore toxic, and hydrophobic, as they are composed of group II and IV element. This hinders their application

as sensors/detectors for most medical applications (Karakoti et al 2015; Matos et al., 2019). Moreover, QDs may experience surface oxidation, photochemical degradation, and leaching of metal ions on long term exposure to cellular media. With the disadvantages mentioned above, the main challenge is the design of specific and hydrophilic QDs with suitable biocompatibility (Rana et al., 2019). Researchers have used two approaches to address these challenges of Cd-based QD whereby, (i) one or more biocompatible and long-lasting polymeric layers to encapsulate QDs and prevent a breakdown during in vivo analysis. (ii) Development of Cd-free QDs with performance comparable to or even better than existing Cd QDs.

Present challenges with QDs and solutions

Currently, there is an ongoing development of nano chemistry methods to design and fabricate Cd free QDs. Researchers have focused on fabricating QDs with tuneable emission colours and tested them in diagnosis to traceable drug delivery and for sensing of cancer biomarkers. With the recent developments of Cd-free QDs, the challenge now is to match the high brightness, narrow emission spectrum and high photoluminescence quantum yield (PLQY) of Cd-based QDs (Xu et al., 2016; Girma et al., 2017). To overcome this challenge, over the past years Cd free QDs have been prepared, including copper indium sulphide ($CuInS_2$), silver indium sulphide ($AgInS_2$), tin sulphide (SnS) and silver sulphide (Ag_2S). These share many of the advantageous properties of the Cd-based QDs with respect to their optical properties, colloidal stability, PL stability, and surface chemistry. Cd-free-based QDs are already used for biological applications (in-vivo and in-vitro). However, the review by Xu et al., 2016 highlighted that additional effort is required to improve the performance of Cd free QDs in biomedical applications and optimize their specific applications.

Tin sulphide (SnS) is an important chalcogenide that has emerged as a material of interest due to its abundancy and non-toxic nature to the environment. Sn-based QDs occurs in different phases

such as SnS, Sn_2S, Sn_2S_3, Sn_3S_4, Sn_4S_5. Among these, SnS monosulfide is a p-type semiconductor that has attracted considerable attention in the research field due to its direct band gap (1.3eV) and indirect band gap (1.09eV) (Wu et al., 2018). Furthermore, its absorption coefficient of $10^4 cm^{-1}$ and high conductivity allows the many possible applications which includes solar cells, batteries, and biomedical sensors. Despite these advantages, SnS-based QDs do not give high photoluminescence (PL) and therefore their luminescent colour purity and stability of these products needs to be improved (Díaz-Cruz et al., 2021). The most widely used method in addressing these issues is functionalizing the monolayers to the atoms and the surface of QDs using capping agents (Subramanian et al., 2020).

Capping agents have sparked interest as promising agents to reduce toxicity and improve the reactivity of QDs (Karakoti et al., 2015; Masab et al., 2018). They play an important role in the alteration of colloidal suspension of QDs, making them viable candidates for sensor development and drug delivery (Rajabi and Farsi, 2016). The presence of an S-H group in thiol capping agents aids in stabilizing and improving the surface functionality of QDs (Yadav & Chowdhury, 2021). Thiol capping agents also convert insoluble QDs to hydrophilic dots to improve the detection of cancer biomarkers.

HER-2 breast cancer biomarker.

Among the most widely known breast cancer biomarkers, human epidermal growth factor receptor-2 (HER-2) is an important biomarker that can be used for the detection and routine monitoring of breast cancer (Caselli et al., 2021). HER-2 contains three domains: extracellular domain (ECD), transmembrane domain, and an intracellular tyrosine kinase domain with similarities to the other epidermal growth factor receptors (EGFR) (Swain et al., 2022). Currently, the main detection methods for HER-2 biomarker are based on enzyme linked immunosorbent assay (ELISA) and biopsy. These methods are limited by long term assay times, high cost and low

sensitivity (Shamshirian et al., 2020).. Electrochemical sensors address these limitations due to their significant properties which includes high specificity, sensitivity, selectivity, low cost, and fast response (Campuzano et al., 2021). Electrochemical sensors are very important because they convert biological samples into electrical signal that easily process information.

1.2. Statement of research problem

Quantum dots (QDs) have drawn much interest due to their application in biological and medical fields. Besides being the best simple sensors, they have proven to be unique fluorescent labels due to their exceptional fluorescence properties. The development of methods to solubilize QDs and attach them with biological molecules has gained remarkable growth and use in the biomedical field. They play a vital role in diagnosing and detecting diseases (Bilan et al., 2015). Although QDs have these exceptional advantages, they have received much criticism due to the toxicity of binary QDs. This is because traditional QDs are made up of toxic heavy metals such as Pb and Cd (Kays et al., 2020), reducing their bio-applications. Moreover, their synthesis methods use high volumes of organic solvents, high temperature and time time-consuming which contributes to them being considered non-environmentally friendly. Thiol capping agents have proven to be the most preferred because they possess molecules with strong binding energy, consequently forming a dense layer on the surface of the particle resulting in the enhancement of the stability of the QDs (Subramanian et al., 2020). Currently HER-2 biomarker is detected via ELISA and biopsy methods. These methods are costly and are not reliable. Therefore, this study will focus on the synthesis of thiol capped quantum dots for the fabrication of a facile sensors for sensing human epidermal growth receptor factor. These QDs will be less toxic and have increased solubility.

1.3. Aims and Objectives.

This study aims to design a suitable method for the synthesis of thiol capped SnS QDs for the development of a facile sensor to detect human epidermal growth factor receptor.

Specific objectives of the study are to:

1. Synthesize SnS-based QDs.
2. Functionalizationalize QDs using different thiol capping agents.
3. Optimize and spectroscopically characterize the as-synthesized SnS QD using various spectrochemical, optical and structural based techniques.
4. Fabricate an electrochemical based sensor using thiol based QDs.
5. Apply the fabricated thiol-capped QDs as asensor platform for the detection of Human epidermal growth factor receptor (HER-2).

1.4. Hypothesis

In this study, only cadmium free SnS based QDs will be synthesized using a facile and eco-friendly method. The QDs will be bio-functionalized with different thiol moieties. This is expected to enhance the optical properties of the QDs, which will be used in the development of an electrochemical sensor.

1.5. Expected outcomes of the study.

1. This study will generate new knowledge on the synthesis of Cd-free QDs.
2. Gain new knowledge of tin-based quantum dots in the sensor applications.
3. Better understanding of the Spectro-chemical and electrochemical properties of the synthesized QDs.
4. Publication of research articles and a thesis for academic qualification is envisaged.

1.6. Delimitations and ethics.

The study will only focus on the synthesis of SnS and SnS/ZnS thiol-based quantum dots. Sensing of Human Epidermal growth factor receptor will only be via electrochemistry. No ethical application will be required for this study.

1.7. Research structure

The current chapter includes an introductory overview of the research theme, the aims and objectives, the research approach and structure of the study. The succeeding chapters will be as follows:

Chapter 2: Literature Review

A detailed review of QDs, their potential as sensors is highlighted and the influence of capping agents on QDs is discussed. The chapter reviews the theoretical background of human epidermal growth factor receptor (HER-2) and the various detection methods used to detect HER-2. This is followed by in-depth description of various sensors being used in the detection of HER-2.

Chapter 3: Synthesis, optimization, and characterization of SnS quantum dots.

Chapter 3 involves the synthesis and characterization of the SnS-based QDs. It concentrates on the general experimental procedures for the synthesis of SnS QDs and the optimization of various parameters that affect the quality of the SnS QDs. The optical properties of the QDs will be evaluated by photoluminescence(PL), ultra-violet spectroscopy (UV-vis), Fourier transform infrared spectroscopy (FTIR) and energy dispersive spectroscopy (EDX). The morphological characterization will be done using transmission electron microscopy (TEM), scanning electron microscopy (SEM), and dynamic light scattering (DLS).

Chapter 4: Fabrication of electrochemical biosensor

Focuses on the electrochemical characterization of the as-synthesized thiol-capped QDs. Optimization of the sensor fabrication will be analyzed by looking at various parameters. This

chapter also examines the application of the fabricated biosensor based on thiol-capped QDs for detecting HER-2.

Chapter 5: General Discussion, Recommendations and Conclusion.

The study is concluded with a concise discussion of the most significant points from all the preceding chapters. Finally, directions for future work are suggested.

1.8. References.

Bilan, R., Fleury, F., Nabiev, I. and Sukhanova, A., 2015. Quantum Dot Surface Chemistry and Functionalization for Cell Targeting and Imaging. *Bioconjugate Chemistry*, 26(4):609-624.

Caselli, E. *et al.* (2021) 'Looking for more reliable biomarkers in breast cancer: Comparison between routine methods and RT-qPCR', *PLOS ONE*, 16(9). doi:10.1371/journal.pone.0255580.

Campuzano, S., Pedrero, M., Yáñez-Sedeño, P. and Pingarrón, J.M. (2021). New challenges in point of care electrochemical detection of clinical biomarkers. *Sensors and Actuators B: Chemical*, 345:130349. doi: 10.1016/j.snb.2021.130349.

Díaz-Cruz, E.B., Regalado-Pérez, E., Santos, J. and Hu, H., 2021. Development of SnS/PVP core/shell quantum dots with tunable color emission synthesized by microwave heating. *Journal of Solid State Chemistry*, 300:122264.

Girma, W., Fahmi, M., Permadi, A., Abate, M. and Chang, J., 2017. Synthetic strategies and biomedical applications of I–III–VI ternary quantum dots. *Journal of Materials Chemistry B*, 5(31):6193-6216.

Karakoti, A., Shukla, R., Shanker, R. and Singh, S., 2015. Surface functionalization of quantum dots for biological applications. *Advances in Colloid and Interface Science*, 215:28-45.

Kays, J.C., Saeboe, A.M., Toufanian, R., Kurant, D.E. and Dennis, A.M., 2020. Shell-free copper indium sulfide quantum dots induce toxicity in vitro and in vivo. *Nano letters*, 20(3):1980-1991.

Lu, S**.,** Li, G., Lv, Z., Qiu, N., Kong, W., Gong, P., Chen, G., Xia, L., Guo, X., You, J. and Wu, Y., 2016. Facile and ultrasensitive fluorescence sensor platform for tumor invasive biomaker β-glucuronidase detection and inhibitor evaluation with carbon quantum dots based on inner-filter effect. *Biosensors and Bioelectronics*, 85:358-362.

Masab, M., Muhammad, H., Shah, F., Yasir, M. and Hanif, M., 2018. Facile synthesis of CdZnS QDs: Effects of different capping agents on the photoluminescence properties. *Materials Science in Semiconductor Processing*, 81:113-117.

Matos, B., Martins, M., Samamed, A., Sousa, D., Ferreira, I. and Diniz, M., 2019. Toxicity Evaluation of Quantum Dots (ZnS and CdS) Singly and Combined in Zebrafish (Danio rerio). *International Journal of Environmental Research and Public Health*, 17(1):232.

Pereira, G., Monteiro, C., Albuquerque, G., Pereira, M., Cabrera, M., Cabral, P., Pereira, G., Fontes, A. and Santos, B., 2019. (Bio) conjugation Strategies Applied to Fluorescent Semiconductor Quantum Dots. *Journal of the Brazilian Chemical Society*.

Rajabi, H. and Farsi, M., 2016. Study of capping agent effect on the structural, optical, and photocatalytic properties of zinc sulfide quantum dots. *Materials Science in Semiconductor Processing*, 48:14-22.

Rana, M. and Chowdhury, P., 2019. L-glutathione capped CdSeS/ZnS quantum dot sensor for the detection of environmentally hazardous metal ions. *Journal of Luminescence*, 206:105-112.

Shamshirian, A. *et al.* (2020). Diagnostic value of serum HER2 levels in breast cancer: A systematic review and meta-analysis', *BMC Cancer*, 20(1). doi:10.1186/s12885-020-07545-2.

Subramanian, S., Ganapathy, S., Rajaram, M. and Ayyaswamy, A., 2020. Tuning the optical properties of colloidal Quantum Dots using thiol group capping agents and its comparison. *Materials Chemistry and Physics*, 249:123127.

Wu, H., Zhou, L., Yan, S., Song, H. and Shi, Y. (2018). Solution synthesis of stannous sulfide and stannic disulfide quantum dots for their optical and electronic properties. *Optics Communications*, 406:239–243. doi: 10.1016/j.optcom.2016.11.060.

Xu, G., Zeng, S., Zhang, B., Swihart, M., Yong, K. and Prasad, P., 2016. New Generation Cadmium-Free Quantum Dots for Biophotonics and Nanomedicine. *Chemical Reviews*, 116(19):12234-12327.

Yadav, P. and Chowdhury, P., 2022. Optical efficiency of CdTe QDs for metal ion sensing in the presence of different thiol-based capping agents. *Chemical Papers*:1-18.

Yadav, H. and Raizaday, A., 2016. Inorganic nanobiomaterials for medical imaging. *Nanobiomaterials in Medical Imaging*:365-401.

CHAPTER 2

LITERATURE REVIEW

This chapter attempts to give an overview of various aspects linked to human epidermal growth factor receptor (HER-2) and various strategies used to detect HER-2. The background of quantum dots (QDs) and the mechanism related to synthesizing QDs and their applications as supporting labels in sensors will also be discussed. This chapter also briefly introduces thiol capping agents and their influence on QDs. The potential use of QDs in fabricating sensors will also be highlighted. Different sensors will be outlined according to their sensing mechanisms and their applications will be discussed.

2.1. Introduction

Cancer is a complex and highly heterogeneous disease caused by an uncontrollable growth of cells (figure 2.1). It is the second deadliest disease worldwide; global demographic characteristic predicts an increase in cancer incidences in the following decades, with > 20 million new cancer cases annually expected by 2025 (Zugazagoitia et al., 2016). For the past decade, breast cancer has been the subject of intense scientific research due to its widespread occurrence and reoccurrence after treatment, high morbidity, and high mortality rate (Roointan et al., 2019). Late stages of breast cancer detection often lack effective treatment. Survival rates increase when breast cancer is identified at early stages. Therefore, detecting cancerous tumours at the earliest possible stage is essential (Milosevic et al., 2018). Currently, oncological imaging and biopsy-cytology of specimens are the most used techniques to detect breast cancer. These methods have drawbacks as they require trained personnel and are tedious and expensive. Therefore, the need for less expensive and feasible breast cancer detection strategies is increasing (Hasan et al., 2021). Thanks, to cancer biomarkers that have enabled early detection of breast cancer. Biomarkers are specific molecules that can distinguish between normal and cancerous conditions. A specific biomarker

indicates the presence of cancer in the body; for example, when the body or cancerous tumour secretes biomarker molecules, this indicates the presence of cancer. Biomarkers are also used to evaluate the body's response to a specific treatment for a disease. Early detection of cancer biomarkers increases the chances of early diagnosis and can be used to predict the risk of developing cancer (Ye et al., 2018).

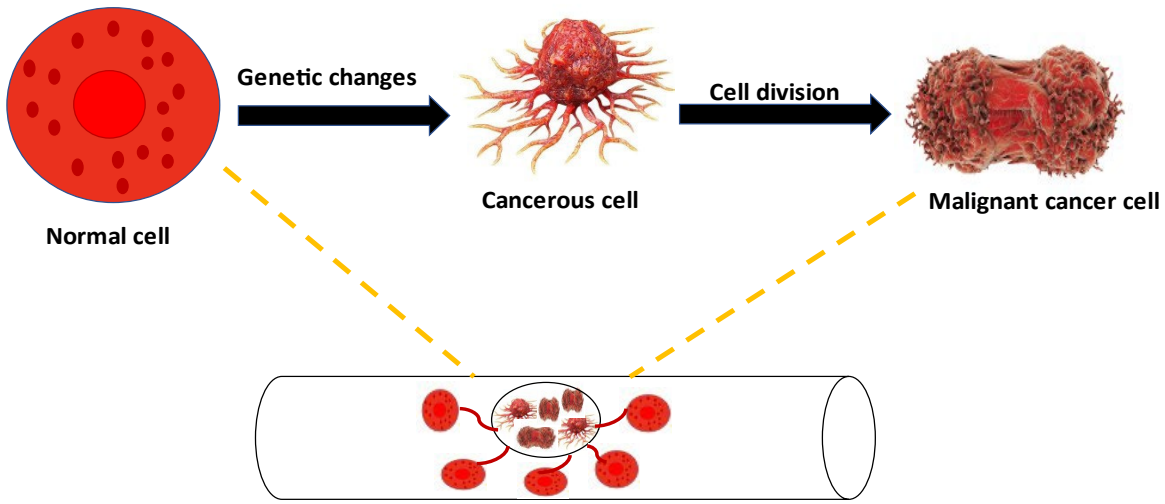

Figure 2.1 The process of cancer cell development.

Currently, various breast cancer biomarkers such as antigen (CA 15-3), mucin 1 (MUCIN), breast cancer type 2 and human epidermal growth factor receptor 2 (HER-2) are utilized in breast cancer management and diagnosis (Seale & Tkaczuk., 2022). Of these biomarkers, HER-2 has been constructed as the most notably tissue marker, whose characterization is now essential for all breast cancers. The overexpression of this biomarker is key in targeting specific immunotherapies for breast cancer diagnosis (Pacheo et al.,2018).

2.2.1. Human epidermal growth factor receptor (HER)

The human epidermal growth factor receptor (HER) is a transmembrane tyrosine kinase factor receptor. This protein is encoded with HER-2 gene and is located on the long arm of a chromosome. It forms part of the epidermal growth receptor family. HER family members share the same structure (figure 2.2), composed of an extracellular domain (ECD), a transmembrane segment, and an intracellular region. The ECD domain is divided into four parts: Domains I and III play a role in ligand binding, and domains II and IV have several residues essential for disulfide bond formation. The transmembrane further consists of 19-25 amino acids residues, as displayed in Figure 2.2 (Furrer et al., 2018).

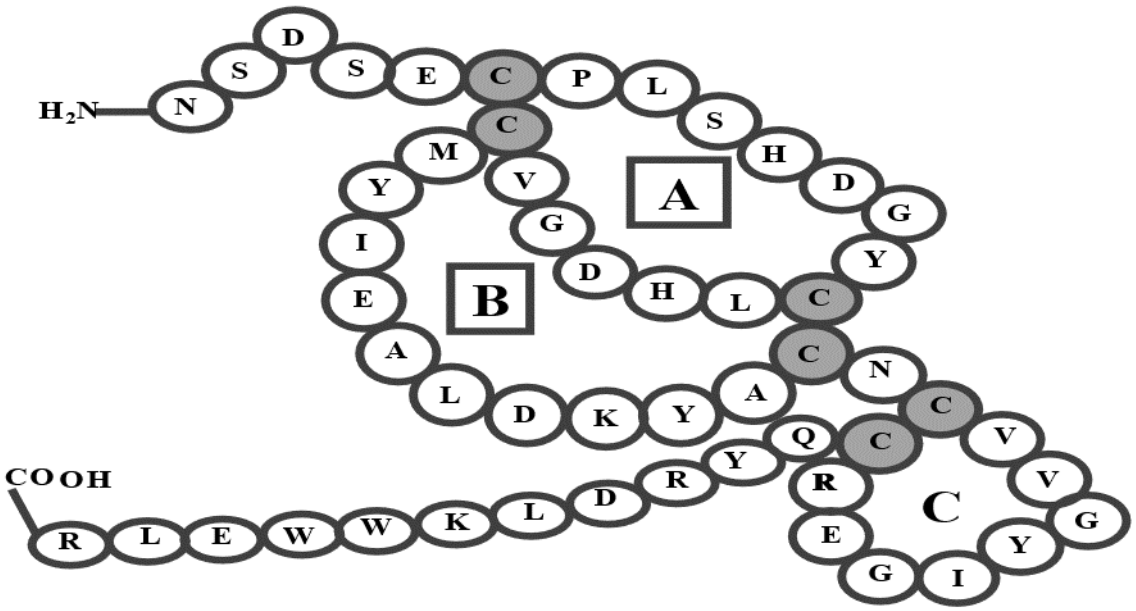

Figure 2.2 Gene structure of HER with the four domains.

Breast cancer can show up to 20-50 copies of HER-2 gene and about 40-400-fold of HER-2 protein, leading to 2 million receptors expressed at the tumour cell's surface (Lah et al., 2019). HER-2 is expressed in many tissues at about 25-25% in breast cancer amplification. HER-2 concentration ranges from 0 to 15 mol/mL^{-1} in healthy women and values above this are considered

overexpressed (Bezerra et al., 2019). HER-2 protein overexpression affects about 1 in 5 women with breast cancer. This type of cancer grows and spreads faster than any other breast cancer. The treatment of this cancer includes surgery and radiation followed by chemotherapy when a combined treatment approach is used. Although these approaches reduce cancer progression, they cause excessive damage to non-cancerous cells due to inherent cytotoxicity in cancer treatment strategies. ECD can be cleaved by Metalloproteases and released in the bloodstream. Consequently, HER-2 can be measured in serum, which is essential for developing quantitative analytical strategies for breast cancer detection (Freitas et al., 2020).

Methods for the evaluation of HER-2 status in breast cancer specimen

Several strategies have been established to evaluate HER-2 status in breast cancer specimens at protein, DNA, and RNA levels. Currently, enzyme-linked immunosorbent assay (ELISA), immunohistochemistry (IHC), and fluorescence *in situ* hybridization (FISH) are the main types of biomarker-based tests accepted for the detection of the overexpression of HER-2 in clinical practice. Figure 2.3 shows various techniques for HER-2 biomarker evaluation.

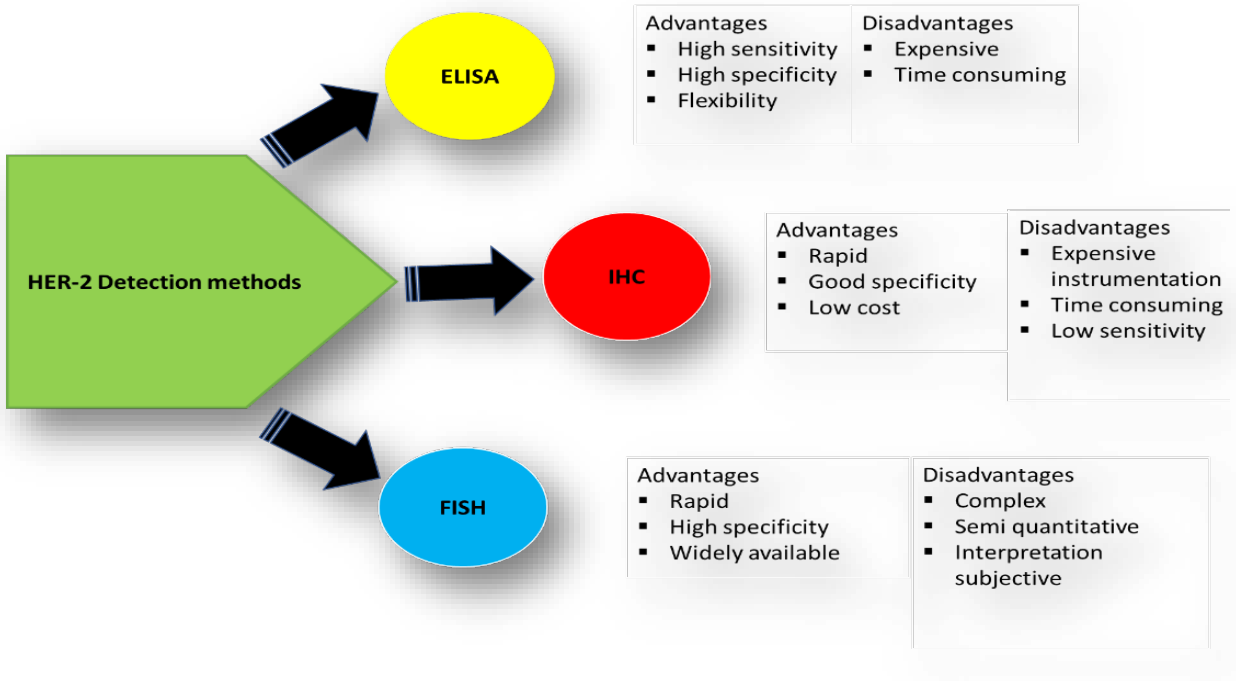

Figure 2.3 Advantages and disadvantages of the currently used biomarker detection methods for HER-2.

Although these methods are sufficient for detecting breast cancer tumours, research shows that breast cancer is still widening significantly in developing countries due to the requirement of highly skilled personnel, complex operations, expensive instrumentation, and long-term analysis (Mostafa et al.,2022). Therefore, developing highly innovative, rapid, affordable, and feasible diagnosis techniques that can measure HER-2 at lower concentrations for clinical diagnosis is urgently needed.

2.2.2. Sensors

A sensor is an analytical device or probe that converts a biological element (i.e., enzyme or antibody) with an electronic device to generate a measurable signal. The electronic component gives information regarding physiological change or the presence of chemical or biological materials in the environment by transmitting, detecting, and recording data (Figure 2.2). Clark and Lyon inverted the first sensor in 1962. Clark and Lyon used electrochemical detection of oxygen and glucose to sense glucose in biological systems. Since then, novel progress has been made in

technology and application of biosensors with different approaches involving electrochemistry, nanotechnology to bioelectronics. Label-based and label-free detections are the two technical strategies used in sensors.

The label-based approach depends on the specific properties of the label compound to target detection. The main disadvantage of label-based detection is that it often requires a combination of specific sensing elements fabricated with an immobilized target protein. On the other hand, the label-free approach allows for the detection of the target molecules that are not labelled or not difficult to tag. Recent biotechnology applications with bioengineering, electrical, and electronics engineering facilitated ways to develop sensors for various detection methods in medical and environmental science applications (Vigneshvar et al.,2016).

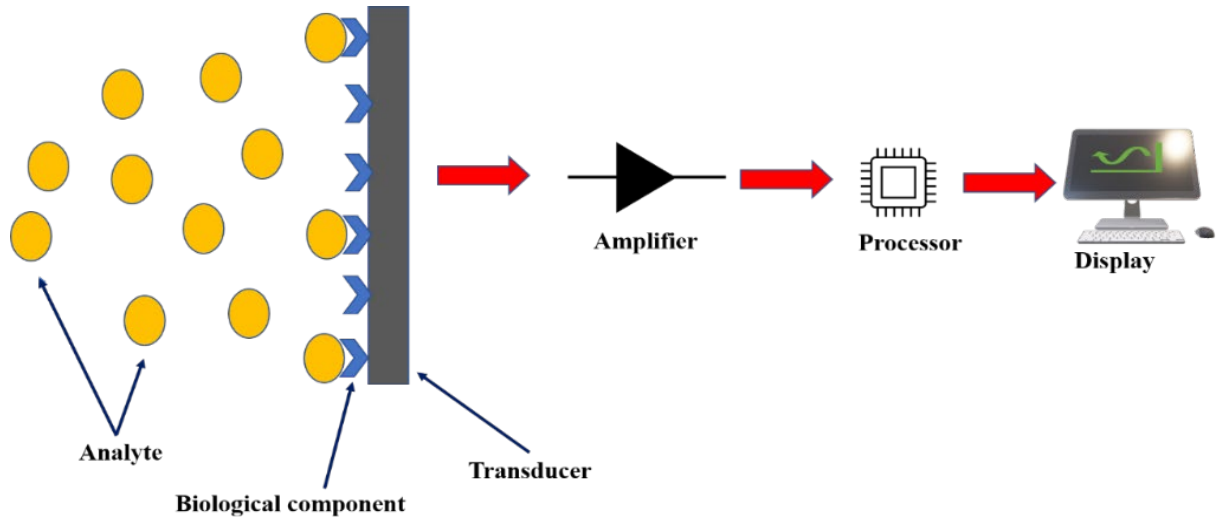

Figure 2.4 Components of a biosensor

Classification of biosensors

Sensors are categorized based on their biological receptors or on the technology used for the transducer. Diagram 1 illustrates different types of biosensors based on signal transduction and

biorecognition element. In most sensors the transducer is attained electrochemically, optically, and mechanically.

Diagram 1. Classification of biosensors/sensors based on transducer systems.

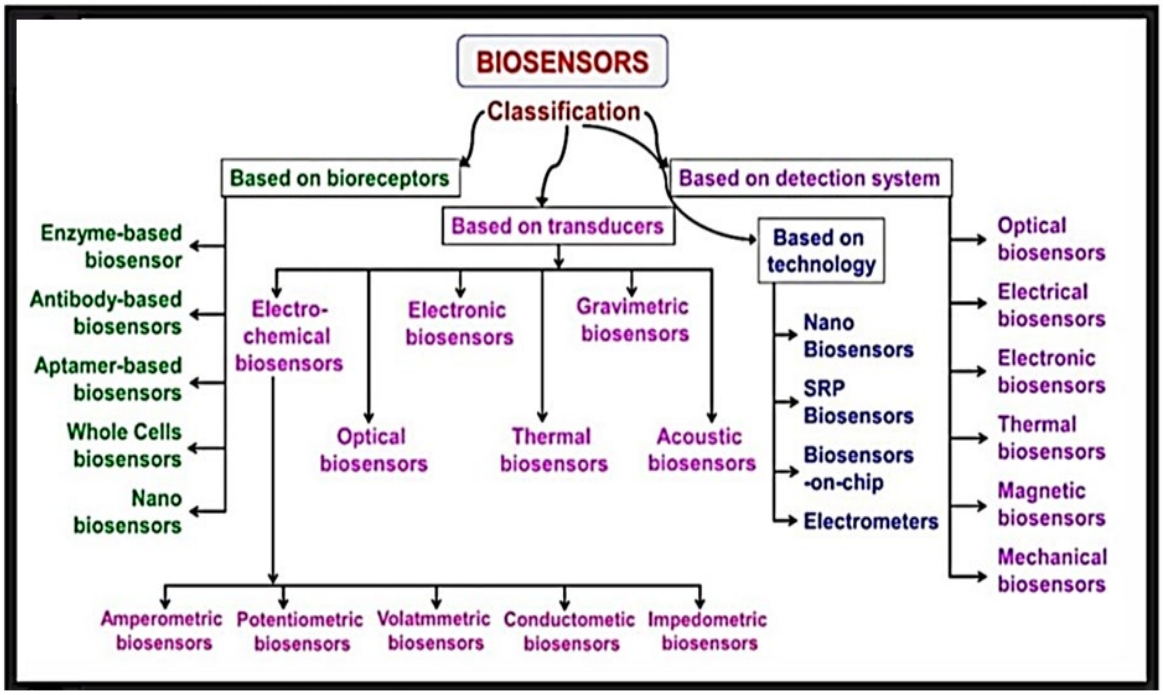

Optical sensors

Optical sensors involve measuring the change in optical properties such as absorption, reflectance, emission or interferometric in the presence of the analyte (Peltomaa et al., 2018). These sensors are based on light scattering of the biorecognition element to study bound antigen-antibody properties. Optical sensors provide a signal proportional to the analyte concentration and interpret the capture in a measurable change in light or refractive index, resonance, intensity, and wavelength (Damborský et al., 2016).

Mechanical sensors

Mechanical biosensors involve changes in mechano-physical properties such as forces, motion, masses etc which are quantified after the biomolecular interaction. Mechanical biosensors are classified into three categories i.e., quartz microblade, surface acoustic wave and nano-mechanical systems. Mechanical biosensors consist of cantilever probe, a mechanical transducer, and a processor. The function of the cantilever probe is to detect the analyte where its performance is a function of its size or shape and proportional to the mass of the cantilever probe (Purohit et al., 2020).

Electrochemical sensors

Electrochemical sensors convert electrochemical data into an analytical signal, either quantitative- or semi-quantitatively, using a biomarker strategy involving an electrochemical transducer (i.e., an electrode). Electrochemical sensors measure signals based on the change in current, potential, conductance, or field effect transducer due to the interaction of the analyte with the biomarker on the sensing surface. Electrochemical sensors play a vital role in point-of-care (POC) systems due to their high specificity, reproducibility, accuracy, and fast miniaturization response (Yoon et al., 2020). These sensors offer low-cost instrumentations, facile methods, portability, and convenient operation. There are five electrochemical sensors i.e. conductive, potentiometric, voltametric, impedimetric and amperometric (Kajal et al., 2022). The conversion of a biochemical reaction into an electric signal can be obtained by Cyclic voltammetry (CV), Differential Pulse Voltammetry (DPV), Square Wave Voltammetry (SWV), and Electrochemical Impedance Spectroscopy (EIS), which are essential for the development of electrochemical sensor. These sensors utilize nanostructured labels at the surface, such as nanoparticles, quantum dots, enzymes, and magnetic beads, which offer high signal biomarker detection (Sinha et al., 2019).

Electrochemical detection of HER-2

Due to their high sensitivity, and fast response with low detection limits (LOD), it is no surprise that electrochemical biosensors are the most preferred for the detection of HER-2 biomarker. Various electrochemical sensors based on QDs (Wahab et al.,2023) have been employed to detect HER-2 biomarker. For example, a highly sensitive QDs-based genosensor was developed with gallium telluride QDs and amine-terminated probe. The sensor was characterized using cyclic voltammetry and electrochemical impendence spectroscopy (Fuku et al., 2015). Lah et al.,2019 constructed an electrochemical sandwich immunosensor based on lead sulfide QDs conjugated with secondary HER-2 antibody to detect HER-2 biomarker. Square wave voltammetry was employed to characterize the developed sensor. The constructed sensor showed a linear concentration of 1 to 100 ng/L, with limit of detection of 0.28 ng/L. An electrochemical magnetic immunosensor was fully fabricated and successfully applied for detecting HER-2 biomarkers in human serum with an assay time of 90min, with a limit of detection of 0. 29ng.mL^{-1} and a linear range between 0.50 to 50ng.mL^{-1}(Freitas et al.,2020). In another study, impedimetric biosensors based on carbon-based graphene QDs and porphyrin framework were designed and investigated towards detecting HER-2. The obtained immunosensor showed good reproducibility and stability (Centane & Nyokong, 2021). The detection of HER-2 biomarker was possible by the development of a precise sandwich immunoassay based on a novel platinum doped cadmium telluride QDs labelled antibody as a probe. The results revealed that the fabricated sensor can be applied in early detection of HER-2 breast cancer biomarker (Ehzari & Safari,2022).

2.2.3. Quantum Dots

Quantum dots (QDs) are referend to as small nanocrystals 2-10 nm in dimension and are composed of groups II–VI, III–V or IV elements. They have been used in the electrochemical sensing of cancer biomarkers due to their surface-to-volume ratio, electrocatalytic activity, electron transport

properties, minimal toxicity, biocompatibility, and water solubility. QDs are made up of a variable number of electrons that occupy a well-defined discrete quantum state and have electronic properties intermediate between a solid and a molecule (Reshma & Mohanan, 2019). Their size and composition are responsible for their unique properties that enable their application in the biomedical field (i.e., medical probes, diagnostics, and sensing of cancer biomarkers) (Wagner et al., 2019). Quantum dots (QD) offer promising opportunities for detecting developing cancer biomarkers and monitoring cancer growth and diagnosis. Their unique optoelectrical properties allow high-quality cancer therapy bioimaging and targeted drug delivery.

Properties of QDs

The structure of QDs consists of a semiconductor core, which is responsible for fundamental optical and semiconducting properties. The inorganic core is made up of surfactants which form atoms on the surface of the core. However, some of the atoms formed are not bound to the surface and are commonly referred to as bare atoms. The coordinating bare atoms on the surface have "dangling bonds" which form traps on the surface, where the electron can get stuck on the hole, quenching the photoluminescence (PL) and decreasing the PL quantum yield due to energy loss (Reshma & Mohanan, 2019). To overcome this challenge, the core is overcoated with an inorganic shell material with a wider bandgap to obtain core-shell QDs structure with improved photoluminescence efficiency compared to their initially uncapped counterparts. The enhancement fluorescence of the QD after shell overcoating is due to increased confinement of the electron and hole pair in the core and the dangling bonds on the surface of the QDs (Vasudevan et al., 2015). Encapsulating the core-shell QD with a capping agent improves solubility in an aqueous buffer solution (figure 2.5).

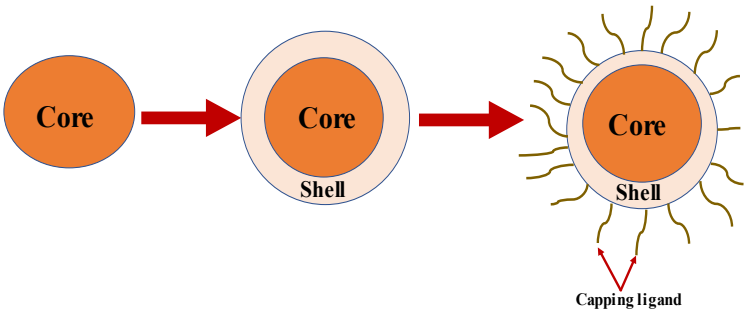

Figure 2.5 Core-shell structure of a capped QD.

In these nanocrystals, the atomic species' highest occupied molecular orbitals (HOMO) interact with each other to form the valance band of the nanocrystal. Similarly, the lowest unoccupied molecular orbitals (LUMO) combine to form the conduction band of the nanocrystal. Since the excitons are confined in all three spatial dimensions, the electrons are quantized to specific energies like those of small molecules. The energy between the valence band and conduction band results in the band gap energy of the nanoparticle (figure 2.6). The bandgap is inversely proportional to the size of a QD, as more and more atoms are bound together, the discrete energy levels combine into energy bands. For most QDs, a decrease in particle size results in a split in the band energy distribution, therefore, higher bandgap energy (Zhao et al., 2017). This phenomenon is called quantum confinement; hence semiconductor nanocrystals are referred to as QDs. Quantum confinement effect is evident in their size-tuneable optical properties. When a semiconductor absorbs energy, electrons are promoted to the conduction band or leaving a positive hole in the valence band as a results electron holes pairs are generated. Since the hole forms a positive charge and the electron forms a negative charge, both the electrons and the hole form strong coulomb attraction causing them to remain relatively localized within a nanometre-sized crystal. This entails that due to the smaller size of the QDs, the electron-hole pair is confined and is smaller than the Bohr radius of the semiconductor. Hence when smaller nanocrystals are formed more energy is needed to confine the exciton and the energy of the emitted photons increases. Therefore, larger nanocrystals absorb and emit in the red region while smaller nanocrystals absorb

and emit in the bluer region. Fluorescence occurs when an excited electron returns to ground state. Therefore, excitation and emission can be easily controlled by changing the diameter and structure of a QD, resulting in broad absorption spectra with narrow, symmetric, and tuneable emission spectra (Zhang, n.d.). Another property of QDs is their large stokes shift (difference between peak absorption and emission wavelength). Large stokes shift reduces autofluorescence, increasing sensitivity and making fluorescent detection possible even at low signal intensity.

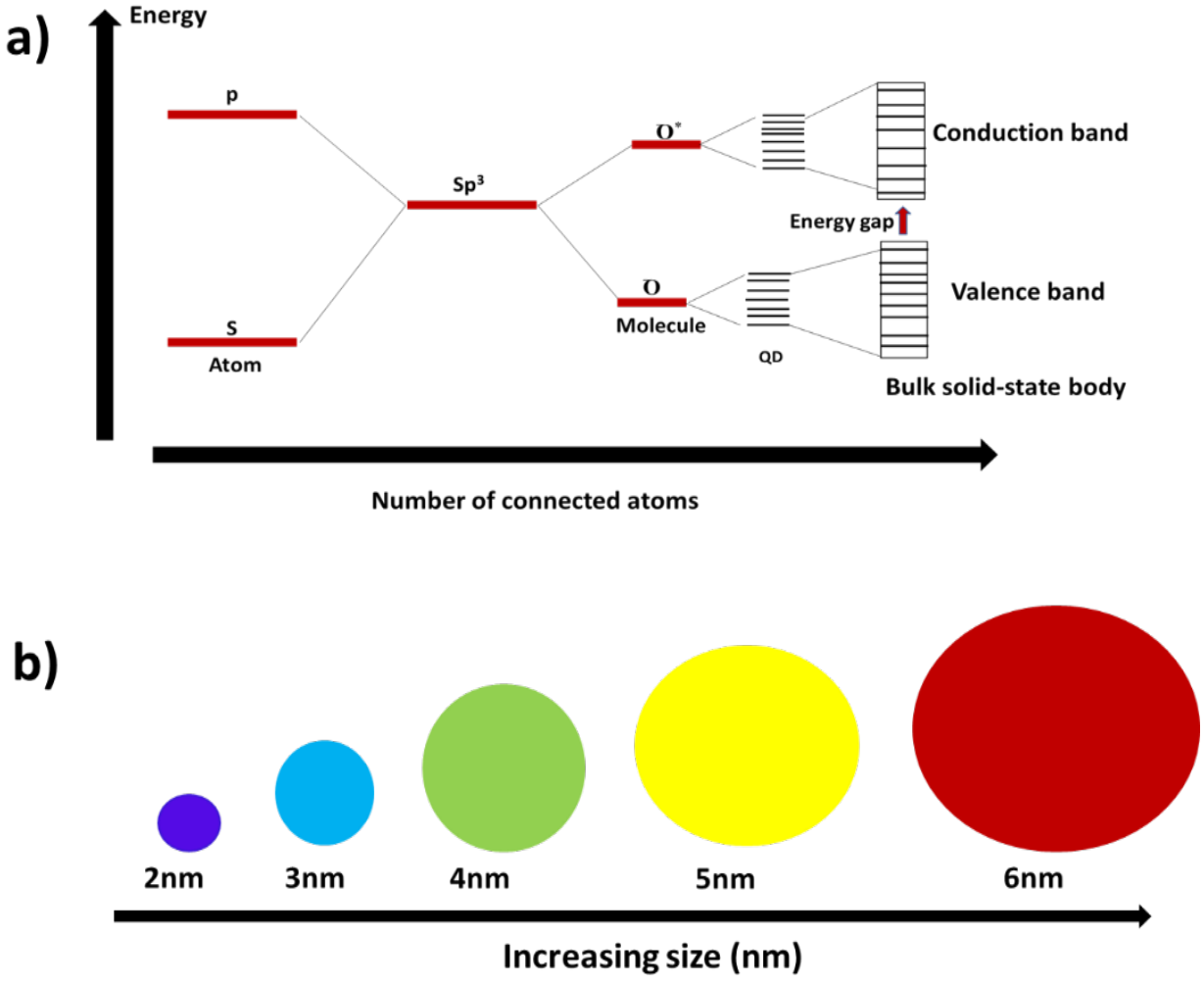

Figure 2.6 a) Electron energy levels depend on the number of bound atoms. b) Particle size dependent of QDs.

Synthesis of Quantum dots

Since QDs were invented, exceptional efforts have been devoted to developing reliable and controllable synthesis methods for the fabrication of high-quality QDs with excellent optoelectronic properties for various applications. In the past decade, the synthetic methodologies for QDs have progressed substantially, and numerous synthetic approaches have been developed to manufacture QDs. The synthesis of QDs involves a sequential process. There are two primary mechanisms by which they grow. Either via coalescence or Ostwald ripening process. Coalescent involves the combination of small masses to form a larger mass, while Ostwald ripening involves the dissolving and redepositing of particles. In the latter, QDs growth is governed by the first step called nucleation (whereby the reaction mixture is heated up to the required temperature and the precursors are changed to monomers) and growth (conversion of monomers into nanocrystals whose continuous growth depends on the surface of the molecules) (Yadav et al., 2020).

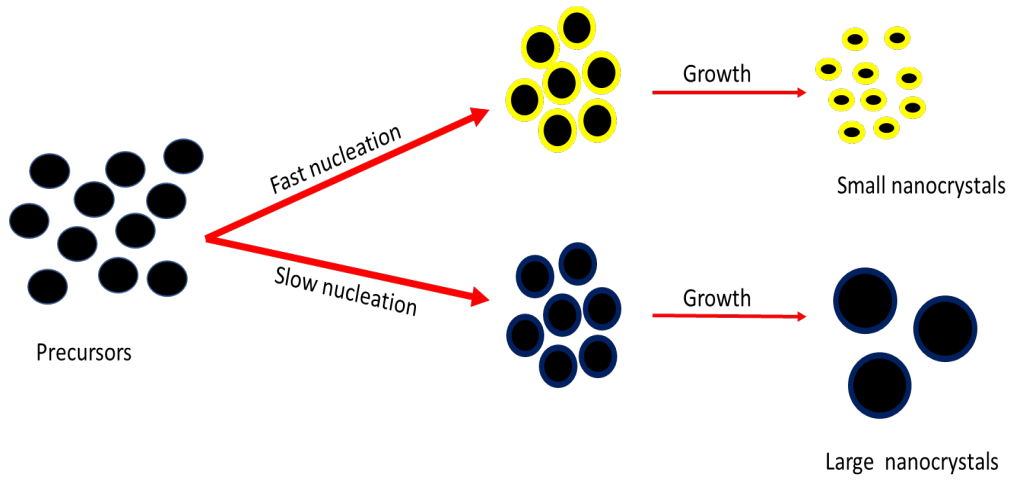

Figure 2.5 Schematic representation of the fast nucleation and slow nucleation and growth of the nanocrystals.

There are generally four major methods (hot injection, hydrothermal, organometallic, and non-injection) used in the synthesis of QDs. The synthesis of SnS-based QDs has focused on hydrothermal, non- hot injection (heat up), and injection methods. The hydrothermal method involves the formation of nanoparticles in an aqueous solution as a reaction system in a unique closed reaction vessel. For example, Modi et al., 2022 synthesized SnS nanoparticles using hydrothermal method. The group used tin dichloride dihydrate, thiourea precursors and distilled water at temperature of 180^0C in an autoclave. Non-injection method involves steadily heating the precursors in the presence of a ligand (Sinatra et al.,2017). Cheng et al., 2020 introduced the non-injection method for synthesizing SnS QDs. The reported improved PL intensities using cysteamine capping agent and ZnS shell at 70^{o}C temperatures. Later, Miranti et al.,2022 synthesized SnS QDs using the hot injection method, which involves the rapid addition of precursors directly to heated solvent with additives. Anhydrous tin chloride was used as Sn precursor, while thioacetamide, oleylamine, oleic acid, trioctylphosphine, octadecene were used as solvents.

Quantum dots as labels in sensors

The outstanding properties of QDs which include, long-term stability, high intensity, and the ability to detect many analytes simultaneously, make them attractive fluorophores that can be used in sensing applications (Schiffman et al., 2018). In sensors, signal detection is based on the registration of the change in one of the sensing material's physical properties (optical, mechanical, magnetic, thermal, electrical) due to the interaction of the analyte (Naresh & Lee, 2021). The optical properties of QDs such as emission, polarization, and emission kinetics, can be tuned and directly used in sensors. The obtained changes can be recorded by human senses or indirectly via signal transformation, amplification, and visualization (Lesiak et al., 2019). All these factors determine the fabrication of sensors and their mechanism in action in detecting various substances

(Lesiak et al., 2019). Table 2 shows various electrochemical detection methods based on QDs for sensing applications.

The human body consists of several organic molecules that naturally absorb and emit light in the near-infrared and visible region (DNA, Proteins, and Collagen) (Reineck & Gibson, 2016). Most conventional organic dyes do not absorb at near-infrared (NIR) emission wavelength (>650nm): this region is critical in biomedical applications due to its reduced light scattering and low tissue absorption (Chang et al.,2019). Therefore, QDs have gained interest due to their optical properties that can be tuned toward NIR. QDs can be used as fluorescence probes for sensing and imaging since they can absorb in the near-infrared region (Matea et al., 2017).

Table 2.1 various electrochemical detection methods sing QDs as sensors

Electroanalytical technique	Bioreceptor	Sensing platform	LOD	Reference
ASV	Antibody	GCE/CdSe/ZnS	2.1 ng/mL	(Freitas et al., 2020)
CV	Antibody	Au PDA/CuZnInS	0.0043nmoL/L^{-1}	(Liu et al., 2018)
ASV	Antibody	SPCE/PbS	0.28ng/L^{-1}	(Lah et al., 2019)
EIS	Antibody	GCE/Sulfur/Nitrogen doped Graphine	0.00141ng/mL	(Centane and Nyokong, 2021)
DPASV	Antibody	SPCE/CdSe/ZnS	0.29ng/mL^{-1}	(Freitas et al., 2020)

*(see glossary for abbreviations)

Quantum Dots limitations

Despite an exceptional promise in sensing applications, an increase in the production of QDs has raised significant health and safety concerns due to the presence of heavy metals such as Cadmium (Cd), Mercury (Hg) and Lead (Pb) (Wang & Tang, 2021). Factors such as their core and core-shell composition, size, and surface chemistry contribute to their toxicity (Gidwani et al., 2021, Zhu et al.,2019). Many strategies have been established to decrease the potential toxicity of QDs such as using Cd-free QDs and introducing ZnS shell on the core, which can slow down the degradation by reducing the transportation of oxygen to the core surface (Mo et al.,2017). In electrochemical applications, QDs may face instability due to their sensitivity in different environmental conditions leading to fluctuations in sensor response and reproducibility. Furthermore, their complex synthetic methods may cause variations in size, shape, and surface properties which may directly impact the performance of the sensor. Moreover, QDs are prone to aggregation which can influence the charge transfer kinetics, hindering the electron transfer processes and compromising the overall electrochemical response of the sensor (Karadurmus et al.,2021). However, for SnS QDs, problems such as low quantum efficiency, low photoluminescence intensity, and poor structural stability still occur (Díaz-Cruz et al.,2021, Gandhimathi et al.,2019, Cheraghizade et al.,2017). SnS QDs also exhibit high solubility in aqueous media for biological applications and dissolve under neutral and basic media. These concerns are significant because they prevent the potential use of SnS QDs in sensing of biomarker applications (Han et al.,2017).

Surface functionalization of QDs

Surface functionalization with capping agents increases the sensitivity, selectivity, and detection efficiency owing to the QD's change in the surface chemistry. A capping ligand is an amphiphilic molecule that consists of a polar head group and non-polar hydrocarbons. Capping ligands act as stabilizers to control QDs from agglomeration and achieve desired nano size. Capping ligands also

reduce the toxicity of QDs by controlling the particle size of a QD, making them hydrophobic and increasing their quantum yield (figure 2.5) (Subramanian et al., 2020). The amphiphilic head confers functionality and enhances compatibility with another phase. During the synthesis of QDs, capping and reducing agents are introduced into the reaction vessel separately. The non-polar group interacts with the surrounding medium, while the polar group interacts with the metal atom of the nano system (Javed et al., 2020).

2.2.4. Thiol capping agents.

Thiol capping agents are amphiphilic molecules that contain a carboxyl group(-COOH) and a thiol (-SH) which helps to bind the surface of the QD very strongly. Thiol capping agents are the most preferred to stabilize nanocrystals due to the strong affinity of the thiol group to the soft metal surface sites that can be employed to introduce a dangling chemical functionality and proximity to the colloidal QDs (Sahm et al., 2022). The formation of thiol-capped QDs involves the reaction between the metal ion and the chalcogenide precursors in a solution. Introducing a thiol capping agent in the reaction results in short-chained thiol molecules forming metal thiolate complexes. These complexes are further consumed to build crystalline thiol-capped QDs. The two terminals affect nucleation and growth during the synthesis of QDs which enhances the photoluminescence properties of QDs. At the energy level, thiol capping agents prevent surface hole trapping which results in high QY without the need to add a coating shell or prolong the process during the synthesis of QDs.

Thiols forms an antioxidant in the human body and are very important in defence against reactive oxygen species (Yadav & Chowdhury, 2021).The electrochemical properties of QDs are significantly impacted by thiol capping agents. These agents are often employed to passivate the surface of QDs providing stability,controlled size, and influencing their electronic structure (Nurerk et al., 2016). The strong interactions between thiols and the QDs surface facilitates

enhanced charge transfare processes enabling effective charge transfer and improving the overall response of an electrochemical sensor (Zou et al., 2009). Figure 2.6 shows some of the most used thiol capping agents. Thiol capping agents prevent aggregation of the QDs and make them accessible for interaction with the analyte of interest. QDs capped with thiols become biocompatible due to the presence of the thiol group which makes the QDs to be bioactive. Different thiols capping agents have been used to improve the optical and electrochemical properties of SnS QDs .

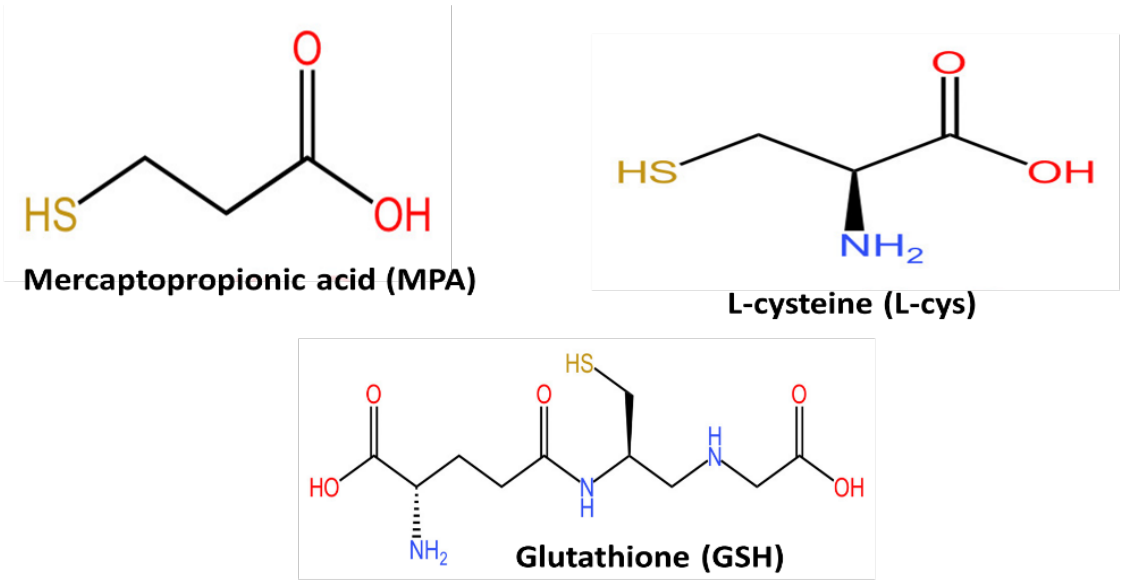

Figure 2.6 Common thiol capping agents utilized in QDs.

Han et al., 2017 synthesized cysteamine capped-SnS QDs in glycerol. The amount of cysteamine and Sn was adjusted as a result of bright photoluminescence, which illustrated excellent size-tuneable optical properties and stability of the synthesized thiol-capped QDs. In another example, Cheng et al., 2020 developed a surface treatment method for SnS with ZnS to form SnS/ZnS core-shell QDs using Cysteamine as a thiol capping agent. The results indicated a 19x increase in PL compared to bare SnS QDs. MPA, another thiol capping agent, increased stability from 8 days to

14 days in glycerol. Das & Dutta et al., 2015 developed stable and crystalline nanorods based on SnS QDs capped with mercaptoacetic acid and proved to be an efficient photocatalyst towards the degradation of trypan blue under sunlight.

2.2 Concluding remarks

Breast cancer is one of the most aggressive malignant diseases among women around the world. HER-2 is a breast cancer biomarker that indicates the presence of cancer. Traditional detection methods for this biomarker are tedious, costly and require a high level of expertise. Biosensors are analytical devices that turn a biological response into a readable electrical signal. Electrochemical detection biosensors are most advantageous than traditional detection methods due to high specificity, fast response time, and selectivity for low concentrations. Recently, quantum dots are receiving great attention due to their attractive properties, allowing them to be used in designing sensors. However, their toxicity limits their use in biological applications. Recent advances have produced Cd-free QDs to reduce the toxicity of QDs. SnS QDs are the most preferred due to their non-toxicity, economic feasibility, and abundance, but reports indicate that these QDs do not exhibit bright photoluminescence and are not stable under aqueous media. These limitations can be addressed through functionalization with thiol capping agents. Thiol capping agents not only reduce toxicity of QDs, but they also stabilize and increase the biocompatibility of QDs and help improve their photoluminescence of QDs.

2.3 References

Aladesuyi, O.A. & Oluwafemi, O.S., 2020. Synthesis strategies and application of ternary quantum dots—in cancer therapy. *Nano-Structures & Nano-Objects*, 24:100568.

Alvi, N.U.H., Gómez, V.J., Rodriguez, P.E.S., Kumar, P., Zaman, S., Willander, M. and Nötzel, R., 2013. An InN/InGaN quantum dot electrochemical biosensor for clinical diagnosis. *Sensors*, 13(10):13917-13927.

Bogdanovska-Todorovska, M., Kostadinova-Kunovska, S., Jovanovik, R., Krsteska, B., Kondov, G., Kondov, B., & Petrushevska, G. (2018). Correlation of Immunohistochemistry and Fluorescence *in Situ* Hybridization for HER-2 Assessment in Breast Cancer Patients: Single Centre Experience. *Open access Macedonian journal of medical sciences*, *6*(4):593–599.

Cancer (no date) *World Health Organization*. Available at: https://www.who.int/health topics/cancer (Accessed: 30 January 2024).

Carvajal, S., Fera, S.N., Jones, A.L., Baldo, T.A., Mosa, I.M., Rusling, J.F. & Krause, C.E., 2018. Disposable inkjet-printed electrochemical platform for detection of clinically relevant HER-2 breast cancer biomarker. *Biosensors and Bioelectronics*, 104:158-162.

Casterá, C. & Bernet, L., 2020. HER2 immunohistochemistry inter-observer reproducibility in 205 cases of invasive breast carcinoma additionally tested by ISH. *Annals of Diagnostic Pathology*, 45:151451.

Centane, S. & Nyokong, T., 2021. The antibody assisted detection of HER2 on a cobalt porphyrin binuclear framework and gold functionalized graphene quantum dots modified electrode. *Journal of Electroanalytical Chemistry*, 880:114908.

Chang, X.H., Zhang, J., Wu, L.H., Peng, Y.K., Yang, X.Y., Li, X.L., Ma, A.J., Ma, J.C. and Chen, G.Q., 2019. Research progress of near-infrared fluorescence immunoassay. *Micromachines*, *10*(6):422.

Cheng, H.Y., Acar, O., Shih, W.Y. & Shih, W.H., 2020. Enhancing the photoluminescence of SnS quantum dots by ZnS treatment. *Chemical Physics Letters*, *754*:137696.

Cheraghizade, M., Jamali-Sheini, F., Yousefi, R., Niknia, F., Mahmoudian, M.R. and Sookhakian, M., 2017. The effect of tin sulfide quantum dots size on photocatalytic and photovoltaic performance. *Materials Chemistry and Physics*, 195:187-194.

Díaz-Cruz, E.B., Regalado-Pérez, E., Santos, J. and Hu, H., 2021. Development of SnS/PVP core/shell quantum dots with tunable color emission synthesized by microwave heating. *Journal of Solid-State Chemistry*, 300:122264.

Damborský, P., Švitel, J. & Katrlík, J., 2016. Optical biosensors. *Essays in Biochemistry.*, 60(1):91-100.

Das, D. and Dutta, R.K., 2015. A novel method of synthesis of small band gap SnS nanorods and its efficient photocatalytic dye degradation. *Journal of colloid and interface science*, 457:339-344.

Ehzari, H. and Safari, M., 2022. A sandwich-type electrochemical immunosensor using antibody-conjugated PT-doped CdTe qds as enzyme-free labels for sensitive HER2 detection based on a magnetic framework. *Frontiers in Chemistry*: 10. Available at: https://doi.org/10.3389/fchem.2022.881960.

Freitas, M., Neves, M., Nouws, H. and Delerue-Matos, C., 2020. Quantum dots as nanolabels for breast cancer biomarker HER2-ECD analysis in human serum. *Talanta* 208:120430.

Freitas, M., Nouws, H.P., Keating, E. and Delerue-Matos, C., 2020. High-performance electrochemical immunomagnetic assay for breast cancer analysis. *Sensors and Actuators B: Chemical*, 308:127667.

Fuku, X., Singh, B., Ajayi, R.F., Jijana, A.N., Baker, P., Dempsey, E. and Iwuoha, E., 2015. A gallium telluride quantum dots bioelectrode system for human epidermal growth factor receptor-2 (Her2/neu) oncogene signalling. *Analytical Methods*, 7(15):6114-6124.

Furrer, D., Paquet, C., Jacob, S. and Diorio, C., 2018. The Human Epidermal Growth Factor Receptor 2 (HER2) as a Prognostic and Predictive Biomarker: Molecular Insights into HER2 Activation and Diagnostic Implications, *Cancer Prognosis.*

Gandhimathi, R., Anitha, D. and Warrier, A.R., 2019, July. Photoluminescence in degenerate states of heavily doped SnS nanoparticles. In *AIP Conference Proceedings*, 2115(1): 030475. AIP Publishing LLC.

Gidwani, B., Sahu, V., Shukla, S.S., Pandey, R., Joshi, V., Jain, V.K. and Vyas, A., 2021. Quantum dots: Prospectives, toxicity, advances, and applications. *Journal of Drug Delivery Science and Technology*, 61:102308.

Guan, Z., Chen, F., Liu, Z., Lv, P., Chen, M., Guo, M., Li, X., Teng, F., Chen, S. & Tang, A., 2019. Compositional engineering of multinary Cu–In–Zn-based semiconductor nanocrystals for efficient and solution-processed red-emitting quantum-dot light-emitting diodes. *Organic Electronics*, 74:46-51.

Han, S., Shih, W.Y. and Shih, W.H., 2017. Charge-Neutral, Stable, Non-Cytotoxic, Near-Infrared SnS Aqueous Quantum Dots for High Signal-to-Noise-Ratio Biomedical Imaging. *ChemistrySelect*, *2*(24):7332-7339.

Hasan, M., Ahommed, M., Daizy, M., Bacchu, M., Ali, M., Al-Mamun, M., Saad Aly, M., Khan, M. & Hossain, S., 2021. Recent development in electrochemical biosensors for cancer biomarkers detection. *Biosensors and Bioelectronics: X*, 8:100075.

Harahsheh, T., Makableh, Y.F., Rawashdeh, I. & Al-Fandi, M., 2021. Enhanced aptasensor performance for targeted HER2 breast cancer detection by using screen-printed electrodes modified with Au nanoparticles. *Biomedical Microdevices*, 23(4):1-11.

Javed, R., Zia, M., Naz, S., Aisida, S., Ain, N. & Ao, Q., 2020. Role of capping agents in the application of nanoparticles in biomedicine and environmental remediation: recent trends and prospects. *Journal of Nanobiotechnology*, 18(1).

Jiang, P., Wang, R. & Chen, Z., 2015. Thiol-based non-injection synthesis of near-infrared Ag 2 S/ZnS core/shell quantum dots. *RSC advances*, 5(70):56789-56793.

Kajal, N., Singh, V., Gupta, R. & Gautam, S., 2022. Metal organic frameworks for electrochemical sensor applications: A review. *Environmental Research*, 204:112320.

Karadurmus, L., Ozcelikay, G., Vural, S. and Ozkan, S.A., 2021. An overview on quantum dot-based nanocomposites for electrochemical sensing on pharmaceutical assay. *Iranian Journal of Pharmaceutical Research: IJPR*, 20(3):187.

Lah, Z., Ahmad, S., Zaini, M. & Kamarudin, M., 2019. An Electrochemical Sandwich Immunosensor for the Detection of HER2 using Antibody-Conjugated PbS Quantum Dot as a label. *Journal of Pharmaceutical and Biomedical Analysis*, 174:608-617.

Lesiak, A., Drzozga, K., Cabaj, J., Bański, M., Malecha, K. & Podhorodecki, A., 2019. Optical Sensors Based on II-VI Quantum Dots. *Nanomaterials*, 9(2):192.

Liu, Y., Chen, X. and Ma, Q., 2018. A novel amplified electrochemiluminescence biosensor based on Au NPs@ PDA@ CuInZnS QDs nanocomposites for ultrasensitive detection of p53 gene. *Biosensors and Bioelectronics*, 117:240-245.

Lu, B., He, Q., He, Y., Chen, X., Feng, G., Liu, S. and Ji, Y., 2018. Dual-channel-coded microbeads for multiplexed detection of biomolecules using assembling of quantum dots and element coding nanoparticles. *Analytica Chimica Acta*, 1024:153-160.

Manole, E., Bastian, A.E., Popescu, I.D., Constantin, C., Mihai, S., Gaina, G.F., Codrici, E. & Neagu, M.T., 2018. Immunoassay techniques highlighting biomarkers in immunogenetic diseases. *In Immunogenetics*, IntechOpen.

Matea, C., Mocan, T., Tabaran, F., Pop, T., Mosteanu, O., Puia, C., Iancu, C. & Mocan, L., 2017. Quantum dots in imaging, drug delivery and sensor applications. *International Journal of Nanomedicine*, 12:5421-5431.

Milosevic, M., Jankovic, D., Milenkovic, A. & Stojanov, D., 2018. Early diagnosis and detection of breast cancer. *Technology and Health Care*, *26*(4):729-759.

Miranti, R., Septianto, R.D., Kikitsu, T., Hashizume, D., Matsushita, N., Iwasa, Y. and Bisri, S.Z., 2022. π-SnS colloidal nanocrystals with size-dependent band gaps. *The Journal of Physical Chemistry C*, 126(11):5323-5332.

Mo, D., Hu, L., Zeng, G., Chen, G., Wan, J., Yu, Z., Huang, Z., He, K., Zhang, C.& Cheng, M., 2017. Cadmium-containing quantum dots: properties, applications, and toxicity. *Applied Microbiology and Biotechnology*, 101(7):2713-2733.

Mohammadpour-Haratbar, A., Boraei, S.B.A., Zare, Y., Rhee, K.Y. and Park, S.J., 2023. Graphene-Based Electrochemical Biosensors for Breast Cancer Detection. *Biosensors*, 13(1):80.

Montaseri, H., Adegoke, O. & Forbes, P.B., 2019. Development of a thiol-capped core/shell quantum dot sensor for acetaminophen. *South African Journal of Chemistry*, 72:108-117.

Mostafa, I.M., Tian, Y., Anjum, S., Hanif, S., Hosseini, M., Lou, B. and Xu, G., 2022. Comprehensive review on the electrochemical biosensors of different breast cancer biomarkers. *Sensors and Actuators B: Chemical*:131944.

Nguyen, A.T., Gao, F., Baucom, D. & Heyes, C.D., 2020. CuInS2-Doped ZnS Quantum Dots Obtained via Non-Injection Cation Exchange Show Reduced but Heterogeneous Blinking and Provide Insights into Their Structure–Optical Property Relationships. *The Journal of Physical Chemistry C*, 124(19):10744-10754.

Naresh, V. and Lee, N., 2021. A review on biosensors and recent development of nanostructured materials-enabled biosensors. *Sensors*, *21*(4):1109.

Pacheco, J.G., Rebelo, P., Freitas, M., Nouws, H.P. and Delerue-Matos, C., 2018. Breast cancer biomarker (HER2-ECD) detection using a molecularly imprinted electrochemical sensor. *Sensors and Actuators B: Chemical*, 273:1008-1014.

Peltomaa, R., Glahn-Martínez, B., Benito-Peña, E. & Moreno-Bondi, M., 2018. Optical Biosensors for Label-Free Detection of Small Molecules. *Sensors*, 18(12):4126.

Purohit, B., Vernekar, P., Shetti, N. & Chandra, P., 2020. Biosensor nanoengineering: Design, operation, and implementation for biomolecular analysis. *Sensors International*, 1:100040.

Ren, X., Zhang, X., Xie, H., Cai, J., Wang, C., Chen, E., Xu, S., Ye, Y., Sun, J., Yan, Q. & Guo, T., 2022. Perovskite quantum dots for emerging displays: Recent progress and perspectives. *Nanomaterials*, 12(13):2243.

Reineck, P. and Gibson, B.C., 2017. Near-infrared fluorescent nanomaterials for bioimaging and sensing. *Advanced Optical Materials*, *5*(2):1600446.

Reshma, V. & Mohanan, P., 2019. Quantum dots: Applications and safety consequences. *Journal of Luminescence*, 205:287-298.

Roointan, A., Ahmad Mir, T., Ibrahim Wani, S., Mati-ur-Rehman, Hussain, K., Ahmed, B., Abrahim, S., Savardashtaki, A., Gandomani, G., Gandomani, M., Chinnappan, R. & Akhtar, M.,

2019. Early detection of lung cancer biomarkers through biosensor technology: A review. *Journal of Pharmaceutical and Biomedical Analysis*, 164:93-103.

Sahm, C.D., Ciotti, A., Mates-Torres, E., Badiani, V., Sokołowski, K., Neri, G., Cowan, A.J., Garcia-Melchor, M. and Reisner, E., 2022. Tuning the local chemical environment of ZnSe quantum dots with dithiols towards photocatalytic CO 2 reduction. *Chemical Science*.

Schiffman, J.D. and Balakrishna, R.G., 2018. Quantum dots as fluorescent probes: Synthesis, surface chemistry, energy transfer mechanisms, and applications. *Sensors and Actuators B: Chemical*, 258:1191-1214.

Seale, K.N. & Tkaczuk, K.H., 2022. Circulating biomarkers in breast cancer. *Clinical Breast Cancer*, 22(3): e319-e331.

Sinatra, L., Pan, J. & Bakr, O.M. (2017) "Methods of Synthesizing Monodisperse Colloidal Quantum Dots," *materials matters,*12(1).

Singh, A.K., Jaiswal, N., Tiwari, I., Ahmad, M. and Silva, S.R.P., 2023. Electrochemical biosensors based on in situ grown carbon nanotubes on gold microelectrode array fabricated on glass substrate for glucose determination. *Microchimica Acta*, 190(2):55.

Sinha, A., Mugo, S.M., Zhao, H., Chen, J. & Jain, R., 2019. Electrochemical immunosensors for rapid detection of breast cancer biomarkers. In *Advanced Biosensors for Health Care Applications*:147-169.

Subramanian, S., Ganapathy, S., Rajaram, M. & Ayyaswamy, A., 2020. Tuning the optical properties of colloidal Quantum Dots using thiol group capping agents and its comparison. *Materials Chemistry and Physics*, 249:123127.

Tian, S., Zeng, K., Yang, A., Wang, Q. & Yang, M., 2017. A copper-based enzyme-free fluorescence ELISA for HER2 detection. *Journal of immunological methods*, *451*:78-82.

Tomar, S., Gupta, S., Priyam, A., Bhushan, B., Singh, A., Dwivedi, U.K. and Choubey, R.K., 2022. Temporal evolution of optical absorption and emission spectra of thiol capped CdTe quantum dots. *Applied Physics A*, 128(10):1-13.

Vasudevan, D., Gaddam, R., Trinchi, A. & Cole, I., 2015. Core–shell quantum dots: Properties and applications. *Journal of Alloys and Compounds*, 636:395-404.

Vigneshvar, S., Sudhakumari, C., Senthilkumaran, B. & Prakash, H., 2016. Recent Advances in Biosensor Technology for Potential Applications – An Overview. *Frontiers in Bioengineering and Biotechnology*:4.

Wagner, A., Knipe, J., Orive, G. & Peppas, N., 2019. Quantum dots in biomedical applications. *Acta Biomaterialia*, 94:44-63.

Wahab, R., Khan, F., Alam, M., Ahmad, J. and Al-Khedhairy, A.A., 2023. Aluminum oxide quantum dots (Al2O3): An immediate sensing aptitude for the detection of urea. *Inorganic Chemistry Communications*, 147:110238.

Wahyuni, H.Y., Misonia, B.S.U., Santhy, W. and Shabarni, G., 2018. A voltammetric immunosensor for detection of HER2 using gold modified screen-printed carbon electrode. *Res J Chem Environ*, 22:294-301.

Wang, X., Yang, Y., Dang, J., McConnell, C., Zhang, J., Wang, J., Yu, S., Ye, W., Gao, Y., Zhang, K., Liu, R. & Jin, L., 2020. Non-invasive early detection of cancer four years before conventional diagnosis using a blood test.*Nature Communications.* 11(1).

Wang, Z. & Tang, M., 2021. The cytotoxicity of core-shell or non-shell structure quantum dots and reflection on environmentally friendly: A review. *Environmental Research*, 194:110593.

Xie, S., Wang, Y., Gong, Z., Li, Y., Yang, W., Liu, G., Li, J., Hu, X., Wang, Y., Tong, Y. & Yuan, P., 2022. Liquid Biopsy and Tissue Biopsy Comparison with Digital PCR and IHC/FISH for HER2 Amplification Detection in Breast Cancer Patients. *Journal of Cancer*, 13(3):744.

Yadav, P. & Chowdhury, P.,2021. Optical efficiency of CdTe QDs for metal ion sensing in the presence of different thiol-based capping agents. *Chemical Papers*, 76(3):1833–1850.

Ye, F., Zhao, Y., El-Sayed, R., Muhammed, M. & Hassan, M., 2018. Advances in nanotechnology for cancer biomarkers. *Nano Today*, 18:103-123.

Yoon, J., Cho, H.Y., Shin, M., Choi, H.K., Lee, T. & Choi, J.W., 2020. Flexible electrochemical biosensors for healthcare monitoring. *Journal of Materials Chemistry B*, *8*(33):7303-7318.

Zhang, F., n.d. *Near-infrared nanomaterials*.

Zhang, M., Gao, G., Ding, Y., Deng, C., Xiang, J. & Wu, H., 2019. A fluorescent aptasensor for the femtomolar detection of epidermal growth factor receptor-2 based on the proximity of G-rich sequences to Ag nanoclusters. *Talanta*, 199:238-243.

Zhang, K., Liu, R. & Jin, L., 2020. Non-invasive early detection of cancer four years before conventional diagnosis using a blood test. *Nature Communications*, 11(1).

Zhao, P., Xu, Q., Tao, J., Jin, Z., Pan, Y., Yu, C. & Yu, Z., 2017. Near infrared quantum dots in biomedical applications: current status and future perspective. *WIREs Nanomedicine and Nanobiotechnology*, 10(3).

Zugazagoitia, J., Guedes, C., Ponce, S., Ferrer, I., Molina-Pinelo, S. & Paz-Ares, L., 2016. Current Challenges in Cancer Treatment. *Clinical Therapeutics*, 38(7):1551-1566.

Zhu, C., Chen, Z., Gao, S., Goh, B.L., Samsudin, I.B., Lwe, K.W., Wu, Y., Wu, C. and Su, X., 2019. Recent advances in non-toxic quantum dots and their biomedical applications. *Progress in Natural Science: Materials International,*29(6):628-640.

CHAPTER 3

Synthesis and optical properties of SnS QDs

This chapter focusses on one-pot heat synthesis and characterization of SnS-based QDs. The QDs were synthesised using two methods with different sulfur sources. In the first method, thiourea is used as a sulfur source, while in the second method, sodium sulfide (N_2S) is used as a sulfur source. The experimental conditions (viz reaction time, pH, Sn:S ratio, shell precursors, solvent and thiol capping agents) for each method were optimized to produce high-quality SnS QDs. Furthermore, the optical, structural, and morphological properties of the obtained SnS QDs in each method are discussed and compared to literature. This chapter concludes based on the optimal method with the best optical results for the synthesis of SnS QDs. The electrochemical properties of the synthesized SnS QDs obtained with the best method will be explored further in chapter 4 as well as in sensor fabrication.

3.1. Introduction

Cadmium free (Cd-free) quantum dots (QDs) are consistently gaining widespread recognition in many applications due to their extraordinary properties. Amongst various types of Cd-free QDs, particular attention is paid to tin sulfide (SnS) QDs. SnS QDs have emerged as a chalcogenide material of interest because of their natural abundance and nontoxic nature to humans and the environment (Cheng et al.,2020). SnS possesses an orthorhombic crystal structure with p-type intrinsic semiconductor nature. It is a layered semiconductor nanocrystal with strong Sn-S bonds

in each layer and weak van der Waals interactions between different layers (Modi etal., 2022). Due to its direct band gap and high absorption coefficient, SnS QDs possess favourable characteristics advantageous for sensors, capacitors, near-infrared detectors, and medical diagnosis. However, despite these outstanding properties that allow for applying SnS QDs in various applications. SnS QDs still suffer from poor stability, high solubility in water, low luminescence, and dissolves under neutral and basic conditions (Cheng et al., 2019).

The quality of these nanomaterials has been the subject of extensive research over the past few years. Subsequently, numerous methods for the production of SnS QDs have been established. The hydrothermal technique (Dar et al., 2022), the non-injection approach (Cheng et al., 2020), and the colloidal technique (Hot injection method) (Liu et al., 2021) are some of these synthetic technologies. Nevertheless, optical properties like narrow photoluminescence (PL) emission wavelength, high stability, and brightness for SnS QDs remain a challenge. It has been shown that various parameters such as reaction time, synthetic method, precursor's concentration and ratio, pH, capping ligand, shell, and synthetic solvents affect PL intensity and the size of the QD. Therefore, it is necessary to optimize these parameters to produce highly luminescent SnS QDs with good optical properties. To achieve optimum synthetic conditions, one experimental variable is changed while the other variables remain constant. Once one variable is optimized, the optimum is further used in the proceeding experiments. These parameters are key in modulating the properties of QDs (Mirzaei, Jahanshahi and Darzi et al., 2018). In addition, understanding the influence of these parameters is mandatory to obtain tailored SnS QDs with precisely controlled emission properties. These properties were varied to produce SnS QDs with optimum optical properties.

3.1.2 Characterization of quantum dots

In this study, optical spectroscopy and microscopy were employed for the characterisation of SnS QDs. Microscopy was used to attain information about the shape and size distribution of QDs. The optical and structural parameters of the material were determined by ultraviolet-visible spectroscopy (UV-vis), photoluminescence spectroscopy (PL), Fourier-transform infrared spectroscopy (FTIR), dynamic light scattering (DLS), transmission electron microscopy (TEM), scanning electron microscope (SEM) and powder X-ray diffraction (XRD) as described below:

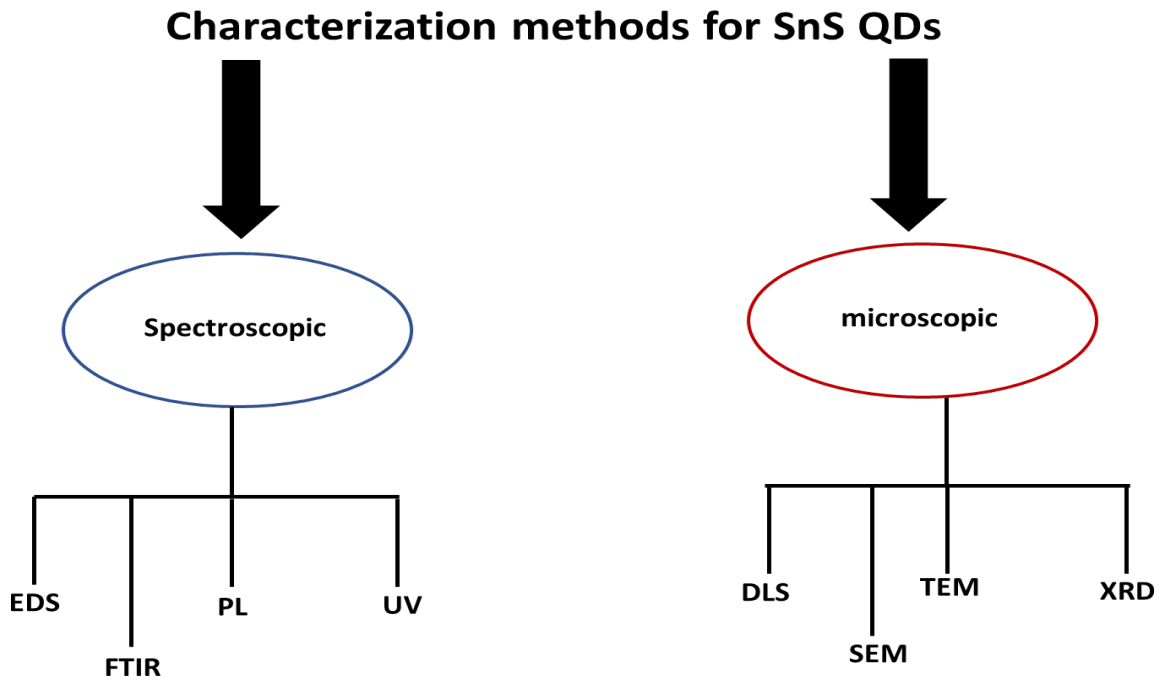

Figure 3.1. Characterization techniques for SnS QDs.

3.2. Experimental

3.2.1. Reagents and Materials

Tin chloride dihydrate ($SnCl_2$-$2H_2O$), sodium sulfide (Na_2S), sodium hydroxide (NaOH), hydrochloric acid (HCl), nitric acid (HNO_3), propylene glycerol ($C_3H_8O_2$), distilled water (H_2O),

thiourea (CH_4N_2S), silver nitrate ($AgNO_3$), zinc nitrate $Zn(NO)_3$, L-Cysteine (L-Cys), Ethanol (C_2H_6O), 3-mercapto-propanoic acid (MPA) and glutathione (GSH) were purchased from Sigma–Aldrich, South Africa. All chemicals were of analytical grade and used without further purification.

3.2.2 Preparation of stock solutions

Tin stock solution (0.08 M) was prepared by dissolving $SnCl_2$-$2H_2O$ (0.30g, 1.32 mmol) in 20 ml of $C_3H_8O_2$. Thiourea stock solution (0.08 M) was prepared by dissolving CH_4N_2S (0.29 g, 3.8 mmol) in 15 mL of $C_3H_8O_2$. Na_2S stock solution (0.08 M) was prepared by dissolving Na_2S (0.29g, 3.71 mmol) in 15 ml of $C_3H_8O_2$. Another stock solution of Na_2S (0.08 M) was prepared by dissolving Na_2S (0.312g, 3.99 mmol) in 5 ml of H_2O. L-Cysteine stock solution (0.32 M) was prepared by dissolving L-Cysteine (0.55g, 4.5 mmol) in 15 ml of $C_3H_8O_2$. MPA stock solution (0.32 M) was prepared by dissolving MPA (0.55g, 5.18 mmol) into 15 ml of $C_3H_8O_2$ and GSH stock solution (0.32 M) was prepared by dissolving GSH (0.55 g, 1.79 mmol) into 15 ml $C_3H_8O_2$.

ZnS shell precursor

Zn stock solution (0.08 M) was prepared by dissolving 0.36 g (Zn (ac) $_2$.$2H_2O$ in 15 mL propylene glycol. The sulphur stock solution (0.08 M) was prepared by dissolving 0.29 g of thiourea in 15 ml of propylene glycol.

3.2.3 Synthetic strategies

Synthetic strategy 1

SnS QDs were synthesized by heating 20 ml of propylene glycerol in an open beaker under magnetic stirring using the modified method by Cheng et al., 2020. 4 ml thiol capping agent (i.e., GSH, L-Cysteine, and MPA) stock solution was added to the reaction solution. This was followed by the addition of 3 ml of tin stock solution. The pH of the reaction mixture was adjusted to the

required pH value. The solution was stirred continuously for 10 min to allow the thiol capping agent to react with Sn while the pH was maintained using NaOH. Then 1 ml of thiourea was added, and the pH of the solution was adjusted using HCl. After the addition of thiourea, the solution turned yellow, and the colour of the solution became intense with an increase in time, confirming the formation of SnS QDs. 4 ml of MPA was added to the synthesis pot to neutralize the positively charged Sn^{2+} followed by 4 ml of the tin stock solution at a constant temperature. The beaker contents were subsequently heated at 70 °C for 60 min to obtain SnS QDs. Different aliquots were taken for every 15 min of the reaction for characterization. The experiment was optimized by varying different synthetic parameters such as the Sn: S ratio (1:1, 1:2, 1:4, 1:6, 1:8), pH (3, 5, 7, and 9), reaction solvent (H_2O vs. $C_3H_8O_2$), thiol capping (GSH, MPA, and L-Cysteine).

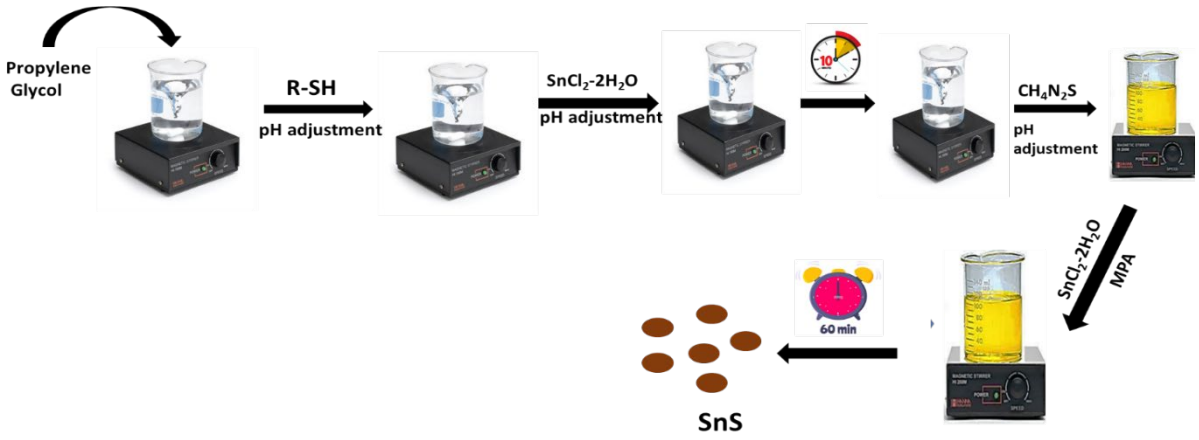

Figure 3.2. Schematic representation of SnS QDs (method 1).

The synthesis of SnS / ZnS-10 ml of the prepared SnS QDs was heated to 70 $^{\circ}C$ and the pH of the solution was adjusted to 9 with NaOH. Then 0.08 M of Zn precursor was added to the solution and the solution was mixed for 30min then after 0.08M of the thiourea (sulfur source) was added to the solution and the solution was mixed for another 30min. The solution was precipitated out by adding the mixture on a diluted solution of water and propylene glycol on a 1:1 ratio. Then the

entire solution was centrifuged at 6000 rpm for 5 min; the process was repeated three times to obtain SnS/ZnS in powder form.

Synthetic strategy 2

In this method, SnS QDs were synthesized via heat-up method. 15 mL of thiol capping agent (L-Cysteine, GSH and MPA) stock solution was heated up to 70 ^{o}C for 10 min. The pH of the solution was adjusted using NaOH/nitric acid. 1 ml of Sn stock solution was added to the solution while maintaining the pH using NaOH. The solution was mixed for 10 min to allow Sn to react with the thiol capping agent as the thiols chelate SnS. Then 1 ml of Na_2S was added to the reaction mixture while maintaining the pH with the addition of nitric acid. At this point, the solution turned from clear to an intense orange colour. An additional 4 ml of Sn precursor was added to the solution to improve luminescence while maintaining pH by adding NaOH. 27 ml of water was added to create 1.6 mmol of SnS QD. The beaker contents were subsequently heated at 70 ºC for 60 min to obtain SnS QDs (Figure3.3). Different aliquots were taken for every 15 min of the reaction. The experiment was optimised by varying different synthetic parameters such as time, pH (pH 3, 5, 7 and 9), thiol capping (GSH, MPA, and L-Cysteine), and shell precursors.

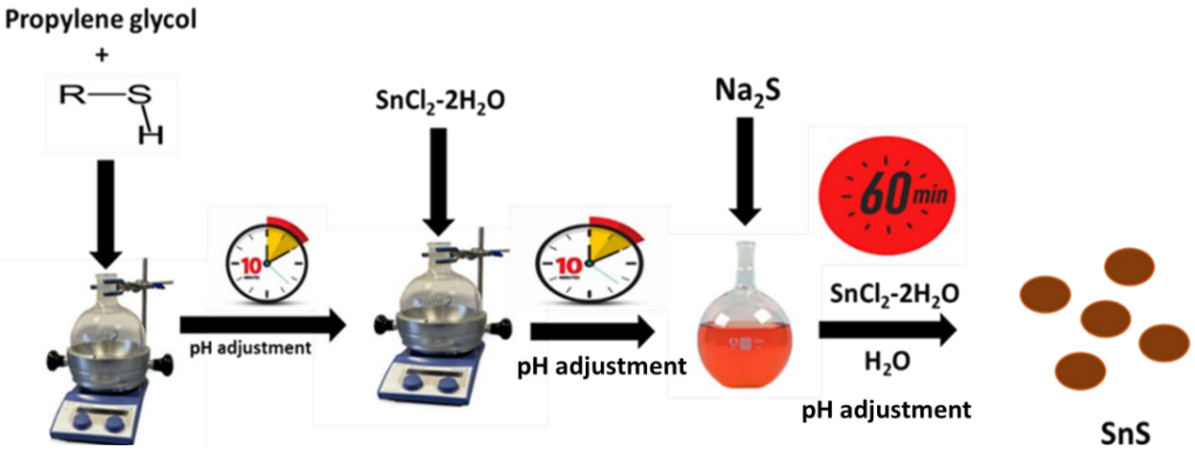

Figure 3.3. Schematic representation of SnS QDs (method 2).

The SnS / ZnS synthesis - 1.6 mmol of the prepared SnS QDs was heated to 70 ° C and the pH of the solution was adjusted to 9 with NaOH. Then 0.08M of Zn precursor was added to the reaction and the solution was mixed for 30min while maintaining pH 9 by addition of NaOH then after 0.08M of Na_2S was added to the solution and pH 9 was maintained with the addition of nitric acid and the solution was mixed for another 30min. The solution was precipitated using ethanol. Then the entire solution was centrifuged at 3000rpm for three minutes then the precipitate was washed with ethanol to obtain pure SnS/ZnS QDs.

3.2.4. Characterization

Ultraviolet-visible spectroscopy (UV-vis)

The optical absorption of the synthesised SnS QDs was characterised using ultraviolet-visible spectrophotometry (UV–vis) (Perkin Elmer UV–Vis Lambda 25 spectrometer, UK) at an absorption wavelength of 200 to 800 nm. The samples were diluted with distilled water and measurements were taken using quartz cuvettes.

Photoluminescence spectroscopy (PL)

Fluorescence analysis of SnS QDs was obtained using PL spectra, and the results were collected using a PerkinElmer spectrometer. Fluorescence analysis was carried out at excitation wavelengths ranging from 200 to 800 nm. All samples were diluted with distilled water (1:3) prior to measurement due to high fluorescence intensity of the concentrated samples.

Fourier transform infrared (FTIR) spectroscopy.

FTIR was implemented for the confirmation of successful thiol capping on SnS QDs, using a Spectrum two UATR spectrometer, Perkin Elmer, UK. The spectrum was recorded at a wavelength of $400cm^{-1}$ to $4000cm^{-1}$. A small drop of the liquid sample was placed on a highly polished diamond sample holder, and it was allowed to dry to obtain a nice, even film for accurate results.

Dynamic Light Scattering (DLS)

DLS is a technique that accurately measures the size of nanoparticle (NP)s in suspension. The size distribution profile of SnS QDs was analysed using Malvern P analytical DLS.

Transmission electron microscopy (TEM)

TEM was applied for determining the structure and diameter of SnS QDs using FEI T20 CRYO FEGTEM. TEM images were captured by the Direct DE-16 camera recording system.

Scanning electron microscope (SEM)

Tescan MIRA 3 RISE SEM was employed to understand the size distribution and structure of the QDs. Distilled water was used into the chamber to improve the quality of SnS QDs images. EDX (Energy- dispersive x-ray) was used together with SEM to confirm the elemental composition of SnS QDs.

Powder X-ray Diffraction (PXRD)

Crystallinity of SnS QDs was determined using XRD (Advance diffractometer with monochromatic Cu-Kα1 radiation (λ = 1.5418 Å).

3.3. Results and Discussion

3.3.1. Synthesis strategy 1 (method 1)

The optical and structural properties of QDs are highly dependent on the synthetic method. Therefore, the appropriate synthesis methods must be performed to obtain optimum QDs quality. Furthermore, optimising synthetic methods further influences the QDs structure and properties (Chand et al., 2017). In this study, the effect of two synthetic methods were investigated: reflux and heat-up method. In both synthesis methods, various synthetic parameters were investigated for optimal results.

Effect of a Synthetic Method: Heat vs. Reflux Method

Figure 3.4 shows the optical properties of SnS QDs (PL and UV) synthesized using heat and reflux methods. For the reflux method (Figures 3.4a-b), the UV-vis (figure 3.4a) exhibited broad absorption excitonic peaks cantering around 238 nm. The absorbance of the QDs increased steadfastly with increasing reaction time.

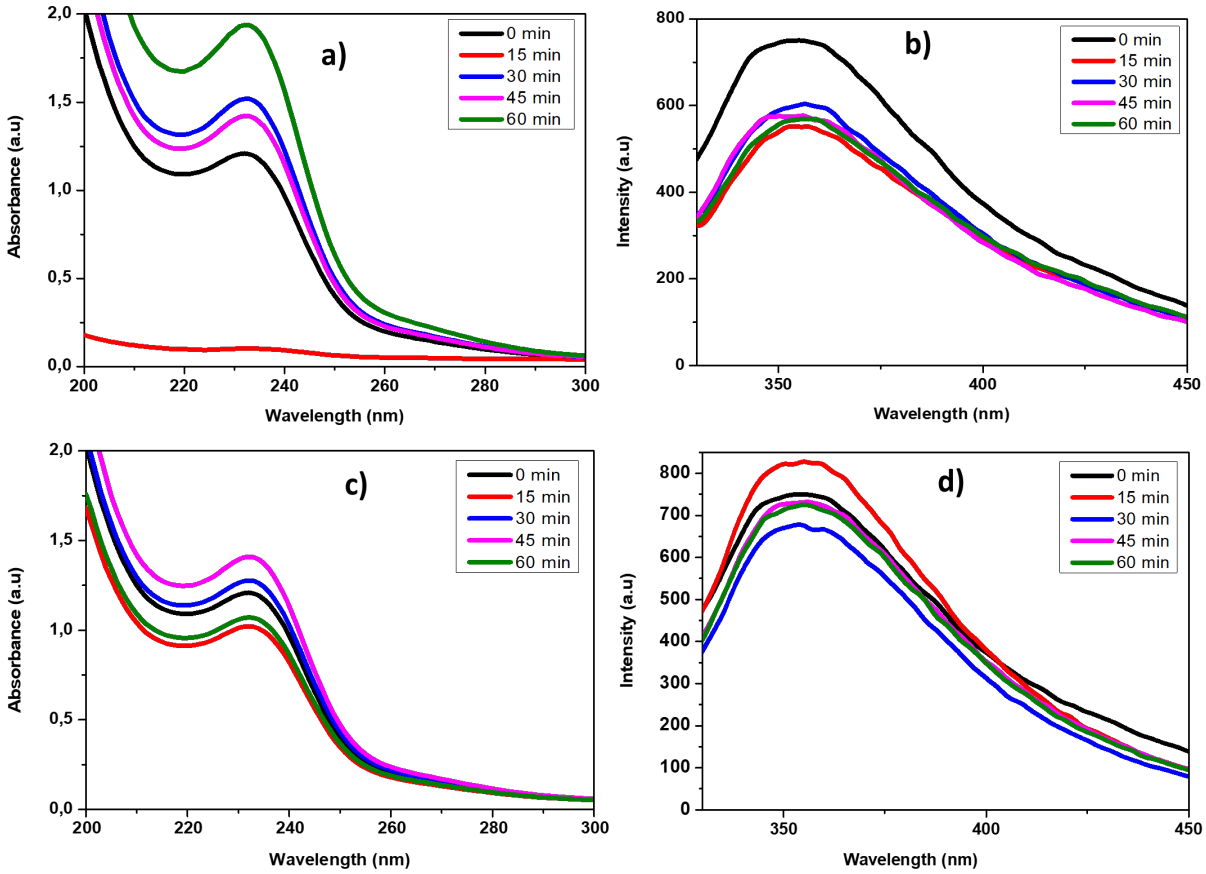

Figure 3.4. a) Absorption spectrum and b) PL spectrum of SnS QDs synthesized via reflux method. c) Absorption spectrum and d) PL spectrum of SnS QDs synthesized via heat method

This suggest an increase in particle size of the QDs (Tsolekile et al., 2020). The corresponding PL (Figure 3.4b) of SnS QDs exhibited broad features with time 0 min (i.e. time 0 denotes 5 minutes after the addition of thiourea) exhibiting highest PL intensities. The PL intensities were then noted to decrease after 10 min, which was most likely caused by the oxidisation of the stabiliser

molecules, which decreased the ability of the ligands to stabilise them while increasing the surface defects of QDs. Similar observation has been reported elsewhere (Yu et al.,2012). Then particle growth was presumed as the intensities increased after 30 min. The PL peak position of the QDs remained relatively stable at ~ 320 nm. Figure 3.4c-d shows UV and PL of the SnS QDs synthesised via the heat-up method, respectively. Figure 3.4c shows the absorption spectra of the synthesised SnS QDs using the heat method at different time intervals. The absorption spectra showed an initial decrease in absorbance for 15 min; this was followed by a steady increase in absorbance with 60 min exhibiting highest intensities. The variations in absorbance was accounted to the formation of small particles which can scatter light and producing random fluctuations resulting in the formation of aggregates. PL spectra (figure 3.4d) show a broad emission wavelength around 378 nm with 15 min exhibiting the highest intensity. Parani et al., 2017 reported that surface area is inversely proportional to nanoparticle size. Therefore, the surface of the emission of the small-sized particles will exhibit higher PL intensities compared to those of larger nanoparticles. Herein, we assume the formation of SnS QDs proceeds via the Ostwald ripening process (bigger particles grow at the expense of smaller particles) because PL intensity increase with a decrease in absorbance. This resulted in broad size distribution (Fig. 3.5); subsequently, an increase in time resulted in a decrease in PL intensity. Therefore, the heat-up method was selected as the optimum synthetic method for forming SnS QDs.

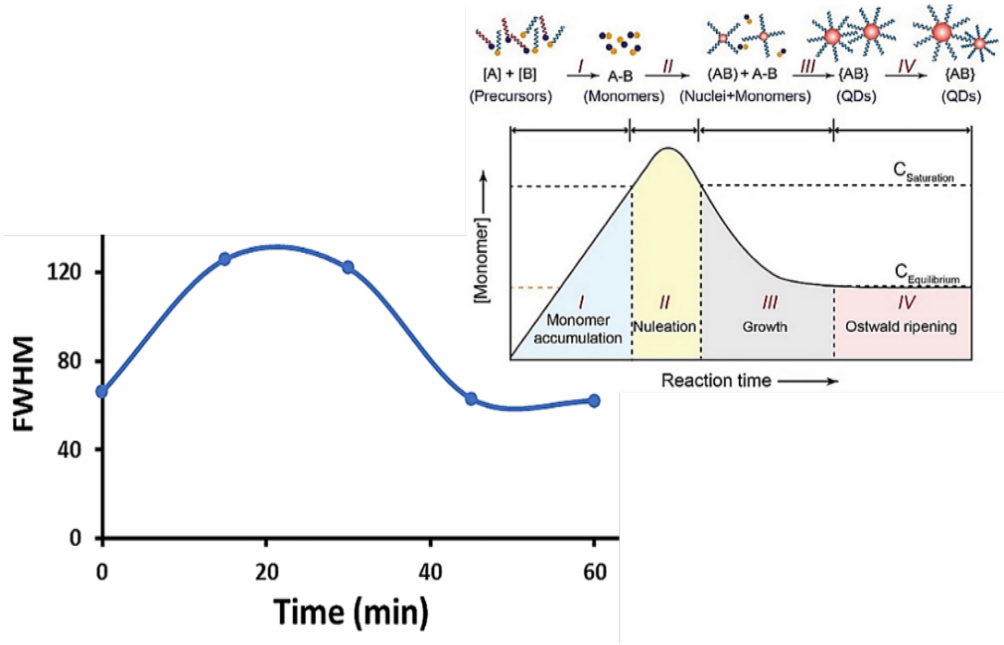

Figure 3.5. Full width half maximum (FWHM) of SnS QDs synthesised at different reaction times (heat method).

The Influence of Sn: S ratio

This study investigated the effect of different molar ratios of Sn^{+}/S^{2+} on the optical properties of SnS QDs. It is known that optical properties. of nanomaterials can be tuned by changing the composition of the metal ions. Hence, obtaining pure phase SnS, elemental control during synthesis is important (Lokhande et al., 2019). Figure 3.6a shows UV absorption at different Sn:S ratio. At 1:1 ratio (Sn:S), a broad absorbance was obtained at 234 nm, while other stoichiometric ratios exhibited band-edge wavelengths. Band-edge absorption was measured at the wavelength where the curve bends the most and deviates from the longer background wavelength (Parani et al., 2017). The corresponding PL (Figure 3.6b) showed a maximum emission intensity at 1:1. According to the literature, an excessive amount of sulfur source leads to the aggregation of QDs (May et al.,2022). This results in surface defects associated with trap sites due to the high surface-to-volume ratio, which may cause non-radiative recombination. PL spectra show this effect; according to literature, the increase in sulfur source results in a reduction in PL intensity (Mei et

al., 2018). Based on UV and PL results, the 1:1 Sn:S ratio was selected as optimum for this study and was subsequently used throughout the study.

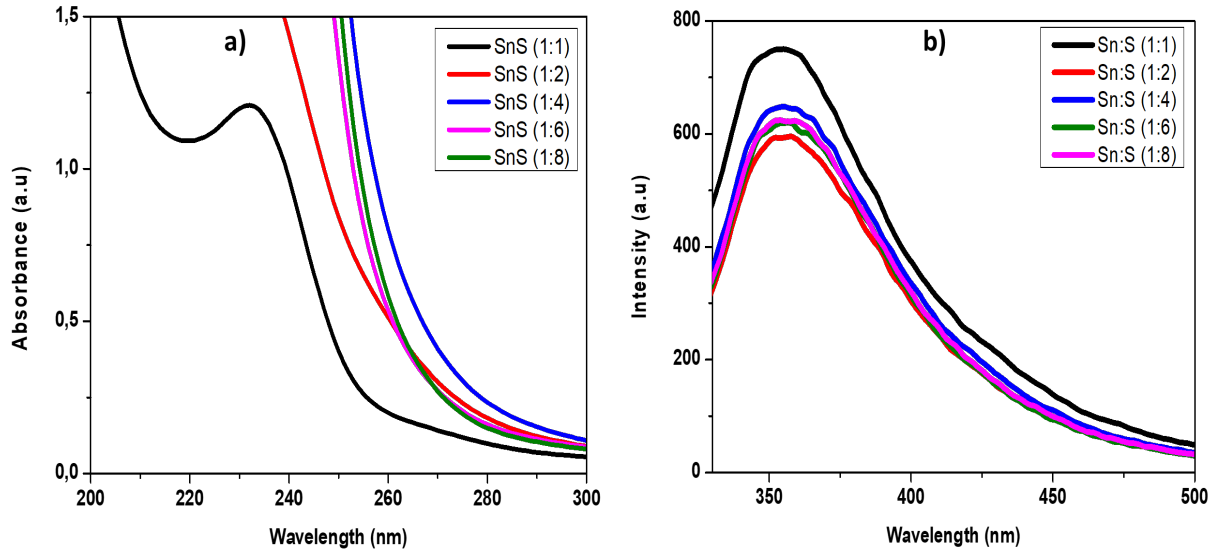

Figure 3.6. a) Absorbance spectra and b) Photoluminescence of SnS QDs synthesised at different Sn:S ratio.

The influence of pH

The effect of pH on the optical properties of the synthesised SnS QDs was investigated. pH plays a fundamental role in the stability, solubility, and agglomeration of QDs. Sn-based QDs are reported to be highly soluble under neutral and basic conditions (Cheng et al., 2020) and unstable under neutral conditions. With an objective of using SnS QDs in biosensing applications, it is important to understand the effect of pH on the PL intensity of SnS QDs. Figure 3.7 depicts the temporal evolution of the optical (UV and PL) properties of the SnS at different pH values. The UV exhibited broad absorbances, which decreased with increasing pH, suggesting a reduction in particle size resulting from the quantum confinement effect (Arya et al.,2021). The UV-vis spectra exhibited broad absorbances, which were slightly red shifted with increasing pH (Fig 3.7a). It was also observed that with increasing pH, the absorbance increased. Figure 3.7b reports on the corresponding PL at different synthetic pHs. Following the same trend as the UV, an increase in

pH exhibited a decrease in PL intensity. This suggests a change in the surface environment of SnS QDs under both acidic and basic conditions. SnS has been reported to dissolve at high pH and show little to no emission (Chen et al., 2020). The reduction in PL intensity was attributed to a lower solubility and instability of SnS under basic conditions. These results highlight the effect of pH on the optical properties of Sn-based nanomaterials and are in line with the literature (Srivastava et al., 2019). Due to the high PL intensities, pH 3 was chosen as the optimum pH for this study.

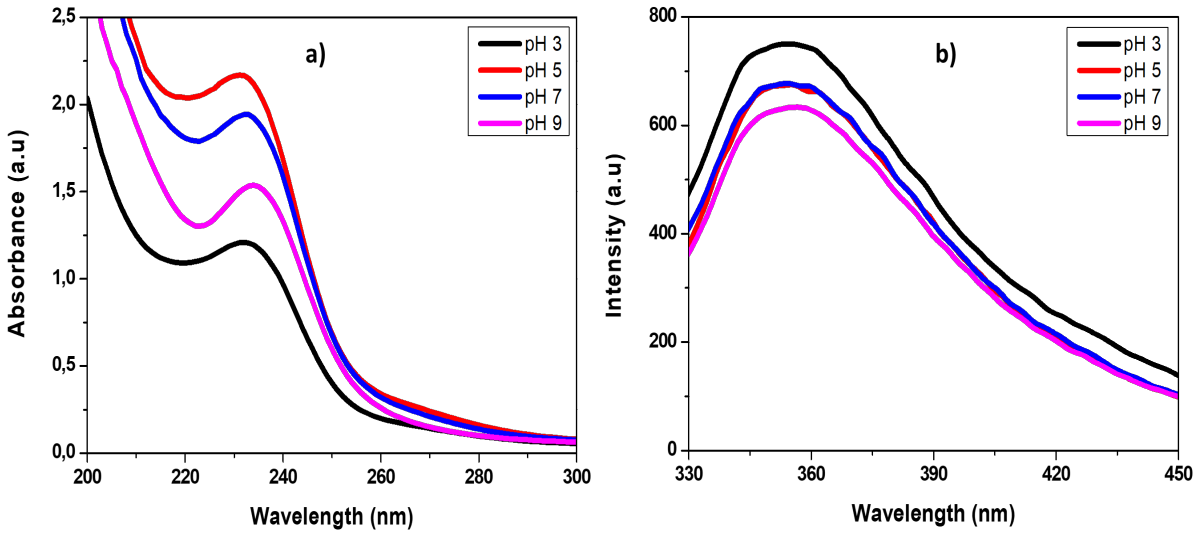

Figure 3.7. Absorption (a) and photoluminescence (b) spectra of SnS QDs at different pH values.

The influence of synthetic solvent

Solvents act as structure-directing agents or soft templates which control the morphology and size of QDs (Kannan et al., 2016). This study examined propylene glycol and distilled water for their potential use as synthetic solvents. Propylene glycol was selected for its high viscosity, which can lower the dissolution of SnS QDs while water provided an eco-friendly and greener alternative for the SnS synthesis. Fig. 3.8 presents the effect of water and propylene glycol on optical properties of SnS QDs.

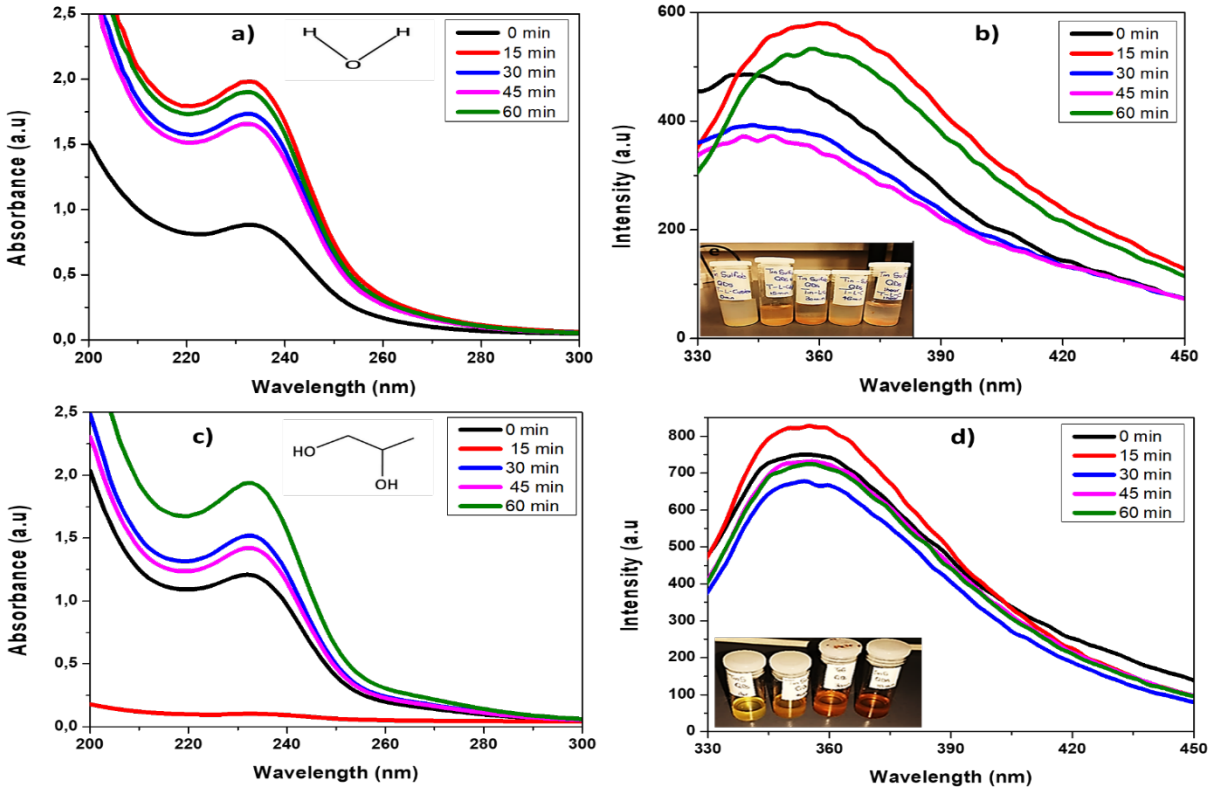

Figure 3.8. The effect of synthetic solvent on (a) absorption spectra, (b) photoluminescence of SnS QDs synthesized in water (*insert* digital photograph of SnS synthesized in water). Effect of propylene glycol as a synthetic solvent on (c) absorption spectra and (d) photoluminescence of SnS QDs (*insert*: digital photograph of SnS synthesized in propylene glycol).

Figure 3.8 shows that the absorption behaviour of water and propylene glycol during the synthesis of SnS QDs was similar. When water was utilized as a solvent, an overall stable absorption pattern was seen (Fig. 3.8a). The corresponding PL for QDs that were synthesised with water revealed a decrease in luminescence intensity with time (Fig. 3.8b) Time-dependent tests revealed that when QDs were synthesised with propylene glycol, absorbance first decreased before stabilising after 20 minutes (Fig. 3.8c). The corresponding PL for propylene glycol-based SnS QDs also exhibited a reduction in luminescence intensity with time. However, after a few days of storage, the aqueous-produced SnS QDs displayed a hard settlement (Fig. 3.8c *insert*), revealing the instability of SnS under aqueous conditions. The SnS QDs synthesised in propylene glycol remained stable for more than 14 days without precipitation (Fig. 3.8d *insert*). Therefore, propylene glycol was selected as the synthesis solvent for SnS and was subsequently used throughout the study.

Proposed mechanism for the synthesis of SnS QDs

During the synthesis, Sn^{2+} forms a complex with propylene glycol (PG) (equation 3.1). The addition of thiourea into the formed Sn-PG complex forms a competition between thiourea and PG. A strong complexation is formed between thiourea and Sn^{2+} is formed, leading to the Sn-thiourea complex (equation 3.2); this prevents the production of many free Sn^{2+} in the solution (Han et al.,2018). Tin and thiourea dissolve easily in propylene glycol solvent, indicating the formation of $[Sn\ (SCN_2H_4)\ n]^{2+}$ complex formation (equation 3.3). The complex produced serves as both tin and sulfur source. On heating, the Sn-thiourea complex undergoes thermal decomposition to produce PG-capped tin sulfide QDs (equation 3.3) due to the rapture of coordinate bonds between Sn^{2+} and thiourea. PG acts as stabilizing ligand. Hydroxyl groups on PG control the size of SnS QDs. The two hydroxyl groups in PG bind more strongly to QD as they grow (Chowdhury et al., 2016, Shih et al., 2019) (Upadhyay et al., 2019).

$$SnCl_2 + n[PG] \rightarrow [Sn\ (PG)_n]^{2+} \quad \text{(Eq 3.1)}$$

$$[Sn\ (PG)_n]^{2+} + SCN_2H_4 \rightarrow [Sn\ (SCN_2H_4)\ n]^{2+} \quad \text{(Eq 3.2)}$$

$$[Sn\ (SCN_2H_4)\ n]^{2+} \xrightarrow{70°C,60min} Sn \quad \text{(Eq. 3.3)}$$

Influence of capping ligand on optical properties

The optical properties of SnS synthesised with different thiol capping agents at pH 3 are presented in Figure 3.9. SnS QDs capped with MPA, and L-cysteine exhibited similar luminescence properties, with MPA showing the highest intensities (Fig. 3.9(a)-(b)). This was attributed to the possible higher chelation of Sn^{2+} by MPA compared to L-Cysteine. L-cysteine is a bifunctional ligand with the amine and carboxyl group as dragging bonds. These may cause competitive coordination with the surface of the QD.

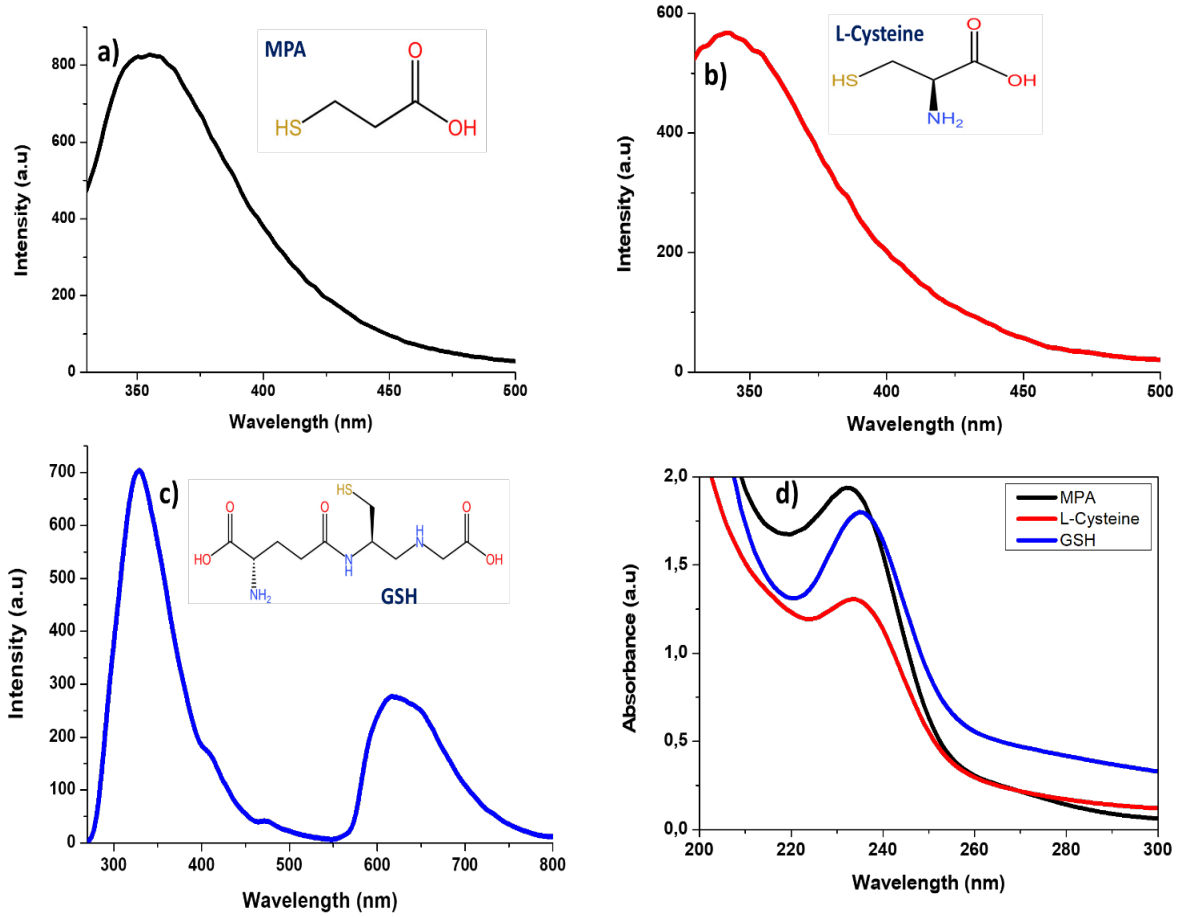

Figure 3.9. The influence of thiol capping agents on SnS QDs: a) MPA, b) L-Cysteine and c) GSH. d) Absorptive spectra of the thiol capping agents.

While MPA has only carboxyl groups, therefore, exhibits more favourable coordination conditions between carboxylate anion and tin metal. In a study by Han et al.,2017 MPA-functionalized SnS QDs were reported to be highly stable even in cell culture due to the MPA neutralization of surface charge. In the case of GSH, two emission peaks (~360 nm and 650 nm) were observed (Fig. 3.9(c)). The peak at 650 nm was attributed to possible deep trap state emissions, while the peak in the UV region is characteristic of surface emissions. The corresponding absoprtion spectra of the thiol capping agents are overlayed in Fig. 3.9(d). The different thiol-capped SnS QDs' UV absorption spectrum shows similar broad absorption bands centred around 236 nm. L-Cysteine exhbited the lowest absorbance, while MPA and GSH displayed comparative absorption spectra. Herein, the

absorption and photoluminescence of QDs were affected by alteration of the capping thiols. As a result of the prolonged stability of MPA- SnS QDs, it was selected as a capping agent in this study.

Effect of ZnS shell

To improve the solubility and stability of the SnS QDs, a ZnS shell was used to passivate the QDs. During the shelling process, the pH of the solution was constantly monitored and maintained at pH 9 using NaOH. ZnS was selected as shell material to (i) convert QDs to type 1 core/shell structure, (ii) to reduce lattice mismatch as the ZnS bandgap (~3.6 eV) fully encompasses that of SnS (~1.5 eV) (Tsolekile et al.,2019). Figure 3.10 shows the optical properties of MPA- SnS/ZnS QDs.

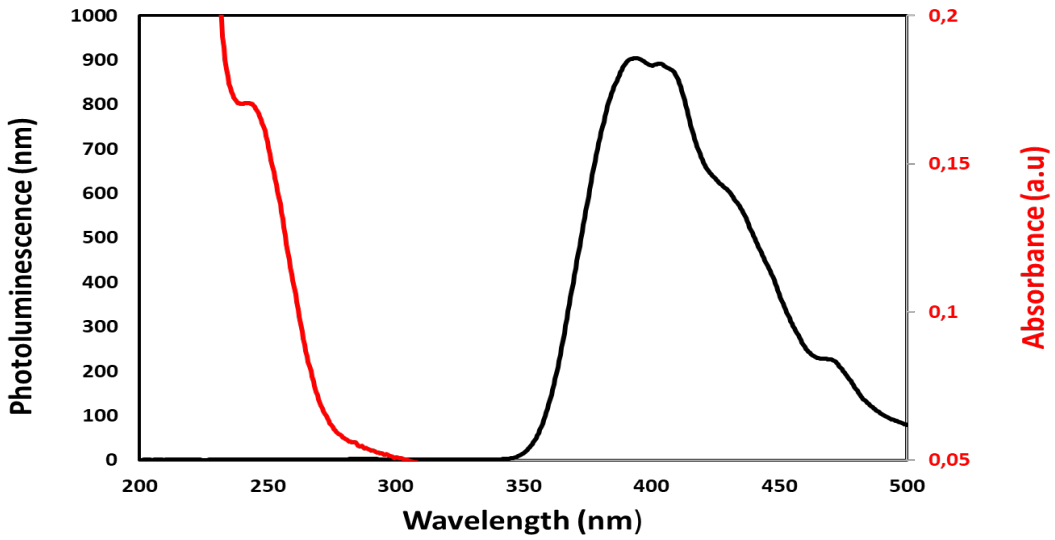

Figure 3.10. Photoluminescence and ultraviolet-visible (UV-vis) spectra of SnS QDs passivated with a ZnS shell.

Following passivation using ZnS, The PL spectra of SnS/ZnS exhibit broad and red-shifted peaks (from 350 nm to 500 nm) compared to the SnS core QDs (350 nm). The peak shift and enhancement in intensity were attributed to the passivation of the SnS QDs surface by ZnS. Similarly, to the PL spectra, the corresponding UV absorbance also exhibited a broad shift toward

longer wavelengths, suggesting a possible increase in the particle size of the QDs after ZnS coating.

3.3.2. Structural and Morphological Analysis of SnS and SnS/ZnS QDs

FTIR Characterisation

Figure 3.11 shows the FTIR spectra of pure powered GSH, MPA, L-Cysteine and thiol-capped SnS/ZnS nanoparticles. Characteristic hydroxyl (-OH) stretching vibration of GSH was recorded at 3321 cm^{-1}, and the -N-H asymmetrical and symmetrical stretching were recorded at 2970 cm^{-1} and 2925 $cm^{-1,}$ respectively (Fig 3.10a). The bands at 1643 cm^{-1} were assigned to –C=O stretching, while the peak at 1376 cm^{-1} was assigned to symmetrical COO. The disappearance of the characteristic GSH thiol (-SH, 2515 cm^{-1}) in the surface capping of GSH on the surface of the SnS/ZnS nanoparticles.

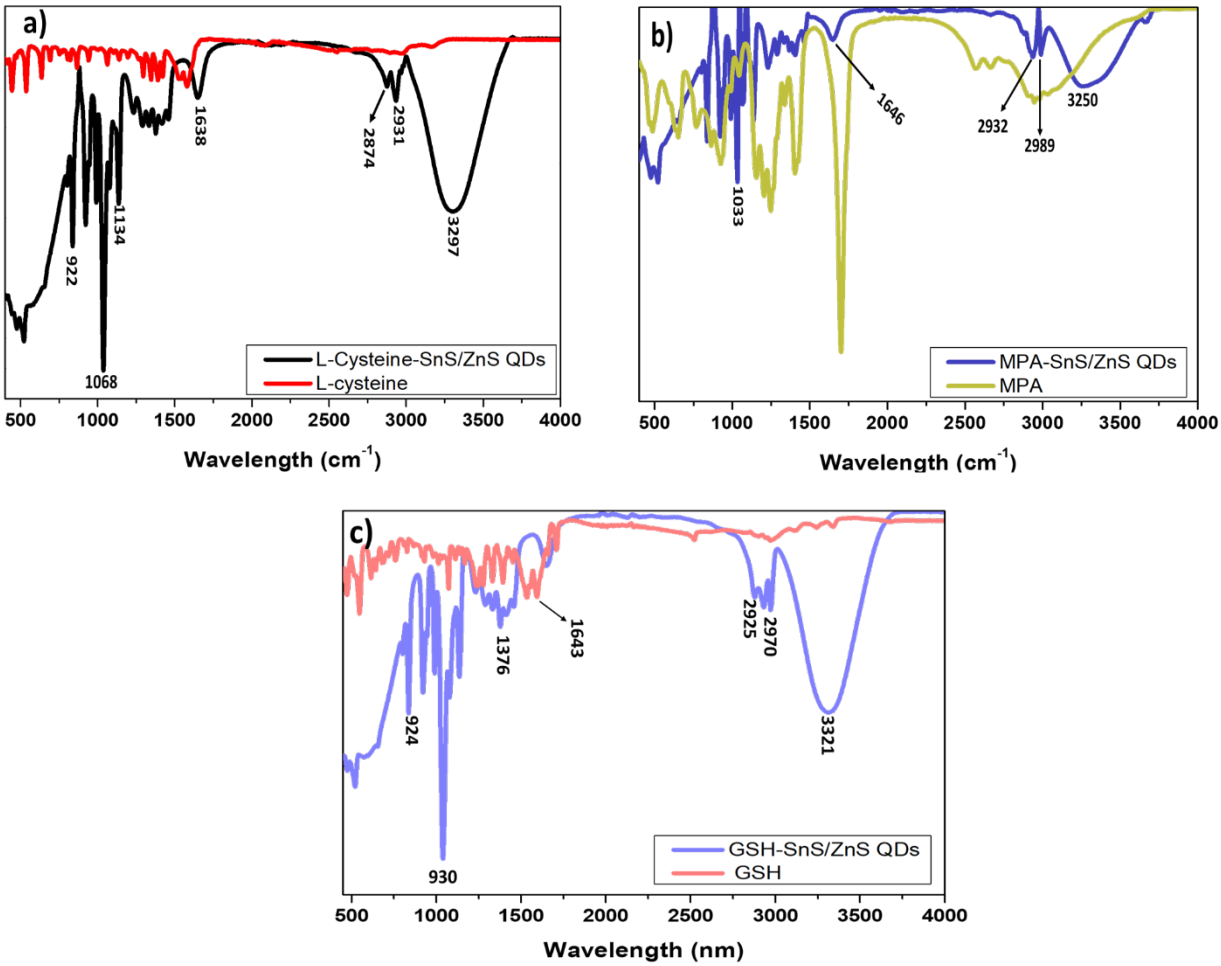

Figure 3.11. FTIR analysis of (a) GSH, (b) L-Cysteine, and (c) MPA capped SnS/ZnS

Fig 3.11b shows the L-cysteine capped SnS/ZnS QDs. According to the FT-IR spectrum of L-Cysteine and L-Cyst-SnS/ZnS nanoparticles, hydroxyl (-OH), anti-symmetrical and asymmetrical stretching vibrations of -CH_2 were recorded at 3297 cm^{-1}, 2931 $cmcm^{-1}$ and 2874 cm^{-1} respectively. The shift at 1638 cm^{-1} (asymmetric stretching vibration of COO-) and formation of the sharp band at 1068 cm^{-1} (-NH_2) structure in L-Cyst-SnS/ZnS not present in the pure L-Cysteine was observed. L-Cysteine is a bifunctional ligand using its thiol group to bond with Sn^{2+} on the QDs surface. The FTIR spectral changes in the Cyst capped QDs suggest L-Cysteine successfully modified the QDs surface. Figure 3.11c shows the IR spectra of pure MPA and MPA-capped SnS/ZnS QDs. The broad peak at 3250 cm^{-1} was attributed to carboxylic acid OH stretching acid in MPA, while the bands at 2989 cm^{-1} and 2932 cm^{-1} (red-shifted from pure MPA) were assigned

to asymmetric and symmetric -CH stretching. The pure MPA bands at 2674 cm^{-1} and 2563 cm^{-1} identified as S-H stretching peaks of MPA disappeared following MPA capping; this was accounted to the formation of SnS/ZnS QDs bond between the sulfur of MPA and dangling bonds on the SnS/ZnS QDs surface. The significant decrease in the intensity of the -C=O (1646 cm^{-1}) band and the other vibrational changes observed after MPA functionalization indicated successful capping of MPA on the surface of the SnS / ZnS QDs. The successful thiol functionalization of the QDs with the thiols with bio-active terminal groups (viz amino and carboxylic groups) allows for further linking of biomolecules on the QDs thus enabling its biological application.

Transmission electron microscope of SnS QDs and ZnS QDs

Figure 3.12 shows the TEM monographs of MPA-capped SnS QDs and SnS/ZnS QDs. The SnS QDs (~ 2.20 nm) and SnS/ZnS QDs exhibited small and spherical particles (Fig. 3.12(a)). As a result of the small particle sizes and interparticle edges of the SnS/ZnS QDs, the TEM images could not be used to approximate the diameter and thickness of the shell (Fig. 3.12(b)). At 20 nm magnification, the SnS/ZnS QDs TEM revealed particle lattice fridges, suggesting nanocrystalline QDs were synthesized.

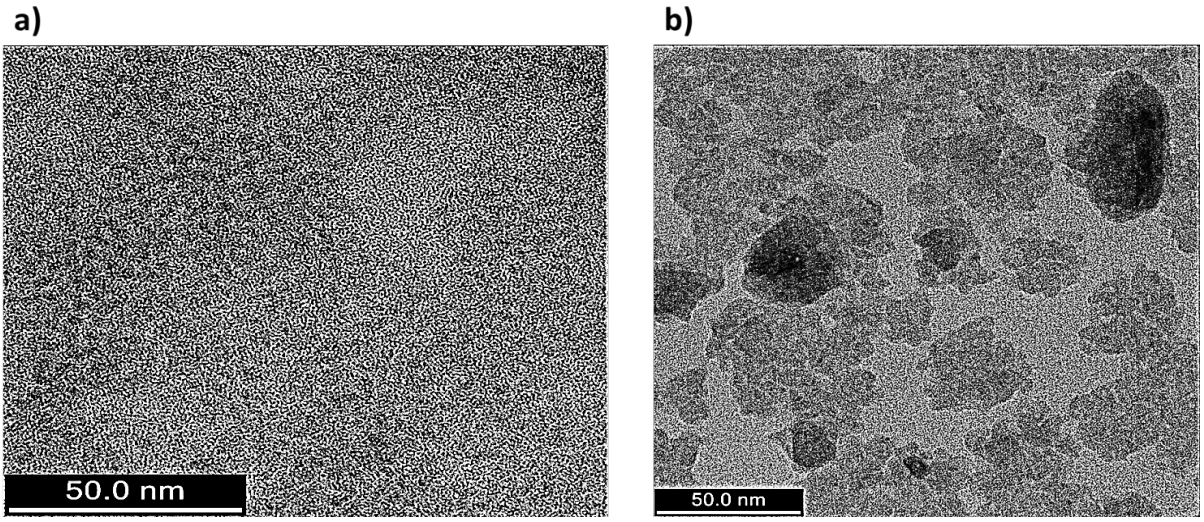

Figure 3.12. TEM images of the MPA synthesized (a) SnS QDs and (b) SnS/ZnS QDs obtained with the molar ratios Sn:S (1:1).

XRD patterns of SnS/ZnS QDs

Fig 3.13 shows the XRD diffraction peaks in powered SnS/ZnS QDs. The three peaks at 2θ of 28.9◦, 48.6◦ and 56.1◦ corresponding to (111), (220), and (311) planes were related to zinc blend structure in-line with literature (Prabha et al., 2018, Chen et al., 2020). In conjunction with the TEM images shown in figure 3.12b, the larger XRD peaks may be attributed to the formation of tiny nanocrystals that lack complete crystallinity.

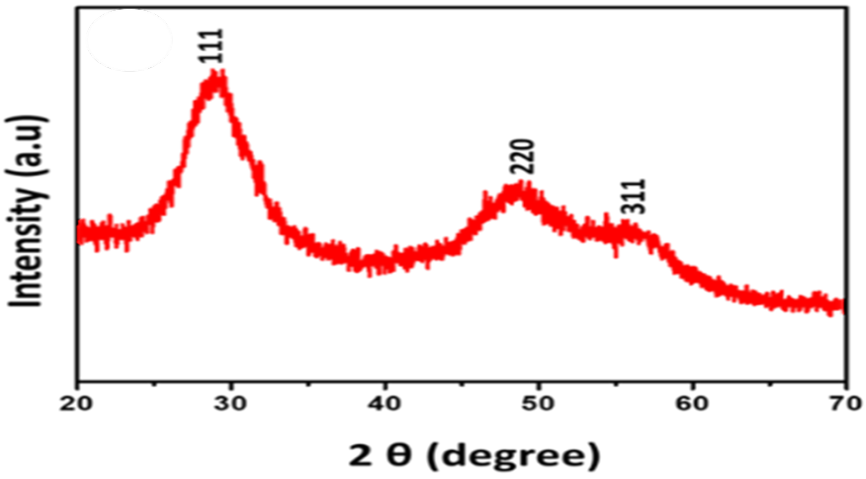

Figure. 3.13. XRD patterns of the SnS/ZnS QDs.

Dynamic light scattering of SnS QDs and SnS/ZnS QDs

The hydrodynamic size of the SnS QDs (3.14a) and SnS/ZnS (3.14b) QDs was measured using dynamic light scattering (DLS), as reported in Figure 3.14 SnS QDs exhibited larger hydrodynamic diameter (HD) sizes than the SnS / ZnS QD, corresponding to UV absorption (figure 3.10).

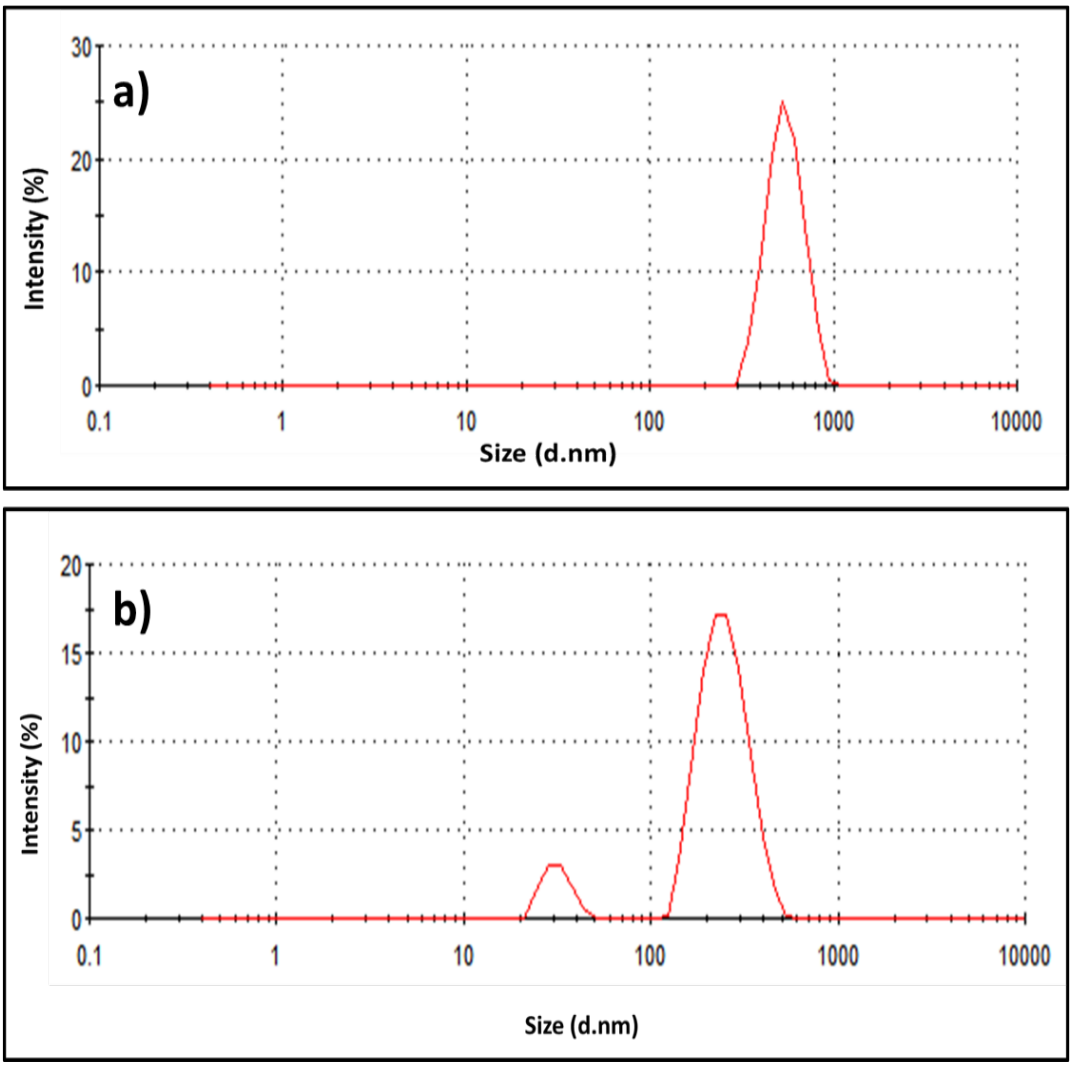

Figure. 3.14. DLS size distribution of (a) SnS QDs and (b) SnS/ZnS QDs.

3.3.3. Synthesis strategy 2 (method 2)

Core/shell structures have been used in the past to significantly increase the PL and stability of a core material by passivating the surface and protecting the core QD from the surrounding medium (Díaz-Cruz et al.,2021). To produce high-quality SnS QDs, a number of parameters need to be tuned because the optical properties of SnS are extremely sensitive to the size of the QD. The encapsulating material is another significant additional component that can impact the optical characteristics of QDs. Herein, we present a technique for treating the SnS core with ZnS precursors. However, we will first examine the impact of two important variables, namely the pH and various thiol capping agents (GSH, L-Cysteine and MPA), on the core SnS QDs.

Effect of capping ligand on SnS

Three thiol capping agents, namely: L-cysteine, Glutathione, and MPA were utilized to investigate the optimum SnS QD-ligand system as shown in figure 3.15.

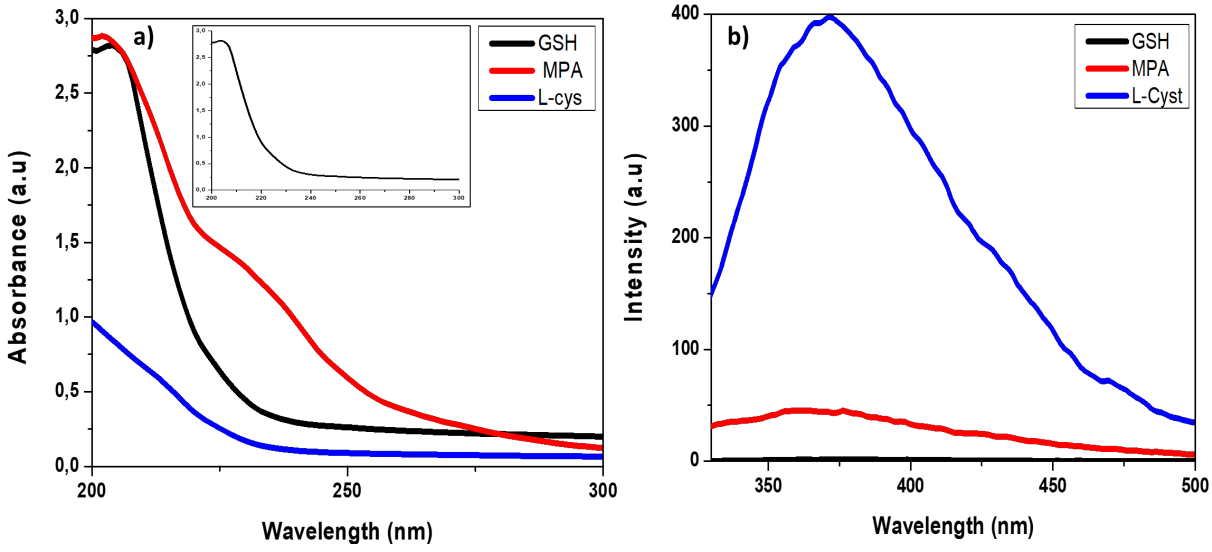

Figure. 3.15. The influence of thiol capping agents on SnS QDs: a) shows the absorption spectra of thiol capping agents (*insert*: UV-Vis of GSH)**.** b) Shows the PL spectra of thiol capping agents.

The optical properties of each capping ligand were studied by comparing the PL and UV spectra for each thiol capping agent, respectively. Figure.3.15a illustrates the UV absorption spectra of SnS QDs capped with different thiols. SnS-MPA and SnS-GSH displayed a band at 227 nm that is attributed to exciton recombination. L-cyst exhibited no notable bend around this region. SnS QDs-MPA showed a slight redshift absorption, indicating an increment in particle sizes of SnS QDs trapped in conditions. Figure.3.15 b displays the influence of each thiol capping ligand on SnS QDs obtained on the PL spectra. The PL spectrum of L-cyst-SnS QDs exhibited one symmetric emission peak around 370nm displaying that SnS QDs exhibit a widened and well-defined band gap with a narrow size distribution. The enhanced PL intensity obtained is due to a better stabilization of SnS QDs through the chelating interaction of Sn^{2+} and -SH, as well as the assistance of the two hydroxyl groups present in PG and the functionalities -COOH and $-NH_2$ present in L-cyst (Tomar et al.,2022). The MPA emission peak was observed at 80 nm, while for GSH the emission peak was observed at 50 nm. The decrease in fluorescence intensity of SnS-GSH and SnS-MPA QDs means that agglomeration is possible. As a result of the variances in the size and length of the capping agent, these nanoparticles might have different optical properties under the same synthetic conditions. Among the investigated thiol-capped SnS QDs, the PL intensity of L-Cyst-capped SnS QDs was found to be the highest, hence it was studied in detail for further investigations.

Effect of pH on SnS QDs

SnS that has been encapsulated with L-Cysteine was chosen in five distinct pH ranges (i.e., pH 1, 3, 6, 9 and 11). Significant variations in the PL and absorption spectra were observed during pH adjustment, indicating the SnS QDs' great dependence on pH for growth. Figure 3.16 a show the absorption spectra of the different pH values of the SnS QDs. SnS QDs exhibited a broad absorption spectrum in the UV region that extended to the visible region. For pH 1 and 3, the UV

spectra showed absorption peaks at 360 nm. Under acidic conditions (pH 1-3), the absorption bands are red shifted, indicating the rapid growth of SnS QDs. The absorption peaks are less prominent in the basic medium (pH 9 and 11), and the PL spectra show a similar trend with red-shifted PL emissions (figure 3.16b) with low luminescence intensities for pH 9 and pH 11 (figure 3.16b *insert*) (Cheng et al., 2020).

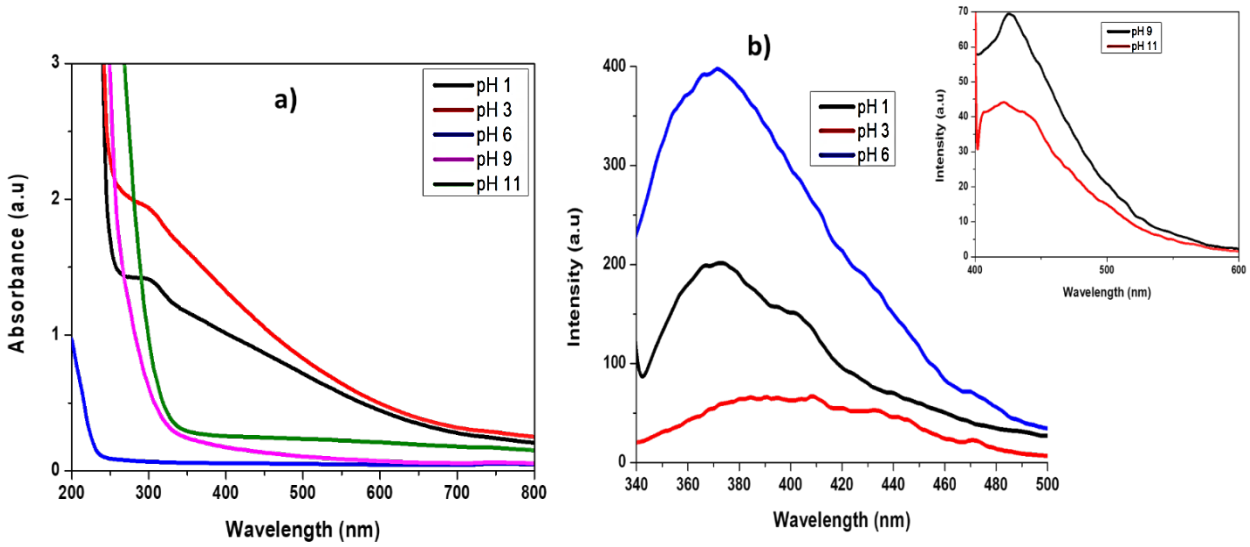

Figure 3.16. The effect of synthetic pH on (a) Absorption and (b) Photolumiscence spectra of synthesised SnS QDs (*insert:* photoluminescence spectra of pH 9 and p H 11).

The reduction in PL intensity and absorption in basic media might be ascribed to the increased number of hydroxyl groups linked to SnS QDs, which reduces the size of the QDs and resulting in lower luminescence and absorption as reported in table 4.1. Moreover, the decrease in absorption of pH 6 and rise in PL intensity imply that the reaction occurs by Oswald ripening, leading to a broad size distribution. Therefore, due to the high intensity of PL, pH 6 was chosen as the optimum for this study.

Table 3.1 Optical properties of SnS based on absorbance and emission intensity

pH values	Absorbance (λ_{max})	Band-edge Absorbance (nm)	Emission intensity (nm)
1	360	300	190
3	360	330	54
6	0	205	400
9	0	400	52
11	0	400	49

Effect of ZnS shell on SnS QDs

To further improve the optical properties of the as-synthesized SnS QDs, ZnS passivation was done on SnS core QDs. ZnS was chosen as a passivating material due to its wider bandgap (~3.6eV) relative to SnS QDs (~1.3eV), which allows charge carriers to be contained to the core region and reduce surface defects (Tsolekile et al., 2020). Moreover, the lattice mismatch of ZnS is relatively low, which reduced the formation of low defect interface between the materials mostly "dangling bonds" caused by undercoordinated metal atoms (Voigt et al.,2021). The temporal evolution of absorption and PL spectra during passivation with the ZnS shell on SnS QDs is shown in Figure 3.17. The absorption spectra of SnS/ZnS QDs (Fig. 3.17a) indicates that longer reaction time causes the absorption peak to consistently move to longer wavelengths, which is an indication of nanoparticle growth. The absorption spectra also show bands at 340 nm for all the reaction times. The corresponding PL spectra in figure 3.17b shows an increase in intensity with an increase in time. Optimum conditions were obtained after 30 min with broad, red-shifted peaks at 394 nm. The enhanced PL intensity might be caused by the passivation of the surface defects by ZnS shell on the surface of SnS QDs (Long et al.,2021).

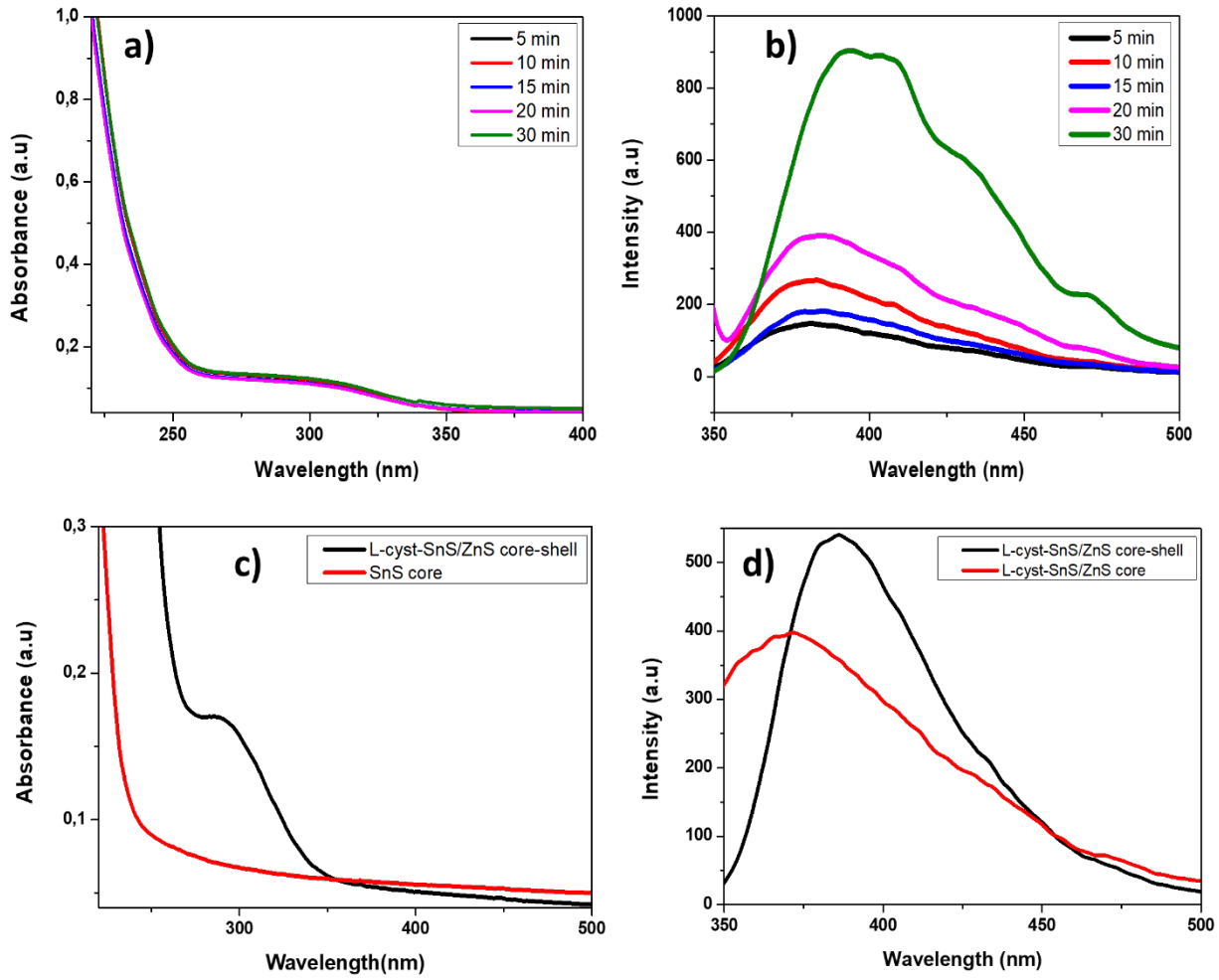

Figure 3.17. Synthesis of L-Cysteine-SnS/ZnS shell QDs at different time intervals: a) Absorption spectra, b) PL spectra, c) Overlay absorption spectra of SnS core and SnS/ZnS core shell QDs and d) Overlay PL spectra of SnS core with SnS/ZnS core shell QDs.

An overlay absorption spectrum of the SnS core and SnS/ZnS shell is shown in figure 3.17c. A red shift was observed, which indicates that the coating process creates a ZnS shell. (Cheng et al., 2020). The redshift in the absorption edge wavelength indicates that the suspension absorbs at a larger range of visible wavelengths. The PL spectra in Figure 3.17d depict a broad PL spectrum of the SnS / ZnS shell with a redshifted peak that agrees with the absorption spectra due to quantum confinement (Harabi et al.,2023). The red-shifted PL peaks indicate that surface defects have been passivated and that the band gap of SnS QDs has decreased when they have been passivated with a ZnS shell.

3.3.4. Structural and Morphological Analysis

Fourier transform infrared (FTIR) spectroscopy characterisation.

FTIR spectroscopy was performed for identification of the adsorbed functional groups and the formation of the as-synthesised QDs. The FTIR overlay spectra of the L-Cysteine-SnS / ZnS core shell and pure L-cysteine are illustrated in Figure 3.18.

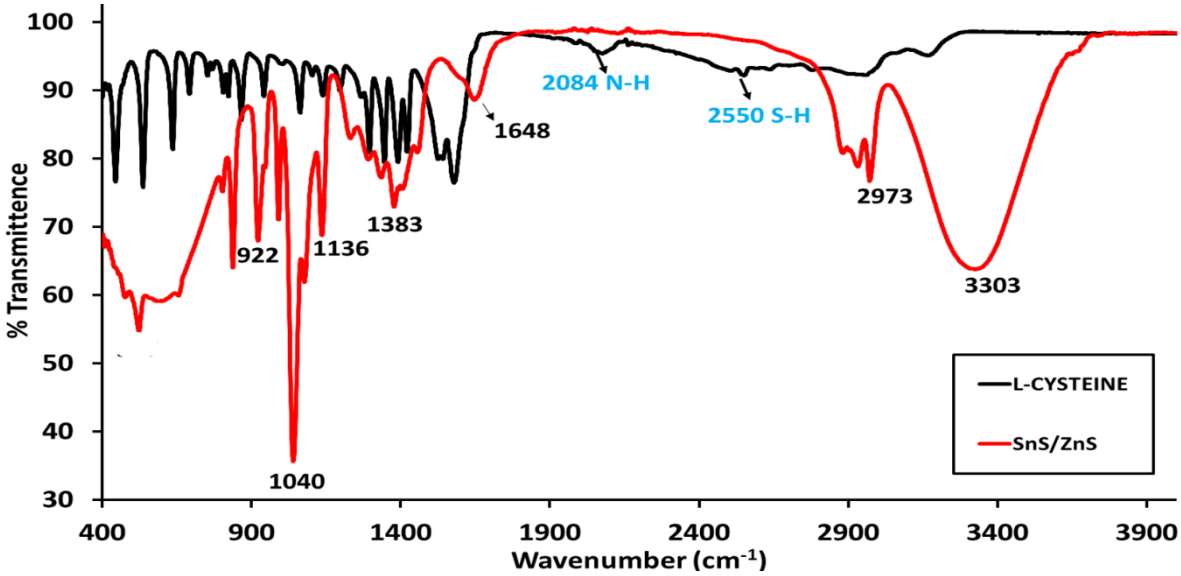

Figure 3.18. FTIR spectra of pure L-cysteine and L-Cyst-SnS/ZnS core-shell QDs

The FTIR spectra of the SnS/ZnS core QDs show the characteristic peak at 3100 cm^{-1} to 3600 cm^{-} which is assigned to stretching vibrations of water molecules (-OH) (Li et al.,2019). The well resolved peaks at 3303 cm^{-1} ,2973 cm^{-1},1648 cm^{-1}, 1383 cm^{-1}, 1136 cm^{-1} and 922 cm^{-1} are assigned to OH- stretching, symmetric -C-H stretching, symmetric stretching of COOH-, C-O stretching, CN- and C-H- bending of L-cysteine respectively. The presence of symmetric stretching of COOH- indicates the chemisorption of L-Cysteine of the QD onto the surface might have occurred through the carboxylate of the thiols which is line with literature (Núñez-Colón & Bailón-

Ruiz.,2023). The formation of a sharp band at 1040 cm^{-1} ($-NH_2$) was observed present in L-cyst-SnS/ZnS not present in pure L-cysteine. Pure L-cysteine exhibited a characteristic peak at 2550 cm^{-1} which is assigned to stretching vibrations of S-H group. This peak completely disappears on SnS/ZnS core-shell QDs due to the cleavage of SH- bonds and the formation of Sn-S bonds (Jia et al.,2021). Since L-cysteine is a cross-linker the cleavage of the SH- bonds might be caused by the presence of thiol group which forms a chemical bond with Sn^{2+} on the surface of the QDs confirming aggregation. Furthermore, stretching vibrations of the N-H of the NH_3^+ group in L-cysteine at 2084 cm^{-1} are also not observed in SnS/ZnS QDs due to the basification of NH_3^+ during the synthesis. This confirms the successful modification of L-cysteine on the surface of SnS/ZnS QDs.

Energy dispersive spectroscopy (EDS) and scanning electron microscopy (SEM) Analysis

EDS and SEM analysis was performed on both L-Cys-SnS QDs and L-cyst-SnS/ZnS QDs. The uncoated L-cyst-SnS QDs in (figure 3.19a) reveals the presence of Sn, S, C, O and N elements. The corresponding EDS spectra of L-cyst-SnS/ZnS QDs in figure 3.19b shows the presence of Zn, C, Sn, O, and S, indicating the successful surface modification of thiol capping in SnS QDs as well as passivation with ZnS shell. The presence of trace amounts of silicon (Si) might be due to contamination during sample preparation. Figure 3.19c shows SEM images of L-cyst-SnS core QDs with a flaky layered structure with no distinct patterns and thickness size of 2µm. The L-cyst-SnS core QDs completely lost their original shape right after passivation with the ZnS shell. Figure 3.19d shows L-cyst-SnS QDs passivated with a ZnS shell. The SEM image reveals a crush-like morphology with a rough surface, indicating the presence of small nanoparticles on the surface with a thickness of 2 µm. The formation of agglomeration in figure 3.19d is attributed to the formation of nanoparticles with extremely small dimensions and high surface energy.

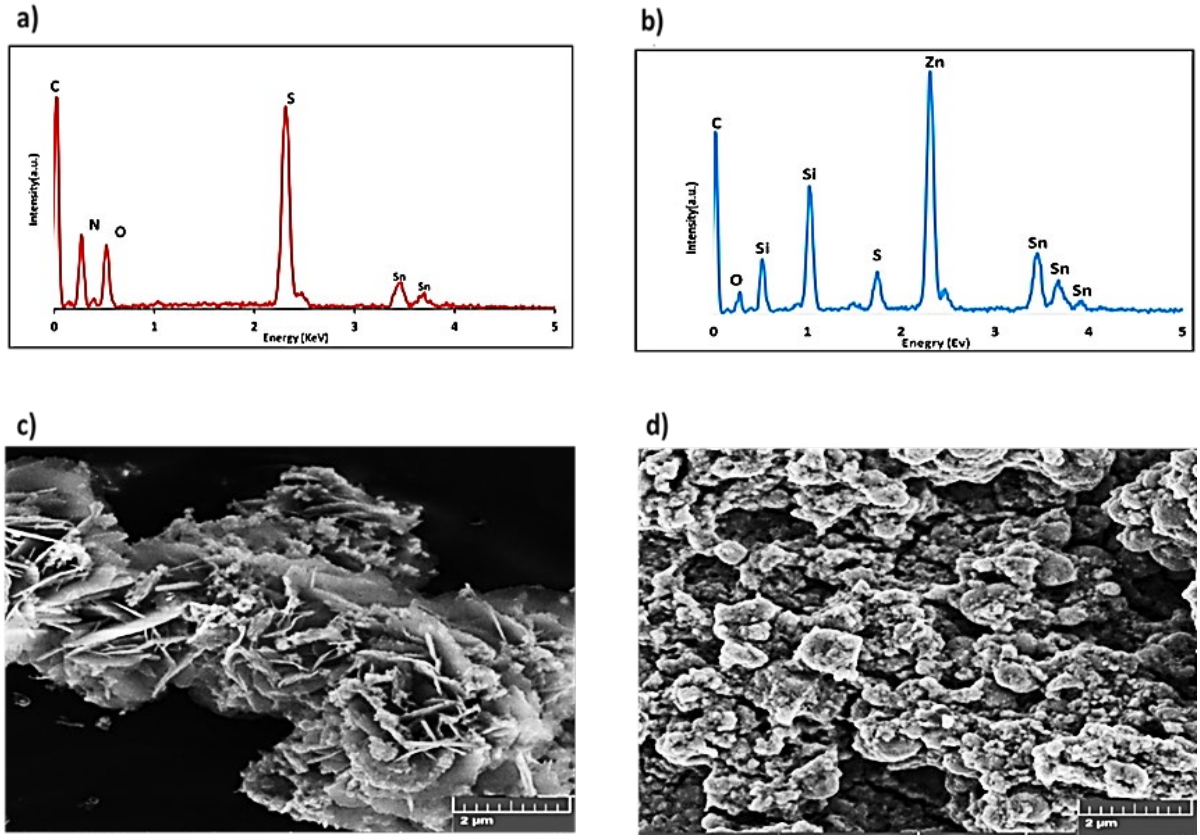

Figure 3.19. EDS spectra of a) L-Cys-SnS QDs and b) L-Cys-SnS/ZnS QDs**.** SEM image of c) L-Cys-SnS QDs and d) L-Cys-SnS/ZnS QDs.

Transmission electron microscope (TEM) analysis

The size and shape of SnS core and SnS/ZnS QDs were examined by transmission electron microscope (TEM) (figure 3.20). Figure 3.20a reveals uniform morphology of SnS QDs. The monograph shows that L-cyst-SnS core QD particles are spherical and monodispersed. In addition, the particles of the core QDs were significantly more stable and did not agglomerate. The estimated average size of SnS was approximately 5.375 nm as shown in Figure 3.20b) which is in agreement with the literature (Li et al.,2019) (Chowdhury et al.,2016).

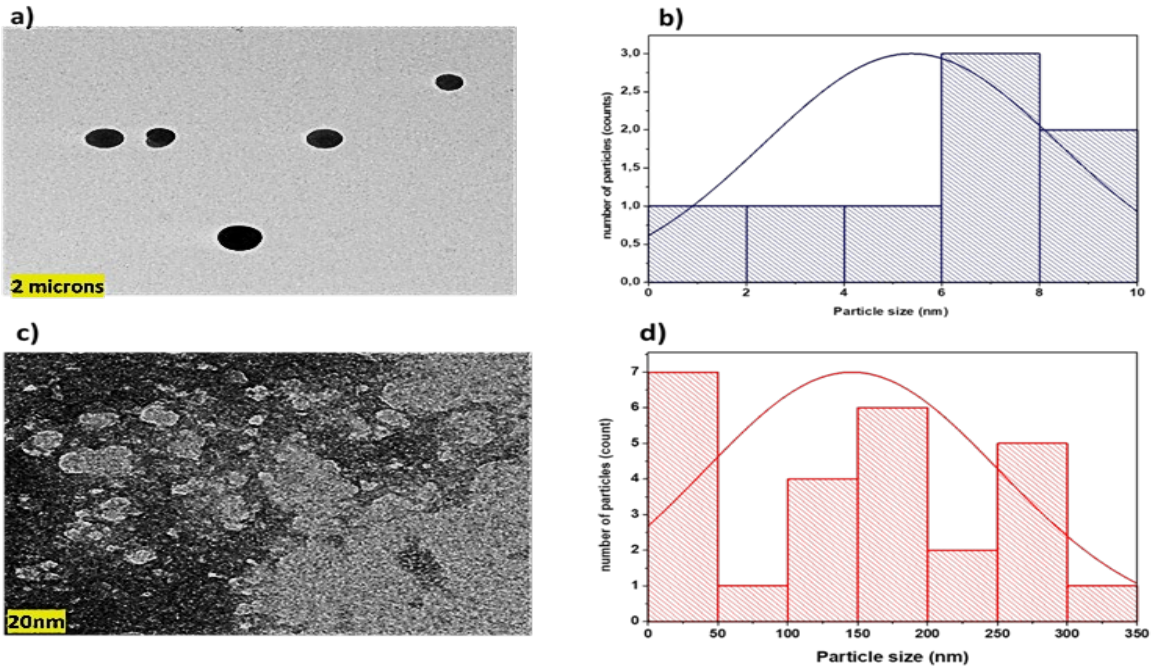

Figure 3.20. Transmission microscopy of a) L-Cys-SnS QDs and b) Histogram of Size distribution of L-Cys-SnS QDs. c) TEM monograph of L-Cys-SnS/ZnS QDs and d) Histogram of size distribution of L-Cys-SnS QDs.

TEM monograph of L-cyst-SnS/ZnS core-shell QDs illustrated in figure 3.20c displays the formation of incomplete hexagonal aggregates on the surface of the SnS QDs. Due to the formation of aggregates the average size of the core-shell could not be estimated. The presence of the aggregates is caused by the ZnS passivation, which might have increased the surface properties of the SnS core QDs. The formation of aggregation based on high surface properties of SnS is quite common and similar observations have been reported by other research groups (Muthuvinayagam et al.,2013) (Cheng et al.,2020). This effect can be further seen in SEM results in Figure 3.19d.

3.4. Conclusion

SnS QDs were successfully synthesized using two methods (viz heat and reflux method). The two synthetic methods for SnS QDs showed that the type of sulfur source influences the quality of SnS QDs. To explore the influence of the two sulfur sources on the optical properties of SnS QDs, we explored different experimental variables (thiol capping agents, pH, Sn:S, solvent, experimental

method: heat vs reflux, ZnS shell). The first method reports the formation of SnS QDs using thiourea as sulfur source and the second method reports the synthesis of SnS QDs synthesized via heat method using N_2S as a sulfur precursor. SnS QDs synthesized using method 1 showed optimal photoluminescence of 1:1 Sn:S ratio, pH 3 using propylene glycol as solvent. Because of the prolonged stability and high luminescence results, MPA was chosen as a capping ligand to synthesise SnS QDs. In method 2, SnS QDs were successfully obtained using Na_2S as a sulfur source and propylene glycol as a solvent and excellent complexing agent. The results indicated that SnS QDs shows optimal intensity at pH 6 using L-Cysteine as a thiol capping agent. In both methods, the addition of ZnS shell on the SnS QDs resulted in increased PL intensity. A comparative study was conducted for both methods. Method 2 was the most rapid and showed a higher intensity, whilst QDs synthesised using Method 1 took longer and had a lower intensity. It was found that the releasing rate of S^{2-} was more rapid in Na_2S than in Thiourea, as results high number of SnS QDs were formed. Characterization of the SnS QDs revealed that SnS/ZnS aggregated to form bigger QD clusters when ZnS was added. Thiol-capping and zinc were introduced into the composition of the QD, as demonstrated by FITR, EDS, and XRD. Both TEM and DLS verified the QD size. In agreement with the SEM findings, TEM images revealed numerous SnS QDs aggregating with ZnS on their surfaces.

3.5 References

Arya, S., Mahajan, P., Mahajan, S., Khosla, A., Datt, R., Gupta, V., Young, S.J. and Oruganti, S.K., 2021. influence of processing parameters to control morphology and optical properties of Sol-Gel synthesized ZnO nanoparticles. *ECS Journal of Solid-State Science and Technology,* 10(2):023002.

Chand, S., Thakur, N., Katyal, S.C., Barman, P.B., Sharma, V. and Sharma, P., 2017. Recent developments on the synthesis, structural and optical properties of chalcogenide quantum dots. Solar Energy Materials and Solar Cells, 168:183-200.

Dar, M.A., Govindarajan, D., Batoo, K.M. and Siva, C., 2022. Supercapacitor and magnetic properties of Fe doped SnS nanoparticles synthesized through solvothermal method. *Journal of Energy Storage,* 52:105034.

Das, P., Bhattacharyya, S., Banerji, P. and Das, N., 2021. Acoustic cavitation assisted synthesis and characterization of photoluminescent carbon quantum dots for biological applications and their future prospective. *Nanostructures & Nano-Objects,* 25:100641.

Deepa, K.G. and Nagaraju, J., 2012. Growth and photovoltaic performance of SnS quantum dots. *Materials Science and Engineering: B*, 177(13):1023-1028.

Drbohlavova, J., Adam, V., Kizek, R. and Hubalek, J., 2009. Quantum Dots — Characterization, Preparation and Usage in Biological Systems. *International Journal of Molecular Sciences*, 10(2):656-673.

Divsar, F., 2020, 'Introductory Chapter: Quantum Dots', in F. Divsar (ed.), Quantum Dots - Fundamental and Applications, IntechOpen, London. 10.5772/intechopen.92151.

Han, S., Shih, W. and Shih, W., 2017. Charge-Neutral, Stable, Non-Cytotoxic, Near-Infrared SnS Aqueous Quantum Dots for High Signal-to-Noise-Ratio Biomedical Imaging. *Chemistry Select*, 2(24):7332-7339.

Harabi, I., Khattak, Y.H., Jemai, S., Ullah, S., Toura, H. and Soucase, B.M., 2023. InP/ZnS/ZnS core quantum dots for InP luminescence and photoelectrochemical improvement. *Physica B: Condensed Matter*:414634.

Jia, Y., Liu, H., Cai, P., Liu, X., Wang, L., Ding, L., Xu, G., Wang, W., Jiao, M. and Luo, X., 2021. Near-infrared emitting Cu–In–Se/ZnS core/shell quantum dots: aqueous synthesis and sulfur source effects. *Chemical Communications*, 57(34):4178-4181.

Kannan, A.G., Manjulavalli, T.E. and Chandrasekaran, J., 2016. Influence of solvent on the properties of CZTS nanoparticles. *Procedia Engineering*, 141:15-22.

Li, H., Li, M., Kan, H., Li, C., Quan, A., Fu, C., Luo, J., Liu, X., Wang, W., Yang, Z. and Wei, Q., 2019. Surface acoustic wave NO2 sensors utilizing colloidal SnS quantum dot thin films. *Surface and Coatings Technology*, 362:78-83.

Liu, M., Wu, H., Liu, X., Wang, Y., Lei, M., Liu, W., Guo, W. and Wei, Z., 2021. Optical properties and applications of SnS 2 SAs with different thickness. *Opto-Electronic Advances*, 4(10):200029-1.

Lokhande, A.C., Babar, P.T., Karade, V.C., Gang, M.G., Lokhande, V.C., Lokhande, C.D. and Kim, J.H., 2019. The versatility of copper tin sulfide. *Journal of Materials Chemistry A*, 7(29):17118-17182.

Long, Z., Zhang, W., Tian, J., Chen, G., Liu, Y. and Liu, R., 2021. Recent research on the luminous mechanism, synthetic strategies, and applications of CuInS 2 quantum dots. *Inorganic Chemistry Frontiers*, 8(4):880-897.

May, B.M., Bambo, M.F., Hosseini, S.S., Sidwaba, U., Nxumalo, E.N. and Mishra, A.K., 2022. A review on I–III–VI ternary quantum dots for fluorescence detection of heavy metals ions in water: optical properties, synthesis and application. *RSC advances*, 12(18):11216-11232.

Mei, S., Zhang, G., Yang, W., Wei, X., Zhang, W., Zhu, J. and Guo, R., 2018. A facile route for highly efficient color-tunable Cu-Ga-Se/ZnSe quantum dots. *Applied Surface Science*, 456:876-881.

Miranti, R., Septianto, R.D., Kikitsu, T., Hashizume, D., Matsushita, N., Iwasa, Y. and Bisri, S.Z., 2022. π-SnS colloidal nanocrystals with size-dependent band gaps. *The Journal of Physical Chemistry C*, 126(11):5323-5332.

Mirzaei, M., Khanbabaie, R., Jahanshahi, M., Najafpour Darzi, G. (2018). 'Preparation, Optimization and Characterization of CuInS2 quantum dots by a D-optimal Design', *Journal of Water and Environmental Nanotechnology,* 3(4):311-320. doi: 10.22090/jwent.2018.04.004.

Muthuvinayagam, A., David, T.M. and Sagayaraj, P., 2013. Investigation on a one-pot hydrothermal approach for synthesizing high quality SnS quantum dots. *Journal of alloys and compounds*, 579:594-598.

Modi, K.H., Pataniya, P.M., Patel, V. and Sumesh, C.K., 2022. Self-powered photodetector functionalized by SnS quantum dots. *Optical Materials*, 129:112504.

Núñez-Colón, A.M. & Bailón-Ruiz, S.J., 2023. Production of Zn-based quantum dots in the presence of different capping agents. *MRS Advances*:1-7.

Oluwafemi, O., n.d. *Ternary quantum dots*.

Parani, S., Tsolekile, N., Pandian, K. and Oluwafemi, O., 2017. Thiolated selenium as a new precursor for the aqueous synthesis of CdSe/CdS core/shell quantum dots. *Journal of Materials Science: Materials in Electronics*, 28(15):11151-11162.

Prabha, D., Usharani, K., Ilangovan, S., Narasimman, V., Balamurugan, S., Suganya, M., Srivind, J., Nagarethinam, V.S. and Balu, A.R., 2018. Thermal behavior and comparative study on the visible light driven photocatalytic performance of SnS 2–ZnS nanocomposite against the degradation of anionic and cationic dyes. *Journal of Materials Science: Materials in Electronics*, 29:18708-18717.

Ramasamy, V. and Vijayalakshmi, G., 2016. Synthesis and characterization of ceria quantum dots using effective surfactants. *Materials Science in Semiconductor Processing*, 42:334-343.

Ramírez-García, G., Oluwole, D., Nxele, S., d'Orlyé, F., Nyokong, T., Bedioui, F. and Varenne, A., 2016. Characterization of phthalocyanine functionalized quantum dots by dynamic light scattering, laser Doppler, and capillary electrophoresis. *Analytical and Bioanalytical Chemistry*, 409(6):1707-1715.

Salman, H., 2016. *Synthesis, Characterization, and Fabrication of All Inorganic Quantum Dot LEDs*. masters, post-graduate. University of Baghdad.

Shambharkar, B.H. & Chowdhury, A.P., 2016. Ethylene glycol mediated synthesis of Ag 8 SnS 6 nanoparticles and their exploitation in the degradation of eosin yellow and brilliant green. *RSC advances*, 6(13):10513-10519.

Shih, W.H., Shih, W.Y., Han, S., Niu, X. and Fang, S., Drexel University, 2019. Tin sulfide quantum dots for in vivo near infrared imaging. *U.S. Patent*, 517(10):967.

Singh, I., Arora, R., Dhiman, H. and Pahwa, R., 2018. Carbon Quantum Dots: Synthesis, Characterization and Biomedical Applications. *The Turkish Journal of Pharmaceutical Sciences*, 15(2):219-230.

Srivastava, R.R., Mishra, H., Singh, V.K., Vikram, K., Srivastava, R.K., Srivastava, S.K. and Srivastava, A., 2019. pH dependent luminescence switching of tin disulfide quantum dots. *Journal of Luminescence*, 213:401-408.

Tsolekile, N., Ncapayi, V., Obiyenwa, G.K., Matoetoe, M., Songca, S. and Oluwafemi, O.S., 2019. Synthesis of meso-tetra-(4-sulfonatophenyl) porphyrin (TPPS4)–CuInS/ZnS quantum dots conjugate as an improved photosensitizer. *International Journal of Nanomedicine*:7065-7078.

Tsolekile, N., Parani, S., Vuyelwa, N., Maluleke, R., Matoetoe, M., Songca, S. and Oluwafemi, O.S., 2020. Synthesis, structural and fluorescence optimization of ternary Cu–In–S quantum dots passivated with ZnS. *Journal of Luminescence*, 227:117541.

Tomar, S., Gupta, S., Priyam, A., Bhushan, B., Singh, A., Dwivedi, U.K. and Choubey, R.K., 2022. Temporal evolution of optical absorption and emission spectra of thiol capped CdTe quantum dots. *Applied Physics A*, 128(10):944.

Upadhyay, M., Thakur, A. and Daimary, M., 2019. Synthesis and Chraracterization of

Tin Sulfide Nanoparticles. Science & *Technology Journal*.,7(2):102-104.

Veerasubramani, G.K., Park, M.S., Choi, J.Y. and Kim, D.W., 2020. Ultrasmall SnS quantum dots anchored onto nitrogen-enriched carbon nanospheres as an advanced anode material for sodium-ion batteries. *ACS applied materials & interfaces*, 12(6):7114-7124.

Voigt, D., Bredol, M. and Gonabadi, A., 2021. A general strategy for CuInS2 based quantum dots with adjustable surface chemistry. *Optical Materials*, 115:110994.

Yu, Y., Zhang, K. and Sun, S. (2012) "One-pot aqueous synthesis of near infrared emitting PBS Quantum Dots," *Applied Surface Science*, 258(18):7181–7187.

Yu, Y., Xu, L., Chen, J., Gao, H., Wang, S., Fang, J. and Xu, S., 2012. Hydrothermal synthesis of GSH–TGA co-capped CdTe quantum dots and their application in labeling colorectal cancer cells. *Colloids and Surfaces B: Biointerfaces*, 95 : 247-253.ttps://doi.org/10.1016/j.apsusc.2012.04.031.

CHAPTER 4

FABRICATION OF ELECTROCHEMICAL HER-2 SENSOR USING GLASSY CARBON ELECTRODE (GCE)

This chapter discusses electrochemical characterization of the L-cyst-SnS/ZnS quantum dots (QDs) (synthesis and spectroscopic characterisation of this material is discussed in chapter 3) using non film (solution) and film (modification on the surface of glassy carbon electrode (GCE) forming L-cyst-SnS/ZnS/GCE) methods. The L-cyst-SnS/ZnS/GCE (film) or L-cyst-SnS/ZnS (non-film) were studied by cyclic voltammetry (CV) and Differential-pulse voltammetry (DPV). Two supporting electrolytes were tested. Important electrochemical parameters of the QDs were determined using different scan rates and interpreted using Randles-Sevcik and Lavron equations. The non-film mode was used to fabricate sensor for detection of HER-2 biomarker. The sensor fabrication was optimized by varying electrochemical techniques, interaction time and use of glutaraldehyde. Optimum conditions were used for establishment of the sensor analytical parameter, which were compared to literature values.

4.1. Introduction

The detection and quantification of HER-2 biomarkers status has continued to be of a great concern to many reseachers due to its wide usage in determing breast cancer at an early stage. Currently, there are two accepted methods in hospitals for the evaluation of HER-2 biomarker and these include immunohistochemistry (IHC) and *in situ* hybridization (ISH), which are not suitable for point-of-care (POC) diagnostics (Sharma et al., 2018). Hence, a considerable effort in developing novel methodologies for the detection of HER-2 biomaker is required. Electrochemical biosensor

technologies are currently gaining phenominal tools for POC analysis. Features such as possibility to maniaturization, low cost, fast response, small sample volume and portability make electrochemical biosensors attractive for the development of new analytical devices (Freitas et al., 2020). Different electroanalytical techniques such as cyclic voltammetry (CV), differential-pulse voltammetry(DPV) and square-wave voltammetry (SWV) and electrochemical impendance spectroscopy (EIS) offer depandable, facile, and highly sensitive approach for the ultrasensitive sensing of HER-2 biomaker (Amir et al., 2024). Over the years, many reseachers have developed different biosensing strategies for the detection of HER-2 biomarker (Harahsheh et al., 2021; Ahmad et al., 2019; Hartati et al., 2020; Freitas et al., 2019; Amir et al., 2024). These strategies rely on modifying the electrode surface with an electroactive material that may provide improved sensor performance.

Electroactive materials are widely employed due to their high surface area which can enhance the adsorption kinetics of the analyte species, excellent catalytic activity, which is useful in systems that utilizes electrocatalysis, faster electron transfer kinetics due to high conductivity resulting in good stability and high surface area which can be optimized towards directing the assembly for targeting analyte species (Ganjali et al., 2018) (García-Mendiola et al., 2018). Electroactive materials have been used in fabrication of sensors, drug delivery systems, cancer biomarker detection and targeting of cancer cells (Olvera and Monaghan, 2021). Different methods are used for proper deposition of electroactive materials on the electrode surface using various methods. A schematic of the methods for depositing electroactive materials on electrode is depicted in Fig. 4.1.

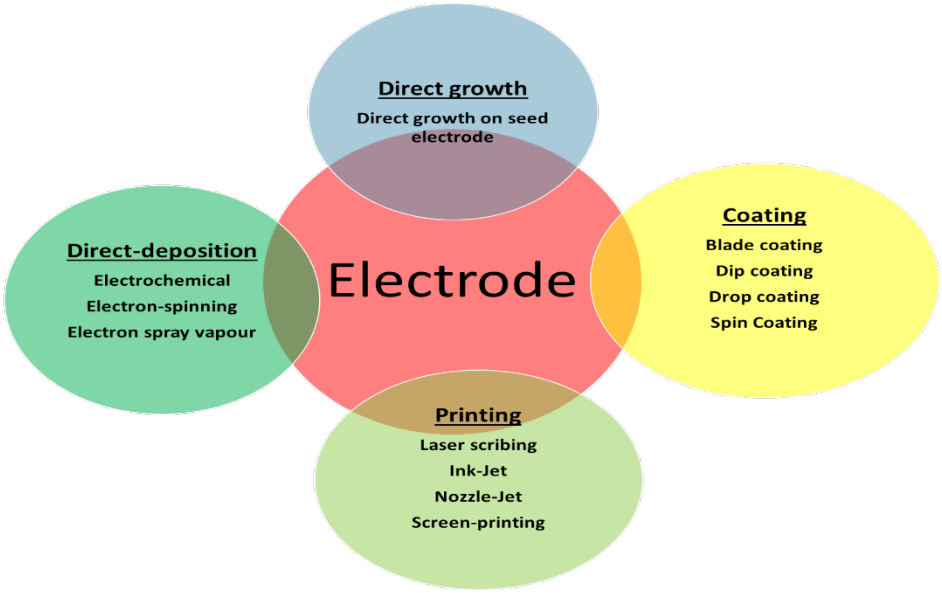

Figure 4.1. Methods used to deposit electroactive materials onto electrode surfaces.

Although these methods are ideal in forming a film on the surface of the electrode, non-film electroactive materials remain the most favoured due to their simplified measuring operation as well as their rapid analysis (Zhang et al., 2017). CV and DPV are the most popular electroanalytical techniques used for assessing the behaviour of electroactive compounds added in solution(non-film) or electrode surfaces (film).

To enhance the kinetics, sensitivity and selectivity of the working electrode, quantum dots (QDs) are amongst the most intensively researched electroactive materials. As the first parts of a sensor, biorecognition components work with QDs to enhance the biosensor's performance. The use of QDs in sensor brings many benefits, including improvement of electrode surface kinetics, increase of electroactive surface area, and increase of selectivity (Mansuriya & Altintas et al.,2020). Quantum dots have been used in several electrochemical methods (fig.4.2.) that have been demonstrated to detect HER-2 biomarker.

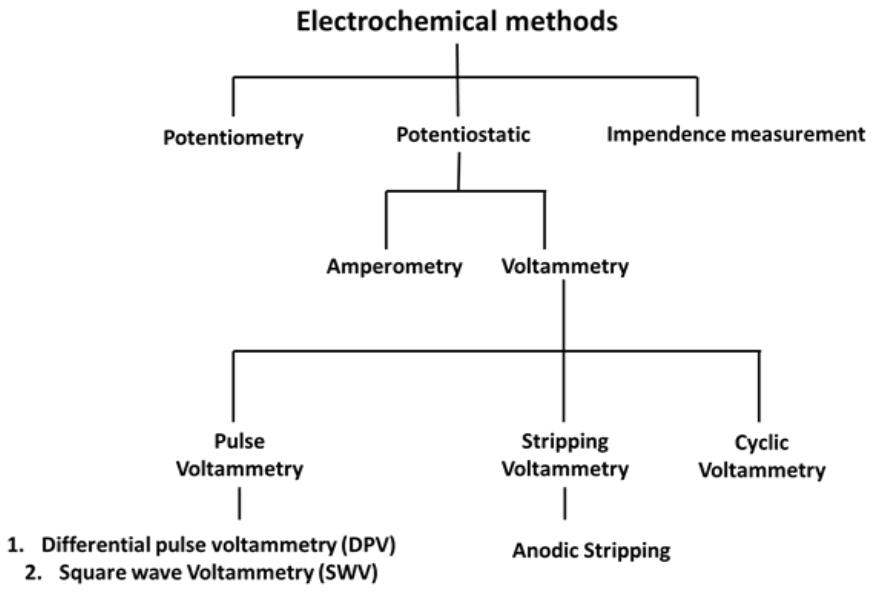

Figure 4.2 A flow chart of the electrochemical methods used to detect HER-2 biomarker.

QDs such as SnS QDs have been widely used in capacitors, sensors, and batteries. Therefore, in this study the electrochemical properties of thiol capped SnS/ZnS QDs were investigated using CV and DPV. Subsequently, the QDs were used to enhance electron transit for HER-2 biomarker sensing applications using film and non-film methods.

4.2. Experimental

4.2.1. Materials and reagents

The SnS/ZnS QDs stated in chapter 3 were employed to fabricate the transducer. The HER-2 antibody, glutaraldehyde binder (25% v/v) potassium dihydrogen phosphate (KH_2PO_4), and sodium hydrogen phosphate (Na_2HPO_4) were all purchased from Sigma Aldrich.

4.2.2. Phosphate buffer saline solution (pH:7.04, 0.1M) supporting electrolyte

Separately, 800 ml of distilled water was used to dissolve 80g of NaCl and 2g KCl. 2.4g KH_2PO_4 and 14.4g of Na_2HPO_4 were then dissolved into the solution. With 1 M NaOH and 1 M HCl, the solutions were brought to a pH of 7.04 and stored at room temperature.

4.2.3. HCl supporting electrolyte preparation (0.1M)

Hydrochloric acid (HCl) working supporting electrolyte was made from 12.1M analytical grade standard solution. 8.26 mL of concentrated HCl solution was pipetted into about 50 mL of distilled water, the solution was stirred and then 100 mL of distilled was added to bring the solution to the mark.

4.2.4. Preparation of SnS/ZnS QDs solution

1mg of SnS/ZnS QDs synthesized using method 2 as mentioned in chapter 3 were dissolved in 2mL of PBS or HCl electrolytes, respectively.

4.2.5. Preparation of HER-2 biomarker solution

A solution of HER-2 was prepared by dissolving 500 µg of HER-2 in PBS solution and stored in a bottle wrapped with aluminium foil and kept refrigerated.

4.2.6. Electrochemical characterization

The electrode was characterized using film by drop coating and non-film by the addition of 5µL soluble SnS/ZnS QDs in the supporting electrolyte. A standard one-compartment, three-electrode system coupled to a potentiostat Autolab PGSTAT 101 (Metrohm, SA) running the program NOVA 2.1 was used to conduct the electrochemical measurements. Glassy carbon (GC) was used as the working electrode, together with a platinum auxiliary electrode and an Ag/AgCl reference electrode. Between experiments, the GCE was polished with 1.0, 0.3 and 0.05 µm alumina powder to get rid of any residue build-up followed by rinsing with distilled water. The synthetic SnS/ZnS quantum dots were dissolved into solution of supporting electrolyte (HCL and PBS). In a quiescent solution, CV measurements were carried out between -1.5V to 1.5V with scan rates ranging from 30 to 270mV/s. Prior to investigating of the SnS/ZnS QD solution, the background signal in the supporting electrolyte solution was evaluated. All electrochemical tests were conducted in solutions that had been purged for one minute with high purity nitrogen gas.

4.2.7. Optimization of the procedure for the detection of HER-2.

Optimization was achieved by detecting HER-2 applying the same variable and varying only the parameter being optimized. Optimizations included the choice of electrochemical technique (CV, DPV and SWV), analyte concentration (0.99ng/mL, 1.32ng/mL, 1.65ng/mL, 2.31ng/mL, 2.64ng/mL, 2.97ng/mL, 3.3ng/mL), analyte interaction time and the influence of adding 5µL of a crosslinking agent (Glutaraldehyde). Scheme 4.1 shows the mechanism for the detection of HER-2 while optimizing the parameters mentioned above.

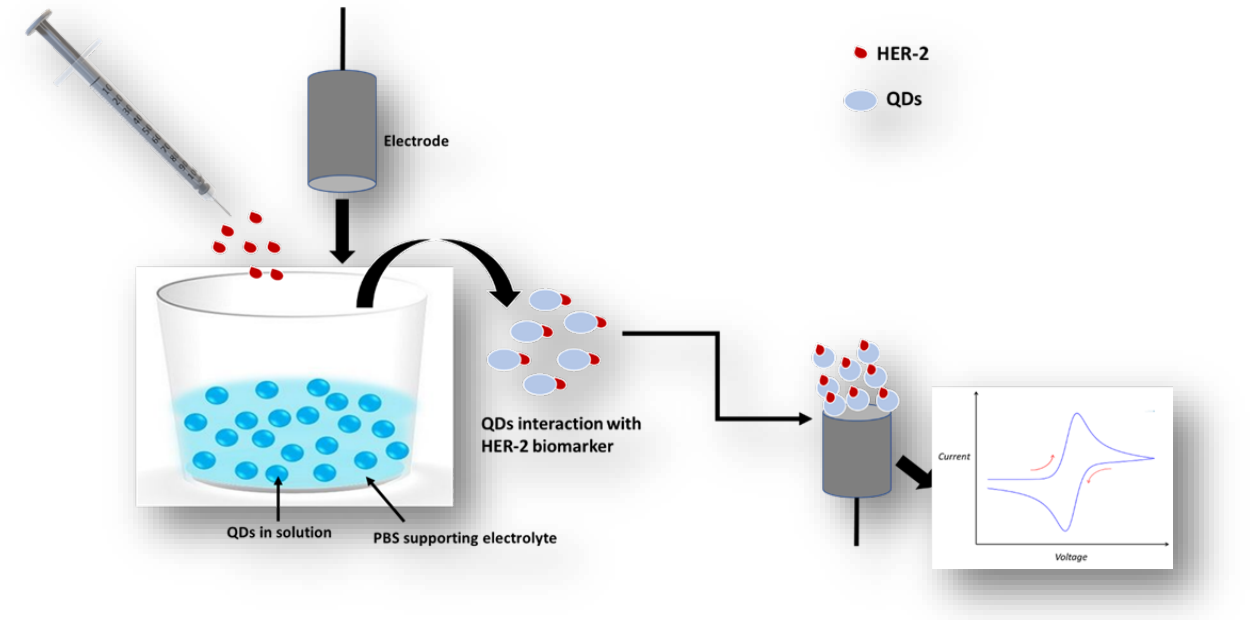

Figure 4.3. Mechanism for the detection of HER-2 based on L-cyst-SnS/ZnS QDs using GCE.

4.3. Results and discussion

4.3.1. Electrochemical Characterization of L-cyst-SnS/ZnS QDs

Film and non-film

Figure 4.4 shows an overlay of film by drop coating (film) (red) and non-film (blue) (addition of soluble L-Cyst-SnS/ZnS QDs in electrolytes) in 0.1 M HCl solution using CV and DPV at a

potential of +1 V to -1V. The blank Voltammogram in CV and DPV has no peaks, indicating that it is non-electroactive. Both film and non-film CV voltammograms (fig. 4.4a) showed two distinct cathodic Sn peaks (+0.13V and +0.15V) and Zn peaks (-0.40V and -0.42V) respectively, confirming the electroactivity of L-Cyst-SnS/ZnS QDs. Similar observations have been previously reported (Zaki et al., 2022) (Ai et al., 2019) (Yang et al.,2011). The potentials are almost the same with non-films values shifting positively for Sn and negatively for Zn. Additionally, non-film displayed an anodic peak at +0.09V which was not present in film. The QDs and their constituent ions[SnS (s) + $H_30^+{}_{(aq)}$= $Sn^{2+}{}_{(aq)}$ + $HS^-{}_{(aq)}$] were likely dissolved by aqueous HCl (strong acid), forming a weak acid which may have been the cause to the absence of the anodic peak in the film.

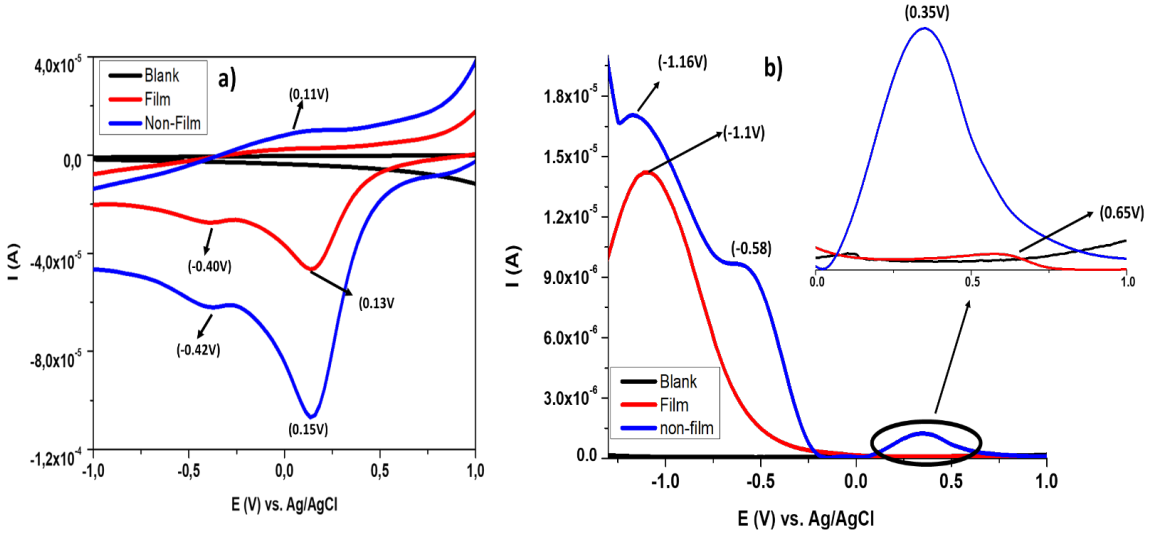

Figure 4.4. An overlay of Film (Red) and non-film (Blue) SnS/ZnS QDs voltammograms obtained using cyclic voltammetry (a) and Differential pulse voltammetry (b) in 0.1 M HCl at a scan rate of 270 mV/s.

Possible chemical reactions responsible for the observed peaks can be explained by eq. 4.3 to eq. 4.5 (Boubakri et al., 2023; Bian et al., 2022):

$Sn^{2+}{}_{(aq)} + S_{(aq)} + 2e^- \rightarrow SnS_{(s)}$ .....(Eq. 4.1)

$Zn^{2+}{}_{(aq)} + S_{(aq)} + 2e^- \rightarrow ZnS_{(s)}$ .....(Eq. 4.2)

$SnS\ (s) \rightarrow Sn^{2+}{}_{(aq)} + S_{(aq)} + 2e^-$ .....(Eq. 4.3)

Further investigations on the electrochemical characterization of L-Cyst-SnS/ZnS QDs was done using DPV (Fig 4.4b). The DPV response of non-film showed three peaks -1.16V, -0.58V and +0.35V (fig 4.3b *insert*) while film depicted two peaks at -1.1V and +0.65 V (Fig 4.4 b *insert*). The non-film current was very high compared with film's current. These data corresponded well with the CV data. The increased signal for non-film suggested that non-film had higher material concentration thus higher electrochemical activity observed. Thus, resulting in faster electron fusion between the L-Cyst-SnS/ZnS QDs and electrode surface. Film fabrication was time consuming due to the high viscosity of propylene glycol which resulted in lengthy evaporation. The film was also found to be unstable. Hence, film by drop coating approach was found to be inappropriate for this study. Therefore, for further studies, non-film was used.

Effect of supporting electrolyte

The electrochemical behaviour of L-cyst-SnS/ZnS in different supporting electrolytes (0.1M PBS and 0.1M HCl) was investigated using CV. The different behaviours observed with different supporting electrolytes are presented in figure 4.5. As observed from the voltammograms, no obvious peak of the L-cysts-SnS/ZnS QDs appears in the blank solution while the prominent peaks of Sn^{2+} (0.15V) and Zn^{2+} (-0.53V) can be observed in HCl electrolyte with a slight positive shift. No anodic peak was recorded when utilizing HCl as the supporting electrolyte, presumably this might be due to the higher tin (II) ion transport coefficient in acidic media (Bakkali et al.,2003).

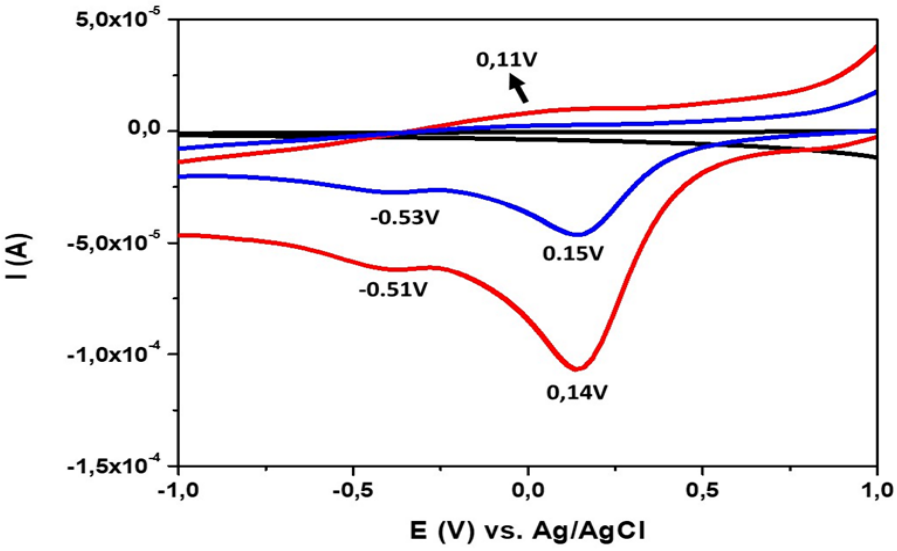

Figure 4.5. a) The cyclic voltammograms of blank (black), HCl (blue) and PBS (Red) supporting electrolytes on the behaviour of SnS/ZnS QDs using GCE (non-film).

For the PBS electrolyte, two cathodic peaks were observed around -0.51V, +0.14V, and one anodic peak at +0.11V. The anodic peak (+0.11V) present in PBS electrolyte was an indication of the occurrence of the reaction in equation 4.3. This peak can also be ascribed to dissolution of the deposited tin (amorphous and crystalline phases). By Considering the currents, PBS showed highest responses, owing to its high specific conductance, which results in superior electrochemical conductivity than HCl. Furthermore, as a buffer solution PBS contains both an acid and a base, but HCl only contains an acid. Hence, it is possible that solubility of the quantum dots is favourable in PBS, resulting in the high current. Additionally, PBS was a preferable choice since the ionic concentration was close to that of the human body; thus, biomolecules are easily hybridized in PBS buffer rather than HCl (Lah et al., 2019). Thus, PBS electrolyte was chosen as the supporting electrolyte for further studies.

Scan rate

The behaviour of L-Cyst-SnS/ZnS QDs (non-film) was evaluated at various scan rates. As demonstrated in Figure 4.6a the anodic (I) and cathodic peak currents (II, III) increased lineally with scan rates, confirming strong kinetic constraints on the electrochemical reaction which could be due to (i) chemical interactions between the electrolyte ions and QDs, (ii) dominance of electrostatic factors, (iii) lateral interactions of the redox pairs on the surface, and/or (iv) non-equivalent sites in the non-film (Opitz et al., 2015) (Karim-Nezhad et al., 2009). It was also observed that when the scan rate was increased, the anodic peak potentials shifted slightly towards a more positive direction while the cathodic peak potentials shifted slightly towards a more negative direction. The shift indicates that both processes are controlled by mass transport.

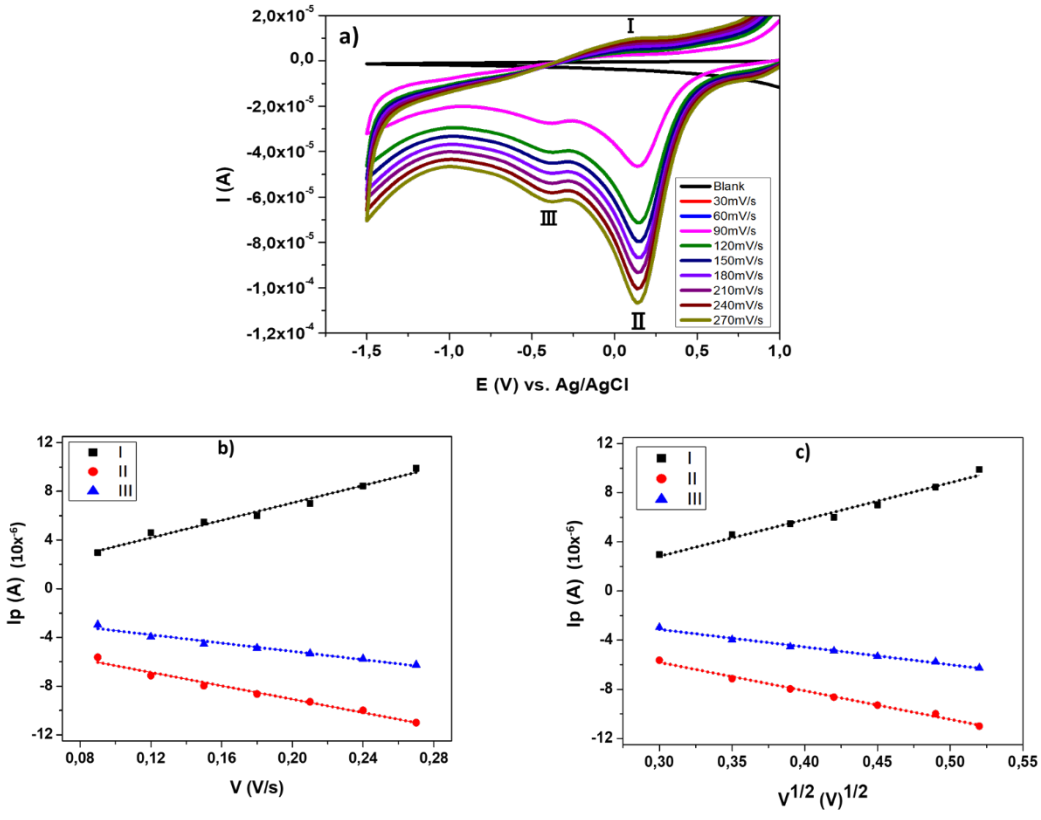

Figure 4.6. a) An overlay of various scan rate Cyclic voltammogram of SnS/ZnS QDs (a) and plots of current versus(b) scan rates as well as (c) square root of scan rate in the range of 30 to 270 mV s-1.

Based on the proximity of the peak potentials in the presented voltammogram (Fig. 4.6a), the processes represented by peak I and II are irreversible. The Lavron's plot presented in figure 4.6a shows a linear increase of anodic peak I and cathodic peaks (II, III) and the linear correlations between Ip and V obtained. The Randles plot (Fig.4.6c) showed a similar trend were the peak current Ip increased linearly with the square root of the scan rate $V^{1/2}$. Based on the correlation values presented in table 4.1, a mixture of adsorption and diffusion-driven processes was evident. However, perfect linearity between Ipa and $V^{1/2}$ was observed for both SnS and ZnS, suggesting that both diffusion and adsorption-controlled process take place, although the dominant process is controlled by diffusion.

Table 4.1: Electrochemical properties of SnS and ZnS QDs based on equations (4.1-4.2)

Parameter	SnS (II)	ZnS (I)
Ipa vs. v (slope) $x10^{-4}$	-2.00	-3.00
Ipa vs. $v^{1/2}$ (slope) x 10^{-4}	-1.00	-2.00
Ipa vs. v (R^2)	0.9718	0.9885
Ipa vs. $v^{1/2}$(R^2)	0.9915	0.9971
ks (s^{-1}) $x10^{-5}$	4.58	6.72
D $x10^{-3}$ cm^2 s^{-1}	7.73	9.43
n (no. of electrons)	2	2

The diffusion coefficients (D) and heterogeneous constants (Ks) were calculated using Randles-sevcik (eq. 4.1) and Lavron's equations (eq. 4.2) as presented in table 4.1:

$i_p = 2.69x\ 10^5$ x n x A x $D^{\frac{1}{2}}$ x C x $V^{\frac{1}{2}}$ ……(Eq. 4.4)

$E_p(V) = E^0 - \frac{RT}{\alpha nF} ln \frac{RTK_s}{\alpha nF} + \frac{RT}{\alpha nF} \ln V$……..(Eq. 4.5)

Where Ip is the peak current, n is the number of electrons involved in a redox reaction, A is the electrode surface area (0.0707 cm^2), D is the diffusion coefficient (cm^2/s), C is the concentration of the electrolyte (mol/cm^3), $V^{1/2}$ is the scan rate (V/s), Ep is the peak potential, E^0 is the standard potential, R is the gas constant ($J.mol^{-1}.mol^{-1}$), F is faraday's constant (96485 C/mol), K_s is the heterogenous constant.

The values for apparent Ks and diffusion coefficient in this study were larger than the reported values (Rudnik, 2013) (Bakkali et al.,2015) (Boubakri et al.,2023). Surface passivation with a ZnS shell and L-cysteine functionalization on the surface of the SnS core may be the reason for this discrepancy. This may also be attributed to the formation of smaller nanoparticles, which move through solutions faster than larger ones whose mass makes them move more slowly, as well as an increase in the capacity of the active sites that are available, which accounts for the high Ks value for L-Cyst- SnS/ZnS in this study (Rupar et al., 2018) (Hareesha et al.,2020) (Timakwe et al., 2023). This is consistent with the results from TEM in Chapter 3 Figure 3.20c. On the other hand, the enhanced value of diffusion coefficient which was calculated using equation (4.1) might be caused by fast transport of electrons which further confirms the formation of small particles. This can also be explained by the good selectivity of the complexing agent chosen for this study, propylene glycol (PG). The steric hindrance of PG had a favorable effect on the complex stability of SnS/ZnS QDs, which can be attributed to the two OH – groups present in PG. For instance, Boubakri et al. 2023 used triethanolamine, which has three OH- groups, as a complexing agent for SnS formation. In their study, they pointed out that a complexing agent with higher OH- groups could cause the destabilization of the system due steric hindrance.

4.3.2. Fabrication of electrochemical HER-2 sensor

Electrochemical identification of HER-2 using GCE

The electrochemical behavior of HER-2 using CV was investigated. The overlay of the QDs in the presence and absence of the HER-2 biomarker is shown in figure 4.7. PBS and PBS+ SnS/ZnS did not show any electrochemical response of HER-2 biomarker while PBS+ SnS/ZnS+HER-2 revealed a single, irreversible peak labelled "HER-2" in the potential window of 1.1 to 1.4V, which was caused by the oxidation of the HER-2 biomarker. Previous studies have reported a similar peak in the same potential range (Pacheo et al., 2018) (Sinha et al., 2019). The oxidation peak potential of the HER- 2 shown shifted negatively to 1.21 V compared to PBS and PBS+ SnS/ZnS. This indicated an effective electrooxidation of HER-2 in the presence of L-cyst-SnS/ZnS QDs. Also, the negative shift in oxidation potential of the HER-2 indicates acceleration in electron transfer. The other peaks observed were the characteristics of L-Cyst-SnS/ZnS QDs as mentioned in section 4.3.1.

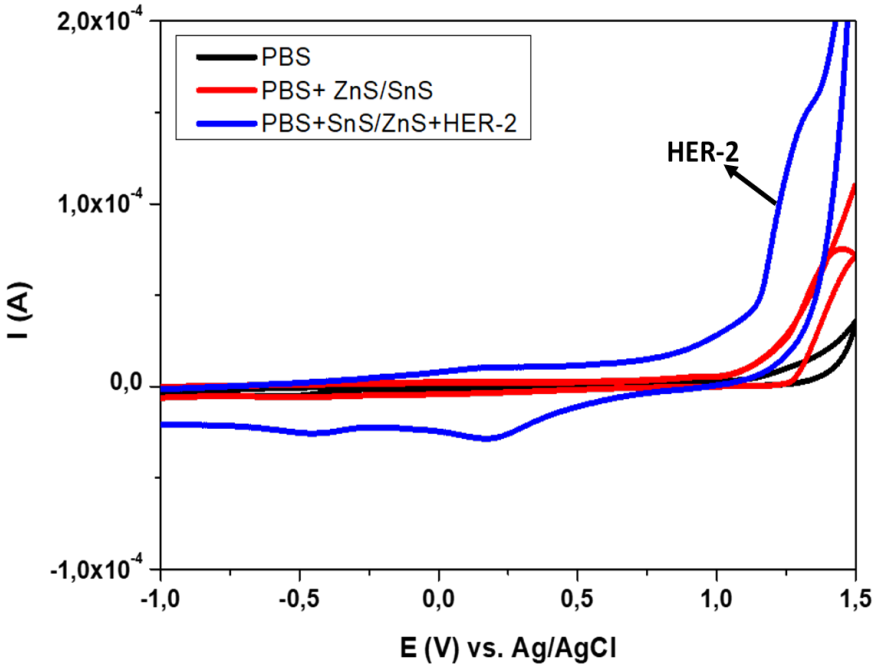

Figure 4.7. Overlay of CV Voltammogram in the absence and presence of HER-2 biomarker at 0.1M PBS, pH 7.1.

4.3.2.1. Optimization parameters

HER-2 interaction with L-Cyst-SnS/ZnS QDs using GCE

The interaction between L-Cyst-SnS/ZnS QDs and HER-2 biomarker on the current response was assessed at different time intervals using CV, DPV and SWV as shown in figure 4.8. The HER-2 peak was utilized to study the influence of interaction time while the other peaks were used to provide information about the interaction of the target analyte with the QDs. The peak current for HER-2 biomarker in both DPV and SWV showed a gradual increase from 10 to 30 min. After 30 min of interaction time, the current response decreased significantly. The CV findings (Fig. 4.8 *inset*) exhibited a similar trend, but the maximum peak current was shown at 40 minutes. Therefore, for further studies 30 min was chosen as the optimum interaction time.

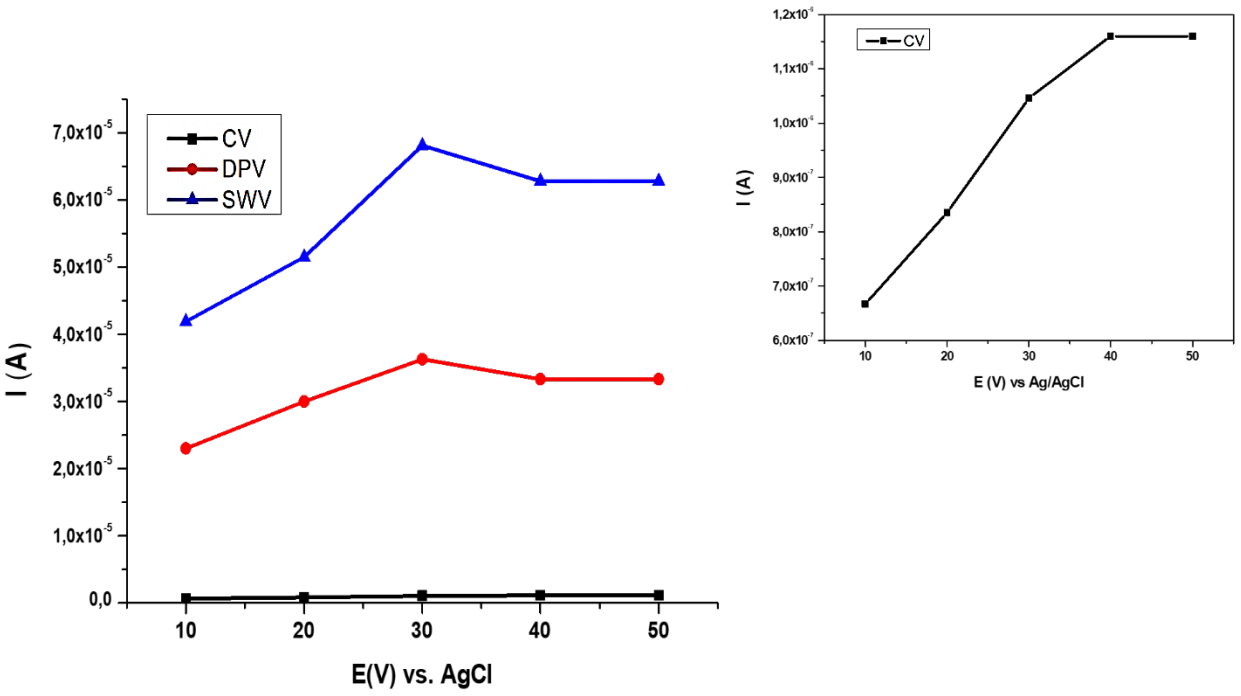

Figure 4.8. Shows the linear graph of time vs. current of the QD-immuno-reaction using different techniques (*insert* of CV: time vs current at different interaction times of QD-HER-2).

The cyclic voltammogram in Figure 4.9 depicts a detailed look at the interaction of the L-Cyst-SnS/ZnS QDs with the target analyte at various times. With the increase in interaction time, the redox peak currents increased markedly with time. The anodic peak potentials (Epa) (figure 4.9 *insert*) of the Sn^{2+} as well as the two cathodic peak potentials (Epc) of Sn^{2+} and Zn^{2+} shifted negatively in the presence of HER-2 biomarker. This electrochemical behaviour indicated a strong interaction between L-cyst-SnS/ZnS QDs and HER-2 to form QDs-HER-2 complex. Duya et al.,2023 observed a similar behaviour, where the addition of the analyte resulted in a negative shift of nanoparticles, demonstrating the formation of a complex.

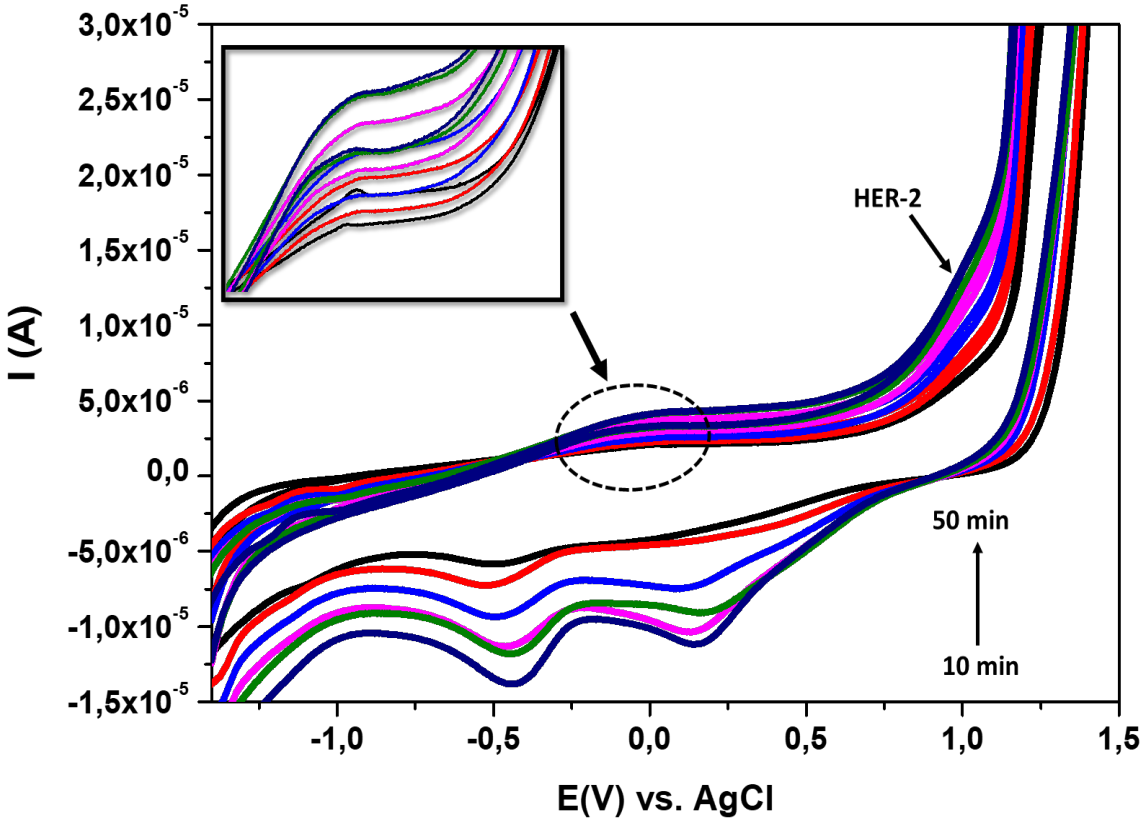

Figure 4.9. CV voltammogram of the interaction time between the QDs and HER-2 at various interaction times.

Electrochemical technique for the detection of HER-2 biomarker

Figure 4.10 shows various electrochemical techniques for the detection of HER-2. All the techniques (Fig.4.10a-c) indicated the presence of the HER-2 biomarker from -1.1V to +1.4V. The results suggested that all the techniques can be employed for the development of the sensor. The HER-2 broad peak on the CV was not clearly defined. DPV and SWV displayed a more pronounced HER-2 peak. In contrast to DPV, the signal change of HER-2 in SWV was more noticeable. As a result, SWV was selected as the main electrochemical method for HER-2 detection.

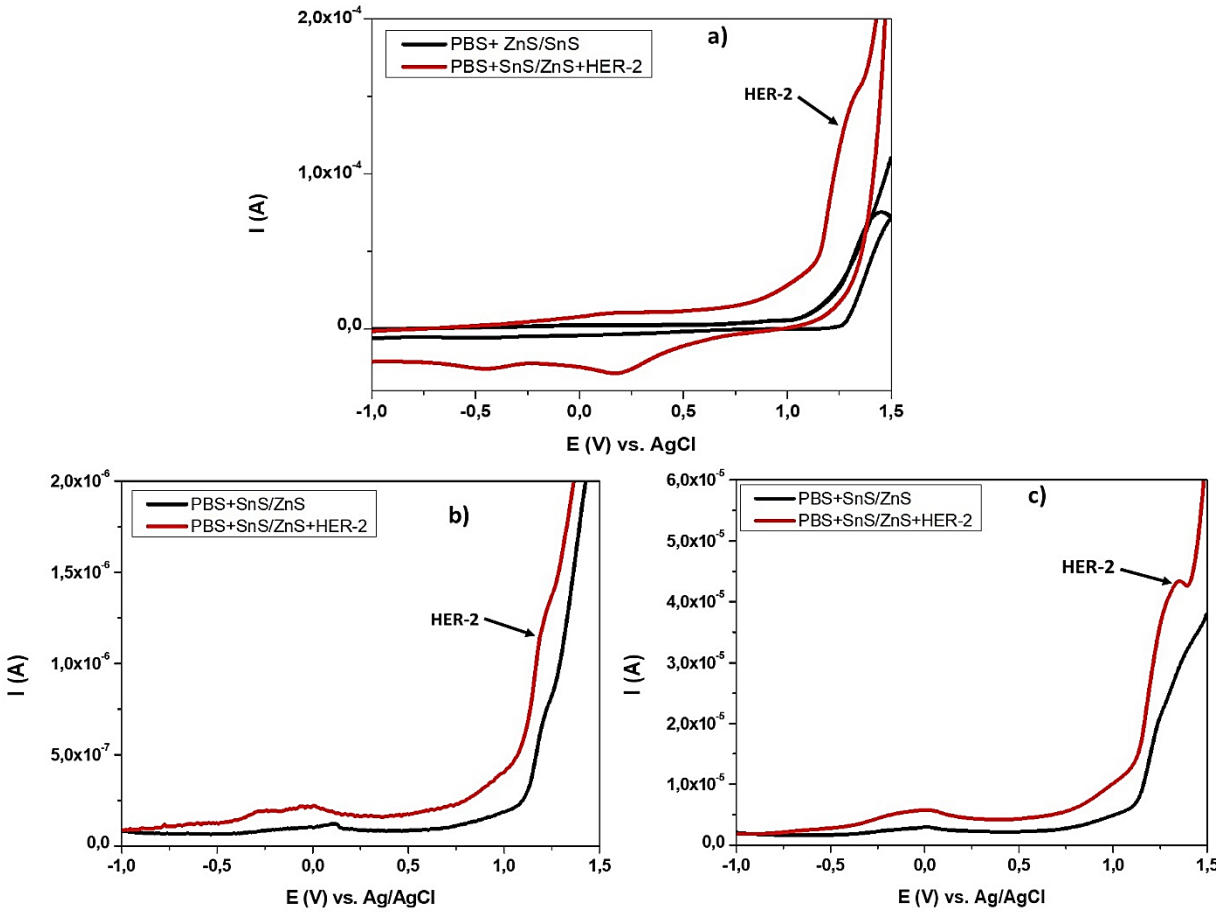

Figure 4.10. Electrochemical responses of HER-2 detection using a) CV, b) DPV, c) SWV techniques at 0.1M PBS, pH 7.1.

Influence of glutaraldehyde (GA) on the response of the biosensor

GA act as a crosslinking agent that is commonly used due to its high stability, which enables strength and water resistance of the obtained structure while reducing its toxicity (Wang et al., 2020). Glutaraldehyde is also used for selective target analyte detection and improved mechanical features (Tahmasebi & Noorbakhsh et al.,2016). In this study the effect of glutaraldehyde (GA) on the current response of the biosensor was examined (Fig.4.11). According to the data obtained PBS+ SnS/ZnS did not exhibit any HER-2 biomarker peak. The HER-2 oxidation peak was visible in both PBS+ SnS/ZnS+HER-2 and PBS+ SnS/ZnS+HER-2+Glut at a potential of 1.2V. Although the peak current was low, the addition of GA resulted in an enhanced peak when compared to PBS+ SnS/ZnS/HER-2.

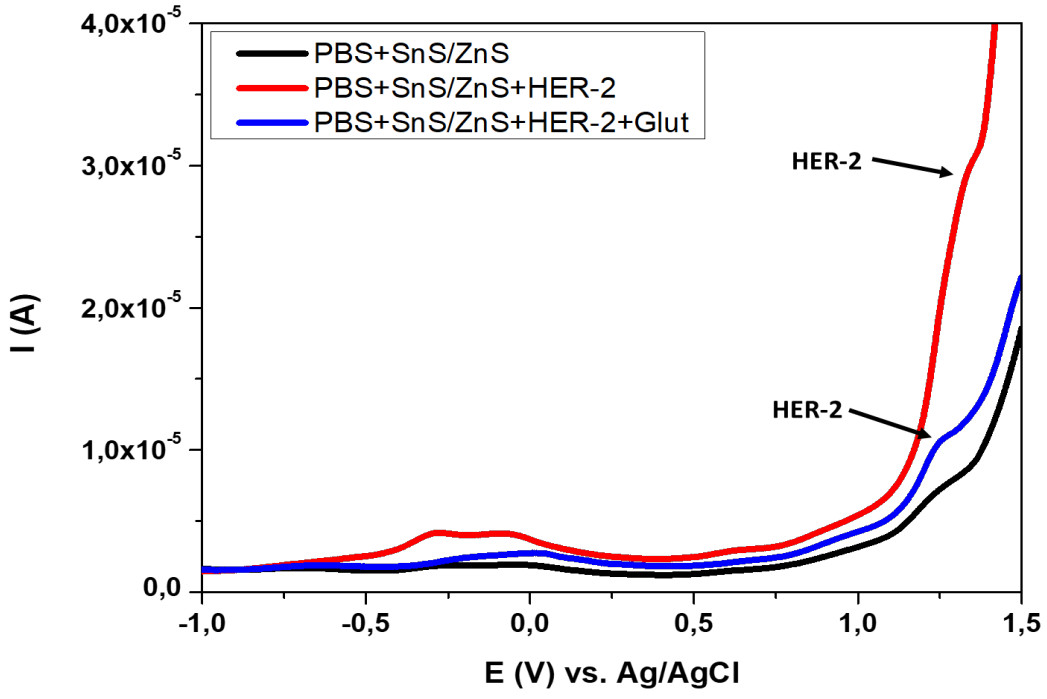

Figure 4.11. SWV curve showing the influence of glutaraldehyde on the detection of HER-2 biomarker.

Determination of electrochemical parameters for HER-2 biomarker

The electrochemical parameters of the HER-2 were determined at various scan rates to study the redox reaction mechanism of the biosensor. The different scan rates ranging from 30 to 270 mV/s were studied at 0.33ng/ml HER-2 in 3mL PBS using GCE (Fig.4.12).

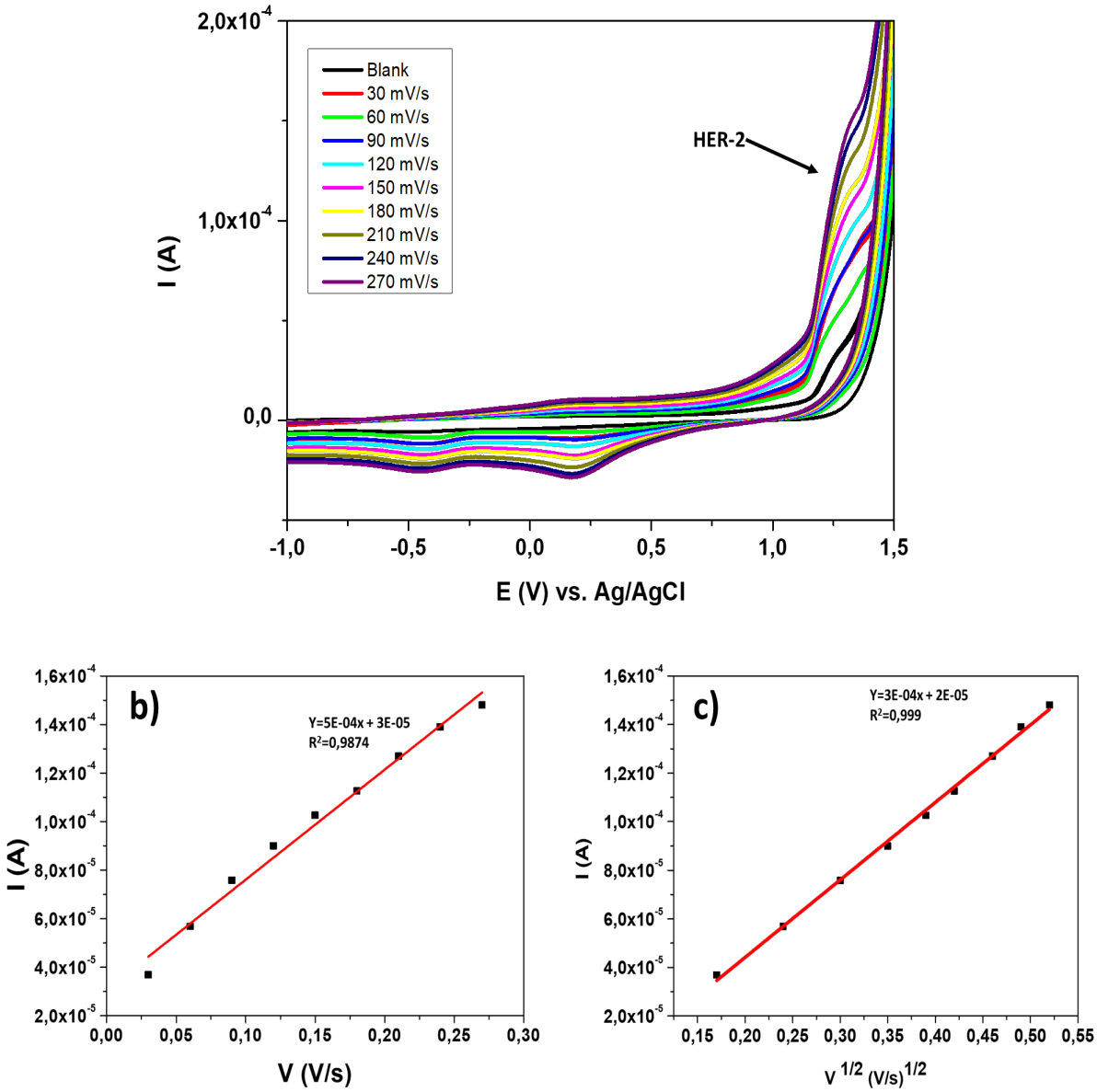

Figure 4.12. a) The influence of various scan rates of HER-2 in 0.1M PBS at SnS/ZnS/GCE(non-film), b) linear relationship for different scan rates and currents, b) Linear relationship of square roots of scan rates and currents.

The CV results in Fig. 4.12 reveal that the redox potentials of HER-2 shift slightly as the scan rate is increased. The slight shift indicates the redox reaction is an irreversible electrochemical process.

The anodic peaks linearly increased with the increasing scan rate from 30 to 270 mV/s. Figure 4.12b) demonstrates how the current increased with scan rate on the Lavron's plot for current vs. scan rate (R^2=0.9874), demonstrating that the oxidation of HER-2 is adsorption controlled. On the other hand, the Randle's plot of current vs. square root of scan rate's linear increase and correlation of 0.9982 (Fig. 4.12c) shows that the oxidation of HER-2 is diffusion-controlled. However, it is clear from comparing the correlation values of figures 4.12b) and c) that diffusion dominates over adsorption in controlling the mass transfer and electrochemical reaction of HER-2. Similar observation has been reported previously (Shepa et al.,2022) (Xia et al.,2023). Table 4.2 presents the electrochemical parameters for HER-2 biomarker.

4.2: Electrochemical parameters of HER-2 determined from Randle's plot.

Parameter	SnS/ZnS/GCE
No. of electrons	0.701
D ($cm^2\ s^{-1}$)	$3.32x10^{-3}$
Ip vs. V (R^2)	0.975
Ip vs. $V^{1/2}$ (R^2)	0.999
Ks (s^{-1})	$6.67x10^{-10}$

Performance of the sensor

The effects of various HER-2 concentrations in 0.1M PBS were examined on the response of the proporsed non-film sensors using the SWV technique. The L-cyst-SnS/ZnS QDs used were dissolved in PBS solution. Various concentrations of HER-2 were tested in figure 4.13a). When the concentration HER-2 was increased from 0.99 to 3.3 ng/mL, the peak current of SWV increased until 3.3 ng/mL (Fig.4.13a). The increase in the response of the sensor might be caused

by the excellent electrocyclic activity of L-cyst-SnS/ZnS QDs, additionally it was evident that the response of the current was due to the recognition of HER-2 by the sensor.

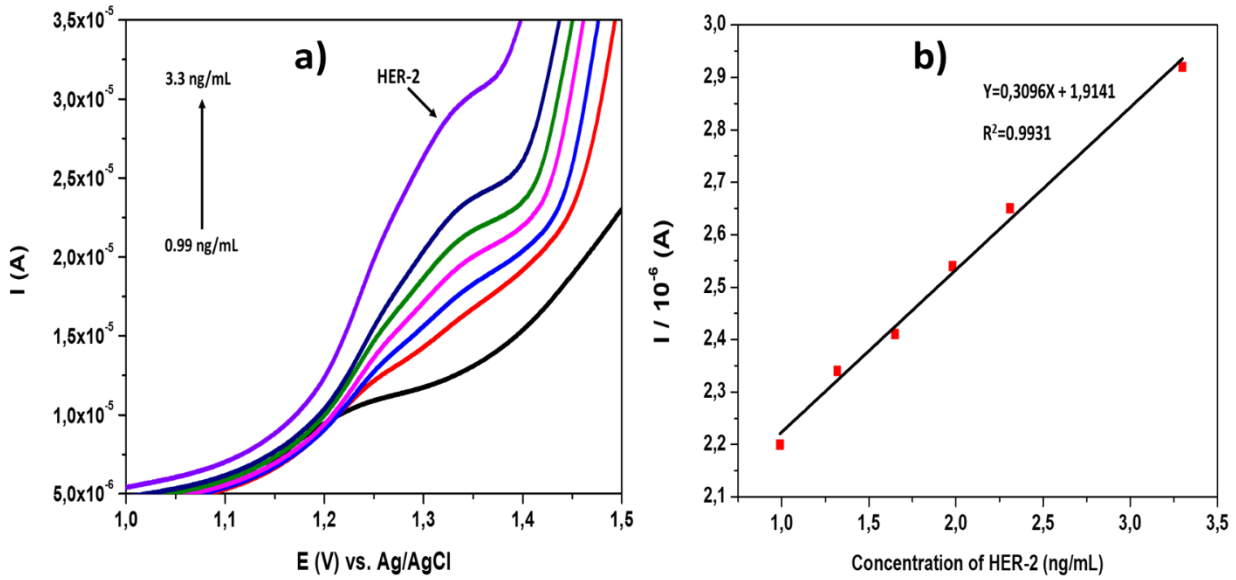

Figure 4.13. a) SWV response of HER-2 using GCE (non-film). b) Shows the linear relationship plot of the different concentrations of HER-2 vs. current.

Figure 4.13b) shows a linear relationship of concentration with peak current. The electrochemical response increase with increase in the concentration of HER-2 following the regression equation: 0.3096x + 1.9141 with a correlation coefficient of 0.9931. To determine the sensitivity of the fabricated sensor, the limit of detection (LOD) and limit of quantification (LOQ) values were calculated using the equations: LOD=3Ơ/m, LOQ=10Ơm, where m is the gradient of the calibration plot and Ơ is the standard error of the y intercept. The LOD was determined to be 0.23ng/mL, while the LOQ was 0.77ng/mL. Considering, the HER-2 biomarker cut off value of 15ng/mL (Freitas et al., 2020), the LOD are clearly lower than the cut off values, implying that the proposed sensor could be effective in breast cancer diagnosis, treatment, and follow-up. Based on the results shown in table 4.3. When compared to other electrochemical methods previously reported (table 4.4), the sensor had lower LOD and LOQ. As a result, the findings in this study

show that the constructed L-cyst-SnS/ZnS QDs based sensor (non-film) has the capacity to detect the HER-2 biomarker.

Table 4.3: Comparison of major parameters for the recently proposed electrochemical methods for the detection of HER-2 biomarker.

Technique	Sensor		LOD ng/mL	LOQ ng/mL	References
	transducer	electrolyte			
DPV	AuNP/SPCE	HCl	2.9	-	Marques et.,2018
SWV	Ab2-PbQDs/ SPCE	PBS	0.28	1	Lah et al.,2019
DPV	CdSe/ZnS QDs/ SPCE	HCl	2.1	7.1	Freitas et al.,2020
DPV	AuNP/PEG /GCE	PBS	1.52	-	Hartati et al., 2021
SWV	GCE	L-Cys-SnS/ZnSQDs in 0.1M PBS	0.23	0.77	This work

4.4. Conclusion

The electrochemical properties of L-cyst-SnS/ZnS were successfully investigated by comparing film and non-film using CV and DPV. The results indicated non-film as the best method for the characterization of L-cyst-SnS/ZnS QDs. Further studies on the characterization of the QDs was undertaken, and the results indicated PBS as the choice of the supporting electrolyte. The behaviour of the L-cyst-SnS/ZnS QDs (non-film) revealed irreversible reaction with a two-electron transfer. Randle's and Lavron's plot showed that the nature of the reaction taking place is

controlled by both diffusion and adsorption. Under the optimum conditions the QDs were further utilized in the fabrication of a sensor.

The fabrication of the sensor for the detection of HER-2 was done by the addition of the L-Cyst-SnS/ZnS QDs in PBS supporting electrolyte solution to form a non-film. CV confirmed the successful detection of HER-2 by the presence of an irreversible HER-2 oxidation peak. The fabricated sensor showed improved electron transfer parameters which was made possible by the optimization of interaction time and detection technique. Under optimum conditions of 0.1M PBS, at 30 min interaction, the sensor exhibited good analytical parameters including low detection of limits and limits of quantification. The developed sensor showed a great potential for real samples detection.

4.5 References

Ahmad, S.A.A., Zaini, M.S. and Kamarudin, M.A., 2019. An electrochemical sandwich immunosensor for the detection of HER2 using antibody-conjugated PbS quantum dot as a label. *Journal of pharmaceutical and biomedical analysis*, 174:608-617.

Ai, J., Zhao, X., Lei, Y., Yang, S., Xu, Q., Lai, C. and Peng, C., 2019. Pomegranate-inspired SnS/ZnS@ C heterostructural nanocubes towards high-performance sodium ion battery. *Applied Surface Science*, 496:143631.

Amir, H., Subramanian, V., Sornambikai, S., Ponpandian, N. and Viswanathan, C., 2024. Nitrogen-enhanced carbon quantum dots mediated immunosensor for electrochemical detection of HER2 breast cancer biomarker. *Bioelectrochemistry*, 155:108589.

Bakkali, S., Jazouli, T., Cherkaoui, M., EbnTouhami, M., El Hajjaji, N. and Chassaing, E., 2003. Influence of M12 organic additive on the electrodeposition of tin from an acid sulfate solution. *Plating and Surface finishing*, 90(1):46-49.

Bakkali, S., Touir, R., Cherkaoui, M. and Touhami, M.E., 2015. Influence of S-dodecylmercaptobenzimidazole as organic additive on electrodeposition of tin. *Surface and Coatings Technology*, 261:337-343.

Boubakri, A., Koumya, Y., Rajira, A., Almaggoussi, A., Abounadi, A. and Achargui, N., 2023. Triethanolamine concentration effect on electrodeposited SnS thin films properties. *Journal of Solid-State Electrochemistry*:1-14.

Duya, C.O., Okumu, F.O. and Matoetoe, M.C., 2023. Impedimetric nano-collision Escherichia coli analysis based on Silver-Gold bimetallic nanoparticles. *Bioelectrochemistry*, 151:108403.

Freitas, M., Neves, M.M., Nouws, H.P. and Delerue-Matos, C., 2020. Quantum dots as nanolabels for breast cancer biomarker HER2-ECD analysis in human serum. *Talanta*, 208:120430.

Ganjali, M.R., Dourandish, Z., Beitollahi, H., Tajik, S., Hajiaghababaei, L. and Larijani, B., 2018. Highly sensitive determination of theophylline based on graphene quantum dots modified electrode. *Int. J. Electrochem. Sci*, 13(3):2448.

García-Mendiola, T., Bravo, I., López-Moreno, J.M., Pariente, F., Wannemacher, R., Weber, K., Popp, J. and Lorenzo, E., 2018. Carbon nanodots based biosensors for gene mutation detection. *Sensors and Actuators B: Chemical*, 256:226-233.

Harahsheh, T., Makableh, Y.F., Rawashdeh, I. and Al-Fandi, M., 2021. Enhanced aptasensor performance for targeted HER2 breast cancer detection by using screen-printed electrodes modified with Au nanoparticles. *Biomedical Microdevices*, 23:1-11.

Hareesha, N. and Manjunatha, J.G., 2020. A simple and low-cost poly (dl-phenylalanine) modified carbon sensor for the improved electrochemical analysis of Riboflavin. *Journal of Science: Advanced Materials and Devices*, 5(4):502-511.

Hartati, Y.W., Syahruni, S., Gaffar, S., Wyantuti, S., Yusuf, M. and Subroto, T., 2021. An Electrochemical Aptasensor for the Detection of HER2 as a Breast Cancer Biomarker Based on Gold Nanoparticles-Aptamer Bioconjugates. *Indonesian Journal of Chemistry*, 21(6):1526-1536.

Karim-Nezhad, G., Hasanzadeh, M., Saghatforoush, L., Shadjou, N., Earshad, S. and Khalilzadeh, B., 2009. Kinetic study of electrocatalytic oxidation of carbohydrates on cobalt hydroxide modified glassy carbon electrode. *Journal of the Brazilian Chemical Society*, 20:141-151.

Lah, Z., Ahmad, S., Zaini, M. & Kamarudin, M., 2019. An Electrochemical Sandwich Immunosensor for the Detection of HER2 using Antibody-Conjugated PbS Quantum Dot as a label. Journal of Pharmaceutical and Biomedical Analysis., 174:608-617.

Mansuriya, B.D. and Altintas, Z., 2020. Applications of graphene quantum dots in biomedical sensors. *Sensors*, 20(4):1072.

Marques, R.C., Costa-Rama, E., Viswanathan, S., Nouws, H.P., Costa-Garcia, A., Delerue-Matos, C. and González-García, M.B., 2018. Voltammetric immunosensor for the simultaneous analysis of the breast cancer biomarkers CA 15-3 and HER2-ECD. *Sensors and Actuators B: Chemical*, 255:918-925.

Olvera, D., and Monaghan, M.G., 2021. Electroactive material-based biosensors for detection and drug delivery. *Advanced drug delivery reviews*, 170:396-424.

Opitz, M., Yue, J., Wallauer, J., Smarsly, B. and Roling, B., 2015. Mechanisms of charge storage in nanoparticulate TiO2 and Li4Ti5O12 anodes: new insights from scan rate-dependent cyclic voltammetry. *Electrochimica Acta*, 168:125-132.

Pacheco, J.G., Rebelo, P., Freitas, M., Nouws, H.P. and Delerue-Matos, C., 2018. Breast cancer biomarker (HER2-ECD) detection using a molecularly imprinted electrochemical sensor. *Sensors and Actuators B: Chemical*, *273*:1008-1014.

Rupar, J., Aleksić, M.M., Nikolić, K. and Popović-Nikolić, M.R., 2018. Comparative electrochemical studies of kinetic and thermodynamic parameters of Quinoxaline and Brimonidine redox process. *Electrochimica acta*, 271:220-231.

Rudnik, E., 2013. Effect of anions on the electrodeposition of tin from acidic gluconate baths. *Ionics*, 19(7):1047-1059.

Sharma, A., Arya, S., Chauhan, D., Solanki, P.R., Khajuria, S. and Khosla, A., 2020. Synthesis of Au–SnO2 nanoparticles for electrochemical determination of vitamin B12. *Journal of Materials Research and Technology*, 9(6):14321-14337.

Shepa, J., Šišoláková, I., Panigaj, M., Bilá, D., Jarčuška, P. and Oriňaková, R., 2022. Electrochemical Biosensors for Soluble Epidermal Growth Factor Receptor Detection. *Electrocatalysis*, 13(5):513-523.

Sinha, A., Mugo, S.M., Zhao, H., Chen, J. and Jain, R., 2019. Electrochemical immunosensors for rapid detection of breast cancer biomarkers. In *Advanced Biosensors for Health Care Applications*:147-169. Elsevier.

Tahmasebi, F. and Noorbakhsh, A., 2016. Sensitive electrochemical prostate specific antigen aptasensor: Effect of carboxylic acid functionalized carbon nanotube and glutaraldehyde linker. *Electroanalysis*, 28(5):1134-1145.

Timakwe, S., Silwana, B. and Matoetoe, M.C., 2023. The impact of silver nanoclay functionalisation on optical and electrochemical properties. *RSC Advances*, 13(3):2123-2130.

Xia, Q., Mu, Z., Qing, M., Zhou, J. and Bai, L., 2023. A sandwich-type electrochemical immunosensor for sensitive detection of HER2 based on dual signal amplification of La-MOF-PbO2 and PEI-MoS2NFs composites. *Bioelectrochemistry*:108431.

Yang, Z., Ren, Y., Zhang, Y., Li, J., Li, H., Hu, X.H.X. and Xu, Q., 2011. Nanoflake-like SnS2 matrix for glucose biosensing based on direct electrochemistry of glucose oxidase. *Biosensors and Bioelectronics*, *26*(11):4337-4341.

Zaki, M.Y., El Khouja, O., Nouneh, K., Ebn Touhami, M., Matei, E., Azmi, S., Rusu, M.I., Grigorescu, C.E.A., Briche, S., Boutamart, M. and Badica, P., 2022. ZnS stacking order influence on the formation of Zn-poor and Zn-rich Cu2ZnSnS4 phase. *Journal of Materials Science: Materials in Electronics*, 33(15):11989-12001.

Zhang, M.R. and Pan, G.B., 2017. Porous GaN electrode for anodic stripping voltammetry of silver (I). *Talanta*, 165:540-544.

CHAPTER 5

Conclusion and Recommendations

This chapter concludes based on the study's main findings and objectives, including further recommendations for future research on determining HER-2 biomarkers. The primary objective of this study was to develop a method for synthesizing thiol-capped quantum dots (QDs) and design a facile sensor based on these QDs for detecting HER-2. To specifically address these objectives, various studies were undertaken, which included: The synthesis and optimization of SnS QDs with novel hybrid surface chemistry to enhance the photoluminescence (PL), stability, and biocompatibility, which formed the first and second objectives. The spectroscopic, optical, and structural properties of the as-synthesized QDs were achieved and discussed. The development and characterization of sensors based on thiol-capped QDs. The last objective entailed sensor optimization and the sensing of HER-2 biomarkers.

5.1. Conclusion

The synthesis and optimization of SnS QDs were successfully conducted. Two synthetic methods for SnS QDs with different sulfur sources (Na_2S and thiourea) were investigated. Various synthetic parameters such as the thiol capping agents (MPA, GSH, and L-Cysteine), pH, Sn:S ratio, solvent, experimental method: heat vs reflux, and ZnS shell were evaluated in each method. Upon optimization, method 2 showed better results of 1:1 Sn:S with L-cysteine exhibiting the highest peak intensity at pH 6. The results also revealed that ZnS shell coating around the core improved the PL intensity compared to that of the core SnS QDs, accompanied by a red shift absorption.

Furthermore, SnS QDs synthesized using method two were more rapid and showed better luminescence results. FTIR verified successful thiol capping on the surface of SnS QDs. Small,

spherical, and uniformly distributed SnS QD and SnS/ZnS QDs particles were revealed by TEM, SEM, and DLS. The elemental analysis by EDS displayed the presence of Zn, S, Sn, C, N, and O, confirming the successful formation of thiol-capped L-cyst-SnS/ZnS QDs. The XRD patterns confirmed the crystalline structure of the SnS/ZnS QDs.

The obtained QDs were added into the supporting electrolyte solution to form non-film (L-cyst-SnS/ZnS), and the film was achieved by the drop coating of the QDs on the glassy carbon electrode (GCE) to form L-cyst-SnS/ZnS QDs/GCE (film). The electroactivity of the QDs in both modes were investigated using cyclic voltammetry (CV) and differential-pulse voltammetry (DPV). The results from the electrochemical parameters showed that non-film (L-cyst-SnS/ZnS) had better electroactivity than film. PBS and HCL were examined as potential supporting electrolytes. PBS displayed higher electroactivity than HCl due to its high conductivity. The behavior of L-Cyst-SnS/ZnS QDs in solution was studied, and the findings revealed an irreversible, adsorption-diffusion mixed redox reaction with a two-electron transfer. The behavior of L-Cyst-SnS/ZnS QDs in the solution was investigated, and the results showed an irreversible, adsorption-diffusion mixed redox reaction with a two-electron transfer.

The obtained L-cyst-SnS/ZnS QDs-based sensor (non-film) was assessed by applying HER-2 detection. Optimization of the sensor was investigated by analysing interaction time and the addition of glutaraldehyde. The optimum QD-HER-2 interaction time was 30min; the addition of glutaraldehyde enhanced the peak resolution of HER-2. The response of HER-2 was examined using different electroanalytical techniques, such as cyclic voltammetry (CV), differential pulse voltammetry (DPV), and square-wave voltammetry (SWV). All the techniques showed a signal in the presence of HER-2; however, the SWV technique's signal was more pronounced, therefore, it was the technique utilized for the sensor fabrication. The developed sensing strategy showed an excellent ability to detect HER-2 with 0.23 ng/mL LOD and 0.77 ng/mL LOQ. The results show

that the developed SnS-based QDs offer a faster, more economical, and simpler alternative as a sensor for detecting HER-2 biomarkers.

5.2. Future work and recommendations

The recommendations for further work on SnS QDs based on the obtained results involve:

- Investigating the effect of different shells, such as the PVP polymers to improve the PL and the stability of the SnS QDs may also reduce the formation of aggregates during the passivating process.
- An extension of the thiol capping molecule which will further enhance stability under neutral conditions and sensing properties of SnS QDs.
- Bio-conjugating the quantum dots with co-polymers like chitosan will provide a diffusion barrier and inhibit QD aggregation.
- Examining the effect of different temperatures during the synthesis of SnS nanoparticles because of temperature dependence on the growth, size, and shape of quantum dots.
- Investigate the influence of pH for detecting HER-2 using the synthesized L-cyst-SnS/ZnS to enhance the sensitivity of the biosensor.
- Further studies on the use of glutaraldehyde.